

Methods to Create Equivalent Models for Power System Studies

by

Moosa Moghimi Haji

A thesis submitted in partial fulfillment of the requirements for the degree of

Doctor of Philosophy

in

Energy Systems

Department of Electrical and Computer Engineering
University of Alberta

© Moosa Moghimi Haji, 2017

Abstract

Adequate modeling of all of the power system components including generators, transmission lines, loads, and neighboring power systems is essential for power system analysis. With nowadays large interconnected power systems, it is common practice to represent only the study system with high accuracy and use simplified equivalent models for the neighboring systems. The type of the required equivalent depends on the type of the study they are intended for. For example, power flow studies require equivalent models at fundamental frequency, whereas high-frequency transient studies require frequency dependent network equivalents (FDNEs).

This thesis research investigates methods to construct three equivalent models for power system studies. They are (1) measurement-based equivalent external system model for online steady-state power system analysis, (2) single-port and multi-port frequency dependent external network model for electromagnetic transient analysis and (3) measurement-based equivalent π circuit parameters estimation of parallel transmission lines.

For the first subject, this research has developed an online network equivalencing method based on synchronized phasor measurement data. The phasor data is used to estimate and update a multi-port Thevenin equivalent circuit continuously. An important issue in implementing this method is that the external network should remain constant during the identification process.

Therefore, a disturbance detection method is utilized to determine if noticeable changes have happened in the external system.

For the second subject, a heuristic optimization method is used to find a FDNE from the frequency response data of an external system. An equivalent circuit consisting parallel branches with positive elements is considered and the problem is formulated as an over-determined nonlinear problem. A proper coding scheme is used and different optimization methods are applied and compared to choose the best one. For the multi-port case, a model consisting of all-positive and all-negative stable branches is considered to be able to fit the non-diagonal elements of the admittance matrix. The non-diagonal elements are fitted one by one and then the diagonal elements are fitted similar to a single-port problem.

For the third subject, synchronized phasor data are utilized to find the π -circuit parameters of a newly constructed transmission line in parallel with an existing transmission line. The method utilizes the induced voltages as the excitation source and uses measurement data collected at both ends of the two parallel lines to estimate the unknown parameters. Different connections of the conductors of the new line are considered for collecting the required data. The parameter estimation problem is divided into two linear sub-problems which are solved using the least-squares method.

Preface

This thesis, including the literature review, idea development, method implementation and analysis, is an original work by Moosa Moghimi Haji. Two chapters of this thesis have been accepted for publication as scholarly articles. Prof. Wilsun Xu was the supervisory author and was involved with developing the ideas for the research and manuscript composition. Dr. Guangchao Geng assisted with method implementation and manuscript edits of the second article.

A version of Chapter 2 has been accepted for publication:

M. Moghimi Haji and W. Xu, “Online Determination of External Network Models Using Synchronized Phasor Data,” *IEEE Transactions on Smart Grid*.

A version of Chapter 3 has been provisionally accepted:

M. Moghimi Haji, W. Xu, and G. Geng, “Single-port and Multi-port Frequency Dependent Network Equivalent with Numerically Stable Branches,” *IET Generation, Transmission & Distribution*.

Acknowledgements

First, I would like to express my sincere gratitude to my supervisor, Prof. Wilsun Xu, for his guidance and support throughout my research work.

I would like to thank the members of my supervisory committee, Prof. Sahar Pirooz Azad and Prof. Hao Liang for their valuable comments and feedback. I would also like to thank other examining committee members, Prof. Udaya Annakkage and Prof. Gregory Kish, for taking the time to review my thesis.

I thank my fellow colleagues at Power Disturbance and Signalling Research Lab and also my friends, especially Dr. Mohammadreza Arani, for their feedback, cooperation and of course friendship.

Last but by no means least, I would like to thank my parents and my fiancée, Reyhaneh, for their continuous love, support, and encouragement.

Table of Contents

| | |
|--|-------------|
| LIST OF TABLES | IX |
| LIST OF FIGURES | X |
| LIST OF ACRONYMS | XIII |
| LIST OF SYMBOLS | XIV |
| CHAPTER 1 INTRODUCTION | 1 |
| 1.1 BACKGROUND | 1 |
| 1.2 THESIS OBJECTIVES AND MOTIVATIONS | 3 |
| 1.3 THESIS OUTLINE | 6 |
| CHAPTER 2 EXTERNAL SYSTEM EQUIVALENT AT FUNDAMENTAL FREQUENCY | 8 |
| 2.1 LITERATURE REVIEW | 9 |
| 2.2 PROPOSED METHOD | 13 |
| 2.2.1 EQUIVALENT MODEL | 14 |
| 2.2.2 MEASUREMENT SCHEME | 15 |
| 2.2.3 FINDING EQUIVALENT PARAMETERS | 15 |
| 2.3 IMPLEMENTATION ISSUES | 16 |
| 2.3.1 DISTURBANCE SIDE | 17 |
| 2.3.2 MEASUREMENT ERROR | 20 |
| 2.3.3 FLUCTUATION LEVEL | 21 |
| 2.3.4 IMPLEMENTATION SUMMARY | 22 |
| 2.4 CASE STUDIES | 23 |
| 2.4.1 CASE 1: IEEE 118 BUS SYSTEM | 24 |
| 2.4.2 CASE 2: MODIFIED IEEE 118 BUS SYSTEM | 32 |
| 2.5 CONCLUSION | 39 |
| CHAPTER 3 FREQUENCY DEPENDENT NETWORK EQUIVALENT | 40 |
| 3.1 LITERATURE REVIEW | 41 |
| 3.2 PROBLEM DEFINITION | 45 |
| 3.3 PROPOSED FDNE METHOD | 46 |
| 3.3.1 SINGLE-PORT FDNE | 46 |
| 3.3.2 MULTI-PORT FDNE | 51 |

| | | |
|--|---|------------|
| 3.4 | CASE STUDIES | 53 |
| 3.4.1 | CASE ONE: SAMPLE ELECTRICAL CIRCUIT | 53 |
| 3.4.2 | CASE TWO: TRANSFORMER | 57 |
| 3.4.3 | CASE THREE: DISTRIBUTION SYSTEM TERMINALS | 60 |
| 3.4.4 | CASE FOUR: IEEE 118 BUS SYSTEM | 64 |
| 3.5 | CONCLUSION | 72 |
| CHAPTER 4 TRANSMISSION LINE PARAMETER MEASUREMENT | | 74 |
| 4.1 | LITERATURE REVIEW | 74 |
| 4.2 | PROPOSED METHOD | 77 |
| 4.2.1 | TRANSMISSION LINE MODEL | 77 |
| 4.2.2 | PARALLEL TRANSMISSION LINES | 78 |
| 4.2.3 | MATHEMATICAL FORMULATION | 81 |
| 4.2.4 | SOLUTION APPROACH | 84 |
| 4.2.5 | MEASUREMENT SCHEME | 87 |
| 4.2.6 | IMPLEMENTATION SUMMARY | 89 |
| 4.3 | CASE STUDY | 90 |
| 4.4 | CONCLUSION | 104 |
| CHAPTER 5 CONCLUSIONS AND FUTURE WORK..... | | 105 |
| 5.1 | THESIS CONCLUSIONS AND CONTRIBUTIONS..... | 105 |
| 5.2 | SUGGESTIONS FOR FUTURE WORK | 107 |
| REFERENCES | | 108 |
| APPENDIX A MULTI-PORT THEVENIN EQUIVALENT | | 118 |
| A.1 | FINDING EXTERNAL NETWORK MULTI-PORT THEVENIN EQUIVALENT PARAMETERS FROM KNOWN NETWORK DATA | 118 |
| A.2 | DECOUPLING THE MULTI-PORT THEVENIN EQUIVALENT | 119 |
| A.3 | IEEE 118 SYSTEM | 120 |
| APPENDIX B HEURISTIC OPTIMIZATION METHODS | | 122 |
| B.1 | SHUFFLED FROG-LEAPING ALGORITHM | 122 |
| B.2 | PARTICLE SWARM OPTIMIZATION | 123 |
| B.3 | DIFFERENTIAL EVOLUTION | 125 |
| APPENDIX C FDNE IN EMTDC/PSCAD | | 126 |
| C.1 | FREQUENCY SCAN..... | 126 |
| C.2 | CREATING THE FDNE MODEL IN EMTDC/PSCAD | 130 |

| | | |
|--------------------------------|-----------------------------|------------|
| APPENDIX D | SIMULINK MODEL | 134 |
| REFERENCES OF APPENDICES | | 135 |

List of Tables

| | | |
|-----------|---|-----|
| TABLE 2.1 | The results obtained by the proposed method for case one | 30 |
| TABLE 2.2 | The results obtained by the proposed method for case two, resistance and impedance values | 36 |
| TABLE 2.3 | The results obtained by the proposed method for case two, equivalent voltage sources | 37 |
| TABLE 2.4 | Accuracy of the contingency analysis results | 38 |
| TABLE 3.1 | Circuit parameters for case one | 53 |
| TABLE 3.2 | Comparison of the results of PSO, DE, and SFLA for case one..... | 54 |
| TABLE 3.3 | Optimal Equivalent circuit parameters for case two..... | 59 |
| TABLE 3.4 | Comparison of SFLA, GA, and VF with passivity enforcement for case two..... | 60 |
| TABLE 3.5 | Number of branches used for creating the equivalent circuit for each element of the admittance matrix | 60 |
| TABLE 3.6 | Objective function value of fitting each element of the first column of the admittance matrix in case three | 64 |
| TABLE 3.7 | Objective function value of fitting admittance elements for case four | 70 |
| TABLE 4.1 | Different connections for phase-A of the new line | 89 |
| TABLE 4.2 | Case study parameters | 91 |
| TABLE 4.3 | Conductor data for the case study..... | 91 |
| TABLE 4.4 | Different connections of the new line conductors for collecting data | 94 |
| TABLE 4.5 | The susceptances obtained by the proposed method compared with the accurate value | 101 |
| TABLE 4.6 | The resistances obtained by the proposed method compared with the accurate value | 102 |
| TABLE 4.7 | The reactances obtained by the proposed method compared with the accurate value | 103 |

List of Figures

| | |
|---|----|
| Figure 1.1 Different network areas..... | 2 |
| Figure 1.2 Applications of the models developed in this research | 3 |
| Figure 2.1 Different fundamental frequency network equivalents | 9 |
| Figure 2.2 The equivalent model in Ward admittance method..... | 10 |
| Figure 2.3 The equivalent model in Ward injection method | 10 |
| Figure 2.4 The equivalent model in REI method..... | 11 |
| Figure 2.5 The equivalent model in pseudo-injection method | 12 |
| Figure 2.6 Multi-port Thevenin equivalent of the external system | 14 |
| Figure 2.7 Measurement scheme | 15 |
| Figure 2.8 Internal and external system representations..... | 18 |
| Figure 2.9 Internal, boundary, and external zones in the IEEE 118 bus system..... | 25 |
| Figure 2.10 Equivalent impedances errors for different numbers of data points ($N_{data}=7, 9, 11, 13, 15$) and different fluctuation levels..... | 26 |
| Figure 2.11 Equivalent voltage sources errors for different numbers of data points ($N_{data}=7, 9, 11, 13, 15$) and different fluctuation levels..... | 27 |
| Figure 2.12 Comparison of the equivalent impedances from 1000 random cases (stars) with actual values (dashed line) for eleven data points and 5% fluctuation level for case one..... | 28 |
| Figure 2.13 Comparison of the equivalent voltage sources magnitudes and phase angles from 1000 random cases (stars) with actual values (dashed line) for eleven data points and 5% fluctuation level for case one..... | 29 |
| Figure 2.14 Real and imaginary parts of the diagonal elements of Z_e from the proposed method (stars) compared with the actual values (dashed line) | 31 |
| Figure 2.15 Average error of non-zero equivalent impedance values and voltage sources with different numbers of data points ($N_{data}=7, 9, 11, 13, 15$) and different fluctuation levels | 32 |
| Figure 2.16 Comparison of the diagonal elements of the equivalent impedance matrix from 1000 random cases (stars) with actual values (dashed line) for eleven data points and 5% fluctuation level for case two..... | 33 |
| Figure 2.17 Comparison of the non-diagonal elements of the equivalent impedance matrix from 1000 random cases (stars) with actual values (dashed line) for eleven data points and 5% fluctuation level for case two | 34 |
| Figure 2.18 Comparison of the equivalent voltage sources from 1000 random cases (stars) with actual values (dashed line) for eleven data points and 5% fluctuation level | 35 |

| | |
|--|----|
| Figure 2.19 Accuracy of the reduced model for contingency analysis | 38 |
| Figure 3.1 Synthesizing the equivalent obtained by VF method | 42 |
| Figure 3.2 Structure of a single module used in [60]..... | 43 |
| Figure 3.3 Configuration of the equivalent circuit in [41]..... | 44 |
| Figure 3.4 Actual admittance data of a transformer | 45 |
| Figure 3.5 Flowchart of the proposed approach for single-port FDNE problem..... | 50 |
| Figure 3.6 The proposed equivalent circuit configuration for frequency responses with negative real parts | 51 |
| Figure 3.7 Sample magnitude and real part of a mutual admittance data | 52 |
| Figure 3.8 Admittance data of case one | 54 |
| Figure 3.9 Convergence rates of different methods for case one..... | 55 |
| Figure 3.10 The effect of increasing the number of branches on the objective function value for case one | 56 |
| Figure 3.11 Comparison of the actual admittance (solid line) with the admittance of the equivalent circuit (dashed-line) for case one..... | 57 |
| Figure 3.12 The effect of increasing the number of branches on the objective function value for case two | 58 |
| Figure 3.13 Convergence rate of the method for case two | 58 |
| Figure 3.14 Comparison of the actual admittance (solid line) with the admittance of the equivalent circuit (dashed-line) for case two | 59 |
| Figure 3.15 Convergence rate of the method for case three | 61 |
| Figure 3.16 Comparison of the actual value (solid line) with the value of the equivalent circuit (dashed-line) for the first three elements of the first column of the admittance matrix in case three | 62 |
| Figure 3.17 Comparison of the actual value (solid line) with the value of the equivalent circuit (dashed-line) for the last three elements of the first column of the admittance matrix in case three | 63 |
| Figure 3.18 Internal, boundary, and external systems | 65 |
| Figure 3.19 External system equivalent circuit configuration | 66 |
| Figure 3.20 Convergence rate of the method for case four..... | 67 |
| Figure 3.21 Comparison of the actual admittance (solid line) with the admittance of the equivalent circuit (dashed-line) for the first column of the admittance matrix in case four..... | 68 |
| Figure 3.22 Comparison of the actual admittance (solid line) with the admittance of the equivalent circuit (dashed-line) for the rest of the lower triangle elements of the admittance matrix in case four | 69 |
| Figure 3.23 Fault current of the full (solid lines) and reduced (dashed-lined) networks..... | 70 |
| Figure 3.24 The eigenvalues of the equivalent network admittance matrix in case four..... | 71 |

| | |
|---|-----|
| Figure 4.1 Transmission line parameter estimation methods | 75 |
| Figure 4.2 Measurement scheme used in [45]..... | 76 |
| Figure 4.3 Equivalent π -circuit model of a transmission line..... | 78 |
| Figure 4.4 The old (connected to the grid) and new (not connected to the grid) transmission lines | 79 |
| Figure 4.5 The circuit diagram showing the mutual couplings between phase A of the new line and other phase conductors | 81 |
| Figure 4.6 The measurement scheme for the proposed method | 88 |
| Figure 4.7 The diagram of the two parallel transmission line | 90 |
| Figure 4.8 Mean error for different numbers of data points for 3, 6, 9, and 15 connections of the new line | 93 |
| Figure 4.9 Comparison between the susceptances of the new line obtained by the method (blue stars) and the actual values (red dashed-line)..... | 95 |
| Figure 4.10 Comparison of the mutual susceptances between the two lines obtained by the method (blue stars) and the actual values (red dashed-line)..... | 96 |
| Figure 4.11 The resistance values obtained by the method (blue stars) and the actual values (red dashed-line) | 97 |
| Figure 4.12 The inductance values obtained by the method (blue stars) and the actual values (red dashed-line) | 98 |
| Figure 4.13 The mutual resistance values between the two lines obtained by the proposed method (blue stars) and the actual values (red dashed-line)..... | 99 |
| Figure 4.14 The mutual inductance values between the two lines obtained by the proposed method (blue stars) and the actual values (red dashed-line)..... | 100 |
| Figure A.1 Decoupled equivalent network configuration | 119 |
| TABLE A.1 Modified loads in IEEE 118 bus system..... | 120 |
| TABLE A.2 PV buses converted to PQ buses for case 2 of Chapter 2 | 121 |
| Figure C.1 The “Harmonic Impedance Component” in EMTDC/PSCAD | 126 |
| Figure C.2 The frequency steps given as the frequency input of the voltage source with external controls..... | 127 |
| Figure C.3 An external source connected to node 1 in an external system with three boundary nodes..... | 129 |
| Figure C.4 Equivalent model for case 4 of Chapter 3 | 130 |
| Figure C.5 The equivalent branch between nodes 33 and 34 | 131 |
| Figure C.6 The parallel RLCG units inside y23 modules of Figure C.5 | 132 |
| Figure C.7 The RLCG branch inside unit 1 of Figure C.6 | 133 |
| Figure D.1 Simulink model for chapter 4..... | 134 |

List of Acronyms

| | |
|--------------|--|
| SCADA | Supervisory Control And Data Acquisition |
| PMU | Phasor Measurement Unit |
| FDNE | Frequency Dependent Network Equivalent |
| REI | Radial, Equivalent, Independent |
| EMTP | Electro Magnetic Transients Program |
| ARMA | Autoregressive Moving Average |
| VF | Vector Fitting |
| GA | Genetic Algorithm |
| GP | Genetic Programming |
| SFLA | Shuffled Frog-Leaping Algorithm |
| PSO | Particle Swarm Optimization |
| DE | Differential Evolution |

List of Symbols

Chapter 2

| | |
|-------------------|--|
| \mathbf{Z}_e | Thevenin impedance matrix of the external system |
| E | Thevenin voltage source of the external system |
| V | The vector of boundary voltage phasors |
| I | The vector of boundary current phasors |
| N_{data} | Number of data points |
| $N_{boundary}$ | Number of boundary nodes |
| V_i^j | Voltage phasor of the i^{th} boundary node from the j^{th} measurement |
| I_i^j | Current phasor of the i^{th} boundary node from the j^{th} measurement |
| \mathbf{Z}_{in} | Thevenin impedance matrix of the internal system |
| U | Thevenin voltage source of the internal system |
| \mathbf{Z}_{eq} | Equivalent Thevenin impedance matrix |
| $Fluc_i$ | Fluctuation index of the i^{th} boundary line |
| $P_{i,old}$ | Active power transferred to the external system before the disturbance |
| $P_{i,new}$ | Active power transferred to the external system after the disturbance |
| $Q_{i,old}$ | Reactive power transferred to the external system before the disturbance |
| $Q_{i,new}$ | Reactive power transferred to the external system after the disturbance |

Chapter 3

| | |
|----------------|---|
| a_n | Poles of the rational function |
| c_n | Residues of the rational function |
| $P_{absorbed}$ | The absorbed power |
| N_F | The number of frequency samples |
| ω_f | Weighting factor |
| R_u | Resistance of the u^{th} branch |
| L_u | Inductance of the u^{th} branch |
| C_u | Capacitance of the u^{th} branch |

| | |
|------------------|---|
| G_u | Conductance of the u^{th} branch |
| Y^f_{actual} | Actual Admittance of the network at frequency f |
| \hat{Y}^f | Admittance of the equivalent network at frequency f |
| $\omega_{res,u}$ | Resonance angular frequency of the u^{th} branch |

Chapter 4

| | |
|------------|--|
| V_S | Voltage at the sending end of transmission line |
| I_S | Current at the sending end of transmission line |
| V_R | Voltage at the receiving end of transmission line |
| I_R | Current at the receiving end of transmission line |
| Z | Series impedance of the transmission line |
| B | Shunt susceptance of the transmission line |
| V_{a2}^S | Voltage phasor of phase-A of the new line at the sending end |
| V_{a2}^R | Voltage phasor of phase-A of the new line at the receiving end |
| V_{a1}^S | Voltage phasor of phase-A of the old line at the sending end |
| V_{a1}^R | Voltage phasor of phase-A of the old line at the receiving end |
| I_{a1} | Phasor of current passing through the coupled impedance of phase-A of the old line |
| I_{a2}^S | Current phasor of phase-A of the new line at the sending end |
| I_{a2}^R | Current phasor of phase-A of the new line at the receiving end |
| I_{a1}^S | Current phasor of phase-A of the old line at the sending end |
| I_{a1}^R | Current phasor of phase-A of the old line at the receiving end |

Appendix

| | |
|----------------|---|
| I_b | The vector of injected current phasors at boundary nodes |
| I_g | The vector of injected current phasors at external system PV nodes |
| V_b | The vector of voltage phasors at boundary nodes |
| V_g | The vector of voltage phasors at external system PV nodes |
| V_l | The vector of voltage phasors at external system load or terminal nodes |
| A_{inc} | Node incidence matrix |
| $Y_{bus_{eq}}$ | Equivalent node admittance matrix |
| F_i | The position of i^{th} frog in SFLA |

| | |
|-------------------------------------|--|
| WF^k | The position of the worst frog in memplex k |
| BF^k | The position of the best frog in memplex k |
| GF | The position of the best frog among the whole population |
| X_i | The position of i^{th} particle in PSO |
| V_i | The velocity of i^{th} particle in PSO |
| $Gbest$ | The best position among the whole particles |
| $Pbest$ | The best personal experience of each particle |
| ω^k | The weighting factor at iteration k |
| $Max\text{-}iter$ | Maximum number of iterations |
| X_i | The i^{th} parameter vector in DE |
| $V_{i,trial}$ | The trial vector for X_i |
| U_i | The new vector for X_i |
| $Y_k(f)$ | Admittance seen at bus k at frequency f |
| $I_k(f)$ | Current injected at bus k at frequency f |
| $V_k(f)$ | Voltage source magnitude connected to bus k at frequency f |

Chapter 1

Introduction

1.1 Background

Power system analysis requires adequate models for all pertinent system component including generators, transmission and distribution equipment and loads. Modeling the transmission lines is a fundamental requirement for many power system applications like fault detection, fault location and relay setting determination [1]. Transmission line parameters are also required for state estimator operation. Many power system studies like power flow analysis, transient and voltage stability analysis, economic load dispatch, and contingency analysis rely on the state estimator data. Inaccurate line parameters lead to inaccurate estimated states which will affect the accuracy of power system analysis [2] -[4].

As the power systems are becoming larger in size and with interconnecting neighboring systems together, representing all of the components in details is a very difficult and time consuming task. In addition, the detailed data of the neighboring systems might not be available. Therefore, when the focus is on a local power system interconnected with other neighboring power systems, power system equivalents are used to represent those neighboring systems. The local power system is represented in details while the neighboring systems are replaced with simpler equivalent networks [5]. The reduced model should be able to represent the external system's response to the disturbances originated at the internal system with good accuracy.

Typically, the system is divided into three parts as shown in Figure 1.1: a) internal system which is fully visible, b) buffer zone or inner external system which has visibility from supervisory control and data acquisition (SCADA), and c) outer external system which usually does not have SCADA measurements except for boundary buses [6].

Different equivalent models have been proposed for different power system studies. Fundamental frequency equivalents are used in system development studies (off-line) and on-line monitoring and control of the power systems [5]. Dynamic equivalents are used in studies involving different types of transient or dynamic phenomena and can be further divided into three categories [7]:

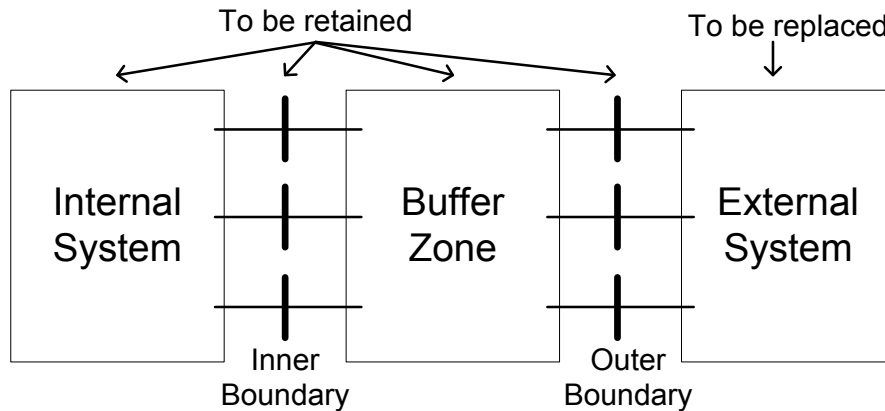


Figure 1.1 Different network areas

- High frequency equivalents which are suitable for high frequency transient studies including lightning and switching overvoltages and power electronic device effects on the system.
- Low-frequency equivalents which are used in studying low-frequency electromechanical oscillations like transient stability analysis.
- Wideband equivalents which are used in studies that involve sub-synchronous oscillations [7].

The focus of this research is on fundamental frequency equivalents, frequency dependent network equivalents, and transmission line electrical

parameters at the fundamental frequency. Application of these models in different power system studies is shown in Figure 1.2. It should be mentioned that system equivalents for transient stability analysis and frequency dependent transmission line model will not be addressed in this thesis.

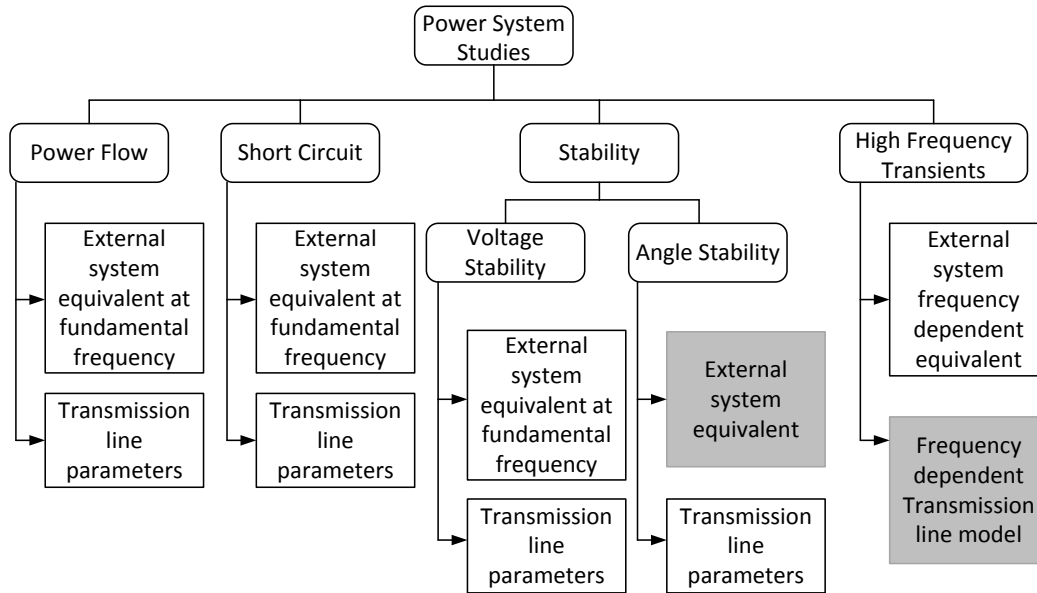


Figure 1.2 Applications of the models developed in this research

1.2 Thesis Objectives and Motivations

Objective 1: Online network equivalencing at fundamental frequency

Various methods have been proposed to derive the equivalent circuit. The majority of the methods are the model-based type [8]- [23]. These approaches need external system network and operating point data at different times and seasons. Such data is very hard to obtain by the owner of the study system in real time due to restructuring of the power industry. To address this major shortcoming, measurement-based approaches have been investigated in the past based on the measurement capability at that time. However, available measurement-based approaches have some drawbacks. For example, the method proposed in [6] uses an oversimplified model for the external system which

cannot model interactions of the various nodes through the actual external system. Other measurement-based methods proposed in [24]-[26] use boundary data from state estimator which needs a model of the external network for its operation. Therefore, these methods have some fundamental obstacles in their implementation.

According to the circuit theory, an external system seen at the boundary nodes can always be represented as a multi-port Thevenin circuit. Therefore, a natural approach to network equivalencing is to identify a series of Thevenin equivalent circuits online through the continuous stream of measurement data. A critical requirement for this measurement-based method is that the voltage and current measurements at the various boundary nodes must be synchronized. The availability of phasor measurement unit (PMU) data makes this approach feasible.

Motivated by the above considerations, the first objective of this research is to propose a method for estimating the multi-port Thevenin equivalent parameters of an external network by utilizing online measurements obtained from PMUs located at the boundary nodes.

Objective 2: Finding single-port and multi-port frequency dependent network equivalents

Several time-domain and frequency-domain approaches are available for finding frequency dependent network equivalent (FDNE). Generally, the time-domain approaches [27]- [31] are not preferred due to the fact the terminal characterization of the external network is usually done in frequency-domain. Vector fitting approaches [32]- [40] have shown good performances. However, they do not guarantee the optimality of the solution. In addition, they do not consider the passivity of the solution. Therefore, there is always a need to apply a passivity enforcement method which might further deteriorate the accuracy and could even fail in some cases [37].

An alternative approach is to directly optimize the parameters of a lumped parameter circuit using an optimization approach. The proposed methods have only considered the single-port FDNE [41], [42] where the equivalent model consists of a number of parallel branches with positive elements. The advantage is

that the passivity of the equivalent is guaranteed, but this model cannot be used for the multi-port case. The reason is that the non-diagonal elements of the admittance matrix could have negative real parts. Such frequency data cannot be fitted using only positive elements. Therefore, a new equivalent model is necessary.

In view of the mentioned shortcomings, the second objective of this thesis is to propose a more general method applicable for both single-port and multi-port problems which can find the equivalents with high accuracy while still considers the stability of the equivalent model during the optimization process.

Objective 3: Finding the electrical parameters of the transmission line

Before a new transmission line is put in service, it is always necessary to find the electrical parameters of this line for applications like protective relay settings. Rapid development of power systems has resulted in increased number of transmission lines sharing the same corridor. In this case, there is a strong electromagnetic coupling between the two lines. Classical calculation-based methods [43], [44] based on the line physical parameters cannot accurately estimate the electrical parameters due to several assumptions made during the calculation process. Therefore, the parameters have to be found through a measurement-based approach.

Conventional measurement-based approaches assume grounded tail end and apply an external voltage source at the head end to measure line impedance. Some methods based on analysing the frequency response of the line have also been proposed [45], [46]. One of the disadvantages of these methods for measuring parameters of parallel transmission lines is that they require an excitation source that is costly. In addition, the excitation source has to withstand a high voltage induced by the other transmission line which could reach more than ten kilo Volts. Therefore, high voltage equipment is required to implement these methods which increases the hardware cost.

Motivated by these considerations, the third objective of this thesis is to propose a new offline method for measuring the electrical parameters of parallel transmission lines. The method has to provide the three phase electrical

parameters or positive and zero sequence parameters. The method should not interrupt normal operation of the other transmission line which is already in service.

1.3 Thesis Outline

The thesis is organized as follows:

Chapter 2 presents the method for finding the multi-port Thevenin equivalent parameters of an external system. A literature review is done at the beginning of the chapter. Then multi-port Thevenin equivalent is explained and the equations representing it are given. Then, the measurement scheme to collect the required synchrophasors is explained. The method to find the equivalent parameters from the collected data is presented and some of the implementation issues are addressed and solutions are discussed. Finally, the method is implemented on two cases and the simulation results and conclusions are presented.

Chapter 3 presents the method for finding single-port and multi-port FDNEs of external networks. After the literature review, the single-port FDNE is addressed and the equivalent circuit model is illustrated. The problem is mathematically formulated and the proposed coding scheme is discussed. Three heuristic optimization methods are then implemented to find the parameters of the equivalent model and the results are compared to choose the best one. The multi-port problem is addressed next and the necessary modifications to the equivalent circuit to apply the method for the multi-port problems are discussed. Several cases are considered to fully evaluate the performance of the proposed methods. Finally, the discussions and conclusions are presented.

Chapter 4 presents a method for measuring the transmission line electrical parameters. The chapter starts with a literature survey. Then the line model is presented and the case of parallel transmission line is discussed. The problem is mathematically formulated and the solution is presented. Measurement scheme to collect the required data is presented and a case study is conducted to evaluate the performance of the method. Finally, the results are analyzed and the chapter is concluded.

Chapter 1: Introduction

Finally, Chapter 5 concludes the thesis and summarizes the contributions. The suggestions for future work are also presented in this chapter.

Chapter 2

External System Equivalent at Fundamental Frequency

In recent years, due to restructuring of the power industry, it is not possible to have detailed information of the whole power system. A natural way to deal with this situation is to model the study system in detail and represent the neighboring external systems with their reduced order equivalents. Thevenin equivalents have been widely used in power system studies for over a century due to their ability to reproduce the behaviour of a system without the need for modeling the system in details [64]- [68].

This chapter proposes a new measurement-based approach to find the multi-port external system Thevenin equivalent parameters. The equivalent is a reduction of the power flow model and can be used for online network applications such as contingency analysis and voltage stability assessment. The external system equivalent is determined by applying the least-squares method to measurements directly obtained at the boundary buses. In addition, a method to detect the changes in the external system from the measurement data collected at the boundary nodes is proposed to make sure that the external system has remained constant during the identification period. The overall computational burden of the method is low which makes the method appropriate to work continuously for creating real-time equivalent model of the external system.

2.1 Literature Review

The most important power system equivalents at the fundamental frequency are categorized in Figure 2.1. The methods can be broadly divided into model-based and measurement-based equivalents. The majority of the methods are model-based which generally require the network data and operating point data of the external system. Equivalent model is then created by simplifying the model of the external system.

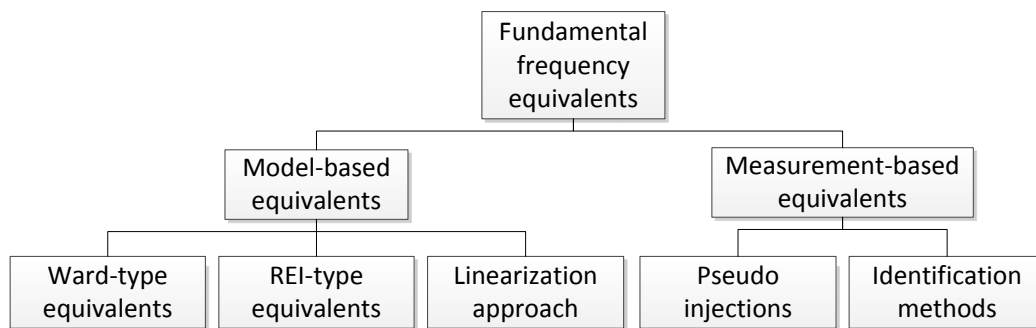


Figure 2.1 Different fundamental frequency network equivalents

One of the most well-known model-based equivalents proposed in the literature is Ward equivalent introduced by J. B. Ward in 1949 [8]. The standard version is Ward admittance method in which all the generations and loads of the external network are converted to shunt admittances. As a result, the equivalent will be a passive network without any injections as shown in Figure 2.2. This approach leads to unusual admittance values which seriously deteriorate power flow convergence [9].

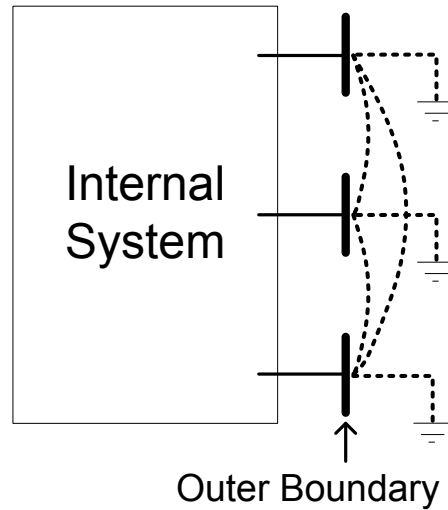


Figure 2.2 The equivalent model in Ward admittance method

The more preferred Ward equivalent is the Ward injection method in which the generations and loads are represented by constant current injections. The external system is modeled by equivalent generator or load at each tie-line terminal and an equivalent meshed network interconnecting these terminals as shown in Figure 2.3.

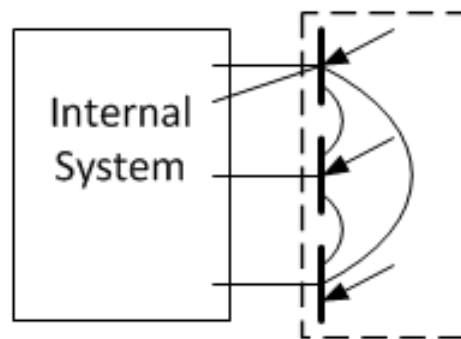


Figure 2.3 The equivalent model in Ward injection method

Failing to appropriately represent the external system reactive power response and boundary-bus type designation problem are some of the drawbacks of these methods. To overcome these problems, several Ward-type equivalents have been proposed [10]- [14].

Another well-known model-based equivalent is REI (Radial, Equivalent, Independent) equivalent introduced by P. Dima in 1970's [15]. In this method, external power system buses are grouped to create REI buses as shown in Figure 2.4.

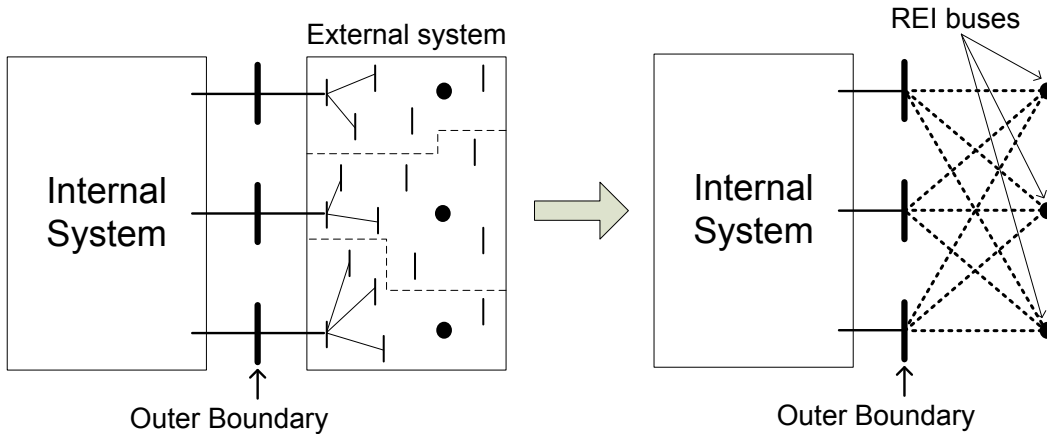


Figure 2.4 The equivalent model in REI method

One important issue regarding REI equivalent is the grouping problem in which the number of equivalent REI buses and the way the real buses are associated to each of them, is determined. The grouping procedure can highly influence the accuracy of the REI equivalent. Some grouping approaches have been proposed in [5], [16], [17]. Some of the drawbacks of this method include difficulties in updating the equivalent in online applications and abnormal nodal voltages. Several approaches have been proposed to solve these problems [18]-[20].

Linearization methods are another well-known model-based approach. In these methods the equivalents are linearization of the external system power flow equations. Various linearization methods have been proposed in the literature [21]- [23]. Accuracy of these methods are compared in [9]. The main drawback of these methods is the fact that the equivalent is an equation, not a network. Therefore, it can only be accommodated by a specially modified power flow model and cannot be incorporated into standard power flow programs.

Chapter 2: External System Equivalent at Fundamental Frequency

As mentioned before, model-based equivalents need the external network data. The main problem encountered by this type of methods is the need for (approximate) external system model at different times and seasons. Such a model is very hard to obtain by the owner of the study system due to restructuring of the power industry.

In recent years, power systems experienced significant expansions in measurement and communication capabilities. Various types of information can be collected through direct or indirect measurements. This has created good opportunities to contemplate measurement-based approaches for creating equivalent circuit models of the external systems.

In fact, measurement-based approaches have been investigated in the past based on the measurement capability at that time. Reference [6] proposed to use the SCADA data of the boundary nodes to build time-varying equivalent loads (or generators) connected to the nodes as shown in Figure 2.5. This method is straightforward, but the external network is oversimplified and cannot fully represent the external system. For example, the interactions of the various nodes through the actual external system cannot be modeled by this method.

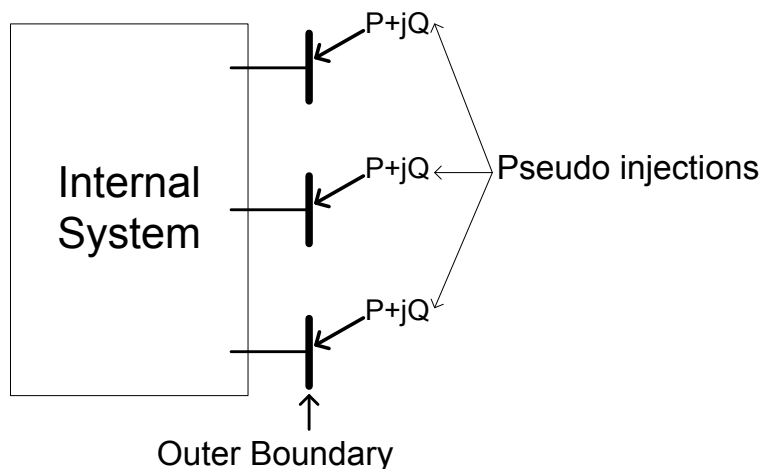


Figure 2.5 The equivalent model in pseudo-injection method

References [24]- [26] proposed to identify the equivalent system through a series of measurements. The external network model is typically fictitious admittances connected between the boundary nodes and ground. These methods need the voltage and current states of the boundary buses calculated from the state estimator. But the state estimator needs a model of the external network model for its operation. Therefore, these methods have some fundamental obstacles in practical implementation.

In view of the drawbacks and limitations of the mentioned methods, this chapter proposes a new measurement-based approach to find the multi-port Thevenin equivalent parameters of an external system. The only data used for identifying the equivalent parameters is measurement data directly obtained at the boundary buses. In addition, since it is necessary to ensure that external system has remained constant during the identification period, a method to detect the changes in the external system is also proposed.

2.2 Proposed Method

According to the circuit theory, an external system seen at the boundary nodes can always be represented as a multiport Thevenin circuit. Therefore, a natural approach to network equivalencing is to identify a series of Thevenin equivalent circuits online through the continuous stream of measurement data. A critical requirement for this measurement-based method is that the voltage and current measurements at the various boundary nodes must be synchronized. The availability of PMU data has made this line of thinking feasible. PMUs have attracted much attention from both researchers and industry in recent years. These devices are expected to be widely installed in power systems. Potential applications of synchronized phasors collected by PMUs have been widely investigated in the literature [69]- [76].

Motivated by the above considerations, this thesis proposes a new measurement-based approach to find the external system Thevenin equivalent. The equivalent is a reduction of the power flow model and can be used for online network applications such as contingency analysis and voltage stability

assessment. The external system equivalent is determined by applying the least-squares method to measurements directly obtained at the boundary buses.

The proposed methodology to find the equivalent external system is presented in this section. First, the equivalent circuit model is introduced and then the measurement scheme to find the unknown circuit parameters is discussed. The mathematical formulas to find the unknown parameters are derived at the end of this section.

2.2.1 Equivalent Model

The idea of a single-port Thevenin equivalent can be extended a multi-port Thevenin equivalent represented by [77]

$$\begin{bmatrix} V_1 \\ V_2 \\ V_3 \end{bmatrix} = \begin{bmatrix} Z_{e,11} & Z_{e,12} & Z_{e,13} \\ Z_{e,21} & Z_{e,22} & Z_{e,23} \\ Z_{e,31} & Z_{e,32} & Z_{e,33} \end{bmatrix} \begin{bmatrix} I_1 \\ I_2 \\ I_3 \end{bmatrix} + \begin{bmatrix} E_1 \\ E_2 \\ E_3 \end{bmatrix} \quad (2.1)$$

Or,

$$V = Z_e I + E \quad (2.2)$$

where V and I are boundary voltage and current phasors, respectively. Also Z_e and E are equivalent Thevenin impedances and voltage sources, respectively. The general circuit model for representing (2.1) is shown in Figure 2.6.

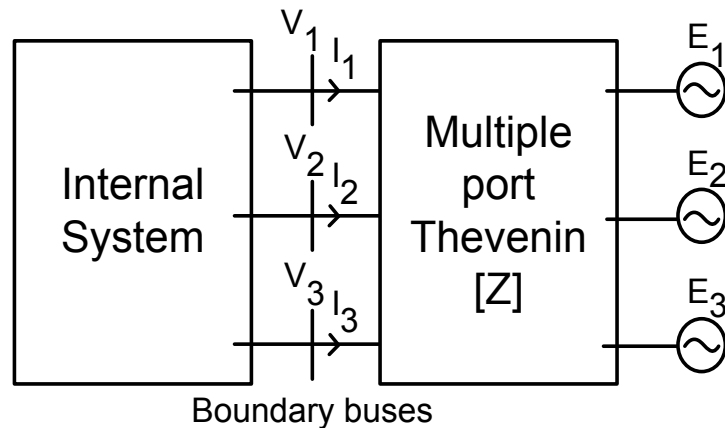


Figure 2.6 Multi-port Thevenin equivalent of the external system

2.2.2 Measurement Scheme

The external system model is determined from measurements directly obtained at the boundary terminals. Voltage and current phasors at the boundary terminals are recorded to find the equivalent circuit parameters as shown in Figure 2.7.

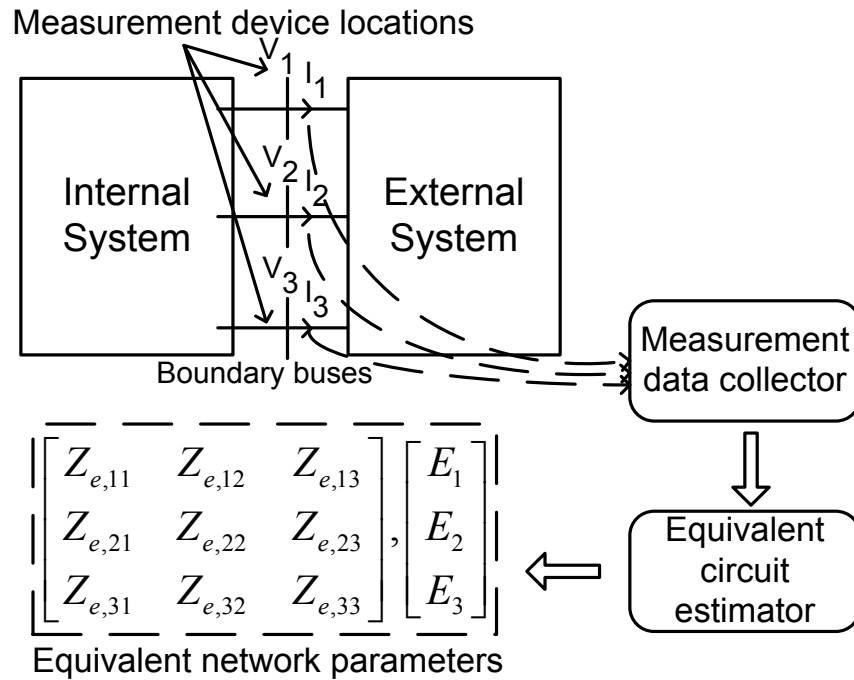


Figure 2.7 Measurement scheme

Due to the multiport coupling characteristics of the equivalent circuit, synchronized measurements of voltage and current phasors are required for circuit parameters estimation. This requirement can be fulfilled by using the PMUs located at the boundary buses. These units measure the bus voltages and the currents flowing into the external system.

2.2.3 Finding Equivalent Parameters

The unknowns of the problem are the complex impedance matrix Z_e and complex voltage source matrix E . As an example, for a problem with three boundary terminals, Z_e is a three by three matrix with eighteen unknowns (real

measurement errors, and fluctuation level. These issues are discussed in the following sub-sections.

2.3.1 Disturbance Side

In deriving the previous formulas, it is assumed that the external system remains constant. This assumption is only true when all of the disturbances are originated outside the external system. A disturbance coming from the external system means that the external system has changed during the identification process and the collected data cannot be used to find the equivalent parameters anymore. Therefore, a criterion is necessary to find the origin of the disturbances and determine which disturbances can be used to find the correct equivalent parameters.

To derive the mathematical basis of the proposed criterion, Thevenin equivalents are considered for both the internal and external systems as shown in Figure 2.8. The following equations could be written for this system.

$$V = Z_e I + E \quad (2.7)$$

$$V = -Z_{in} I + U \quad (2.8)$$

where Z_{in} and U are Thevenin equivalent impedance and voltage source matrices of the internal system.

Using the above equations, boundary voltages and currents could be expressed by

$$V = (Z_e^{-1} + Z_{in}^{-1})^{-1} (Z_e^{-1} E + Z_{in}^{-1} U) \quad (2.9)$$

$$I = (Z_{in} + Z_e)^{-1} (U - E) \quad (2.10)$$

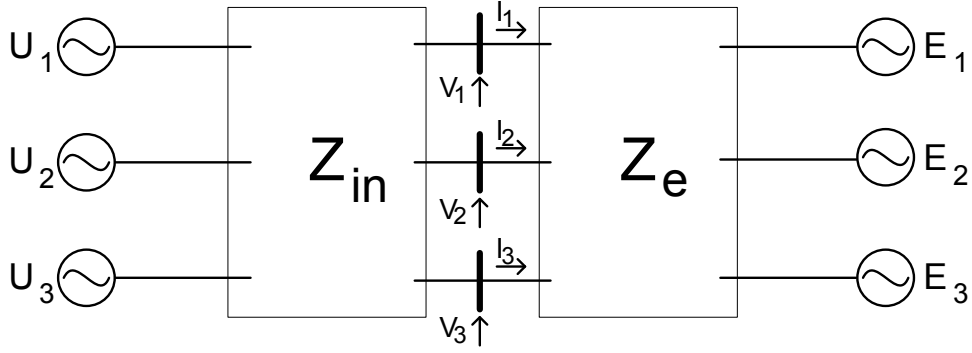


Figure 2.8 Internal and external system representations

Disturbances in both internal and external systems are applied to find the equivalent impedance matrix. For each disturbance, boundary voltages and currents are found using (2.9) and (2.10) and are recorded as a data point. After collecting enough data points (i.e. $N_{boundary}+1$), the equivalent impedances and voltage sources are found using (2.4)- (2.6).

For instance, a three port system is considered and different numbers of disturbances from the external system are considered. In the first case, it is assumed that U_1 , U_2 , and E_3 experience three independent changes of ΔU_1 , ΔU_2 , and ΔE_3 , respectively. The initial boundary phasors are

$$V = (Z_e^{-1} + Z_{in}^{-1})^{-1} (Z_e^{-1} [E_1, E_2, E_3]^T + Z_{in}^{-1} [U_1, U_2, U_3]^T) \quad (2.11)$$

$$I = (Z_{in} + Z_e)^{-1} ([U_1, U_2, U_3]^T - [E_1, E_2, E_3]^T) \quad (2.12)$$

The boundary phasors after applying the first disturbance are

$$V = (Z_e^{-1} + Z_{in}^{-1})^{-1} (Z_e^{-1} [E_1, E_2, E_3]^T + Z_{in}^{-1} [U_1(1+\Delta U_1), U_2, U_3]^T) \quad (2.13)$$

$$I = (Z_{in} + Z_e)^{-1} ([U_1(1+\Delta U_1), U_2, U_3]^T - [E_1, E_2, E_3]^T) \quad (2.14)$$

The boundary phasors after applying the second disturbance are

$$V = (Z_e^{-1} + Z_{in}^{-1})^{-1} (Z_e^{-1} [E_1, E_2, E_3]^T + Z_{in}^{-1} [U_1, U_2(1+\Delta U_2), U_3]^T) \quad (2.15)$$

Chapter 2: External System Equivalent at Fundamental Frequency

$$I = (Z_{in} + Z_e)^{-1}([U_1, U_2(1 + \Delta U_2), U_3]^T - [E_1, E_2, E_3]^T) \quad (2.16)$$

Finally, the boundary phasors after applying the third disturbance are

$$V = (Z_e^{-1} + Z_{in}^{-1})^{-1}(Z_e^{-1}[E_1, E_2, E_3(1 + \Delta E_3)]^T + Z_{in}^{-1}[U_1, U_2, U_3]^T) \quad (2.17)$$

$$I = (Z_{in} + Z_e)^{-1}([U_1, U_2, U_3]^T - [E_1, E_2, E_3(1 + \Delta E_3)]^T) \quad (2.18)$$

By substituting the boundary phasors obtained from (2.11)-(2.18) in (2.4), the following equation is derived for equivalent impedance matrix.

$$Z_{eq} = \begin{bmatrix} Z_{e,11} & Z_{e,12} & Z_{e,13} \\ Z_{e,21} & Z_{e,22} & Z_{e,23} \\ -Z_{in,31} & -Z_{in,32} & -Z_{in,33} \end{bmatrix} \quad (2.19)$$

In the second case, two disturbances are considered in the external system. It is assumed that U_1 , E_2 , and E_3 experience three independent changes of ΔU_1 , ΔE_2 , and ΔE_3 , respectively. Similar to the previous case, the following equation is derived by applying the mentioned disturbances and using equations (2.4), (2.9), and (2.10).

$$Z_{eq} = \begin{bmatrix} Z_{e,11} & Z_{e,12} & Z_{e,13} \\ -Z_{in,21} & -Z_{in,22} & -Z_{in,23} \\ -Z_{in,31} & -Z_{in,32} & -Z_{in,33} \end{bmatrix} \quad (2.20)$$

Finally, in the third case, all of the disturbances are applied in the external system (ΔE_1 , ΔE_2 , and ΔE_3). The following equation is derived by applying the mentioned disturbances.

$$Z_{eq} = \begin{bmatrix} -Z_{in,11} & -Z_{in,12} & -Z_{in,13} \\ -Z_{in,21} & -Z_{in,22} & -Z_{in,23} \\ -Z_{in,31} & -Z_{in,32} & -Z_{in,33} \end{bmatrix} \quad (2.21)$$

As it can be seen in equations (2.19)- (2.21), when at least one of the disturbances is from the external system, a negative value appears in at least one of the diagonal elements. Considering the fact that diagonal values represent self-

impedances, a negative value could be a good sign that the disturbance is coming from the wrong side, i.e. the external system. Therefore, each time a new data point is recorded, the equivalencing method is applied using this new data point and the previous $N_{boundary}$ data points. Then the real and imaginary parts of the diagonal elements of the diagonal elements of the equivalent impedance matrix are examined. If negative values appear in these elements, it indicates that the external system has not remained unchanged.

2.3.2 Measurement Error

In theory, $N_{boundary}+1$ data points would be enough to find the equivalent circuit parameters using (2.4). However, practically this does not give accurate results due to measurement errors and noise. To improve the accuracy of the model, additional data points could be utilized to have more equations. In this case, least-squares method is applied to find the unknown parameters.

Suppose that N data points are available. Each data point gives $N_{boundary}$ complex equations. For example, for three boundary nodes, the following equations can be written for the first data point.

$$I_1^1 Z_{e,11} + I_2^1 Z_{e,12} + I_3^1 Z_{e,13} + E_1 = V_1^1 \quad (2.22)$$

$$I_1^1 Z_{e,21} + I_2^1 Z_{e,22} + I_3^1 Z_{e,23} + E_2 = V_2^1 \quad (2.23)$$

$$I_1^1 Z_{e,31} + I_2^1 Z_{e,32} + I_3^1 Z_{e,33} + E_3 = V_3^1 \quad (2.24)$$

Or,

$$\begin{bmatrix} I_1^1 & I_2^1 & I_3^1 & 0 & 0 & 0 & 0 & 0 & 0 & 1 & 0 & 0 \\ 0 & 0 & 0 & I_1^1 & I_2^1 & I_3^1 & 0 & 0 & 0 & 0 & 1 & 0 \\ 0 & 0 & 0 & 0 & 0 & 0 & I_1^1 & I_2^1 & I_3^1 & 0 & 0 & 1 \end{bmatrix} \begin{bmatrix} Z_{e,11} \\ Z_{e,12} \\ \vdots \\ Z_{e,33} \\ E_1 \\ E_2 \\ E_3 \end{bmatrix} = \begin{bmatrix} V_1^1 \\ V_2^1 \\ V_3^1 \end{bmatrix} \quad (2.25)$$

Writing similar equations for the other data points and combining all of the equations gives

system before and after the disturbance, respectively. A new data point is recorded when the fluctuation index of at least one of the lines is equal to or greater than a predefined fluctuation level.

The fluctuation level should be high enough to give a good accuracy when determining the equivalent system parameters and to make it possible to detect the direction of the disturbance. On the other hand, the fluctuation level should be low enough to detect considerable changes in the external system to ensure that the external system has remained fairly constant during the identification process. The reason behind ignoring small variations in the external system is that the model accuracy requirements are only applied to the internal system. Therefore, the goal is to find an approximate external system model which gives adequate accuracy for studies like contingency analysis and voltage stability analysis performed in the internal system.

In addition, there is a boundary zone between the internal and external systems. As a result, the external system has less effect on the internal system. Therefore, the fluctuation index must be adjusted to detect only large variations in the external system, since small variations do not have noticeable effects on the internal system. The desired fluctuation index should be determined according to utility's accuracy requirements.

2.3.4 Implementation Summary

Disturbances frequently happen in both internal and external systems and new data points are continuously being recorded. The method is implemented according to the following steps:

Step 1) Collect $N_{boundary}+1$ data points.

Step 2) Detect the direction of the disturbances using (2.4)- (2.6).

Step 3) If all of the disturbances are from the internal system, go to Step 5. Otherwise, continue to Step 4.

Step 4) Replace the oldest data point by a new one and go to Step 2.

Step 5) Mark the disturbances as internal disturbances and wait for the next disturbance.

Step 6) Once a new disturbance is detected, use the new data point along with the most recent $N_{boundary}$ data points to determine the disturbance direction using (2.4)- (2.6).

Step 7) If the new disturbance is from the external system, discard the previously recorded data points and start over from Step 1. Otherwise, continue to Step 8.

Step 8) Add the last disturbance to the internal disturbance list and calculate Z_e and E from (2.26)- (2.28) using least-squares method.

Step 9) When a new disturbance is detected, use the newest $N_{boundary}+1$ data points to detect the direction of the disturbance using (2.4)- (2.6).

Step 10) If the disturbance is from the external system, discard the previously recorded data points and go to Step 1. Otherwise, use the new data point along with the previous ones to calculate the equivalent parameters with higher accuracy using (2.26)- (2.28) and go to Step 9.

2.4 Case Studies

The IEEE 118-bus system is considered for simulation studies. The internal, buffer, and external areas are defined as shown in Figure 2.9. The system is simulated in PSS/E and the method is implemented in MATLAB.

It is assumed that PMUs are placed at the boundary nodes 24, 43, 49, and 65 to measure bus voltages and currents flowing into the external system. To account for the measurement errors, a random noise is added to the recorded phasors to create 1% total vector error according to the standard IEEE C37.118.1 [79]. This data is considered to be real measurement data collected by field PMUs at the boundary nodes.

First, the original IEEE 118 bus case is simulated and a sensitivity study is conducted to analyze the effect of fluctuation index and number of data points on the performance of the method. The impedance values obtained from 1000 random cases are then compared with the actual values obtained by the method presented in Appendix A. The performance of the disturbance side detection method is also evaluated in this case.

To further investigate the performance of the method, a second case is created by modifying IEEE 118 bus system. The modifications are presented in Appendix A. The performance of the method is evaluated for different fluctuation indices and numbers of data points. Then, the external system is replaced with the equivalent circuit with the method presented in Appendix A and contingency analysis results of the original and reduced systems are compared.

2.4.1 Case 1: IEEE 118 Bus System

As explained before, to deal with measurement errors it is necessary to use additional data points. A sensitivity analysis is conducted to analyze the performance of the method with different numbers of data points and fluctuation levels. 1000 random cases are considered for each fluctuation level and number of data points. For creating the random cases, voltage sags with random magnitudes are simulated in random locations in the internal system and buffer zone and the boundary voltages and currents are recorded. For each case, N_{data} of these recorded data points with the desired fluctuation levels are selected to find the external system equivalent parameters. The percentage errors of the equivalent impedances and voltage sources are shown in Figure 2.10 and Figure 2.11, respectively.

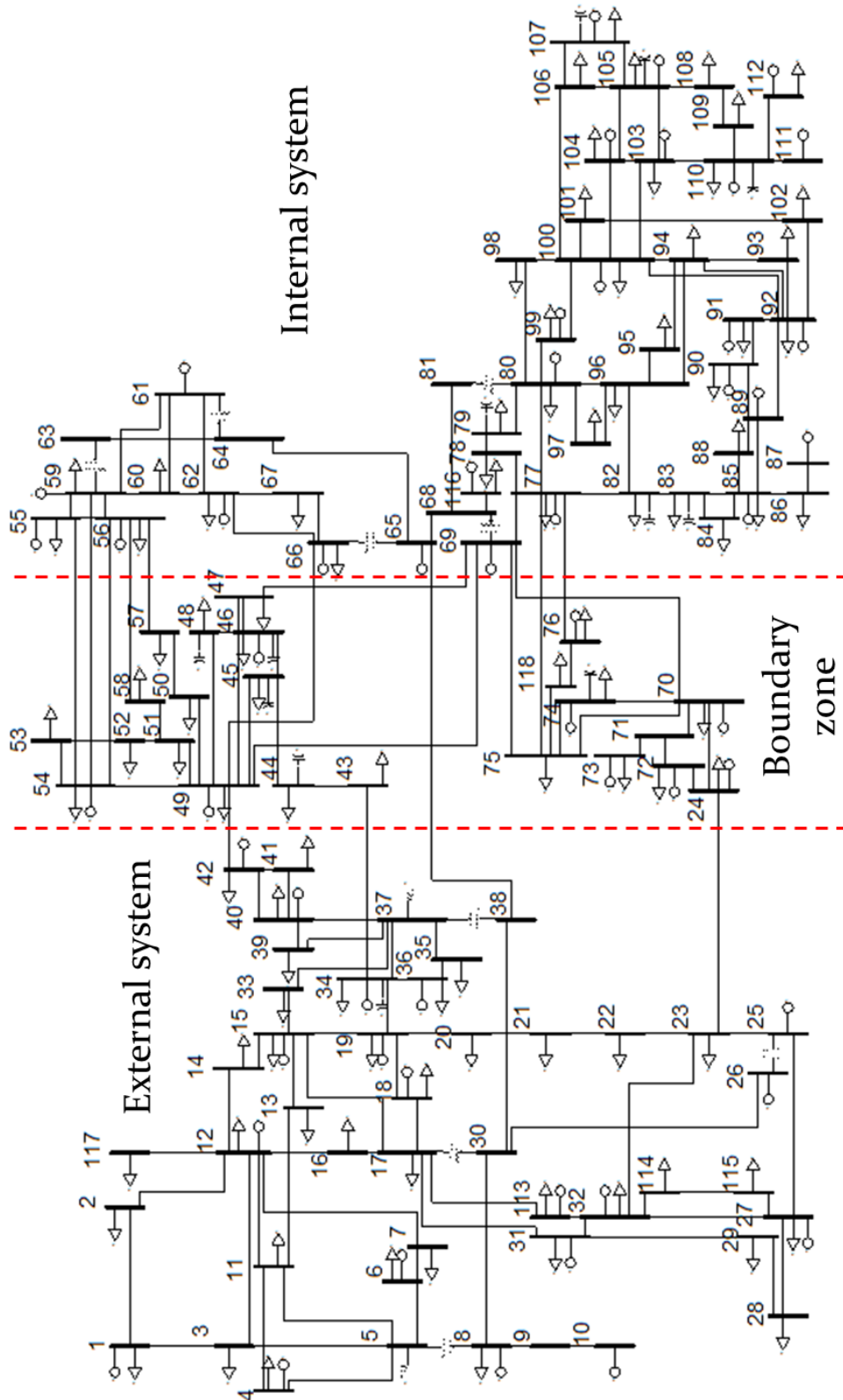


Figure 2.9 Internal, boundary, and external zones in the IEEE 118 bus system

Case 1- Sensitivity Study

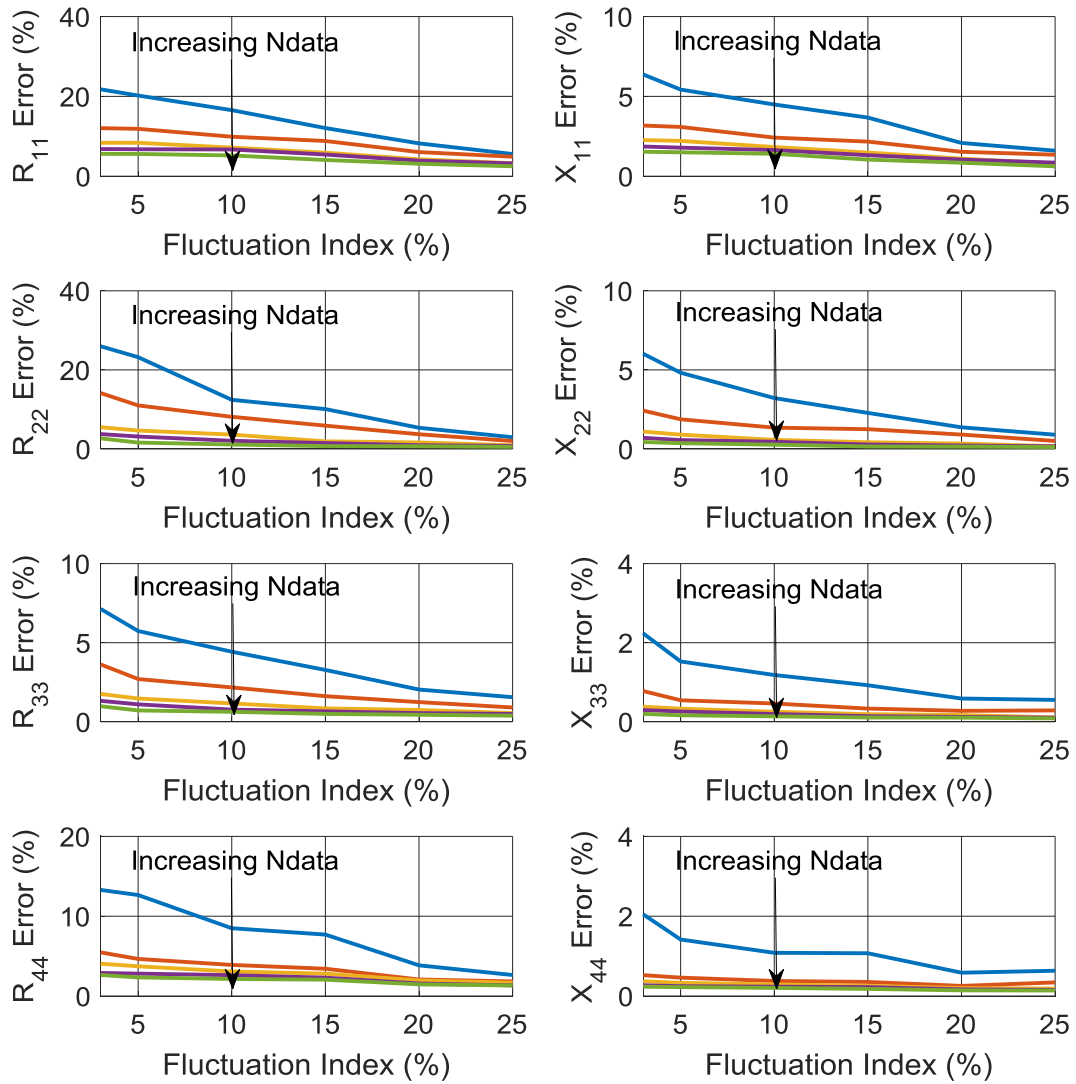


Figure 2.10 Equivalent impedances errors for different numbers of data points ($N_{data}=7, 9, 11, 13, 15$) and different fluctuation levels

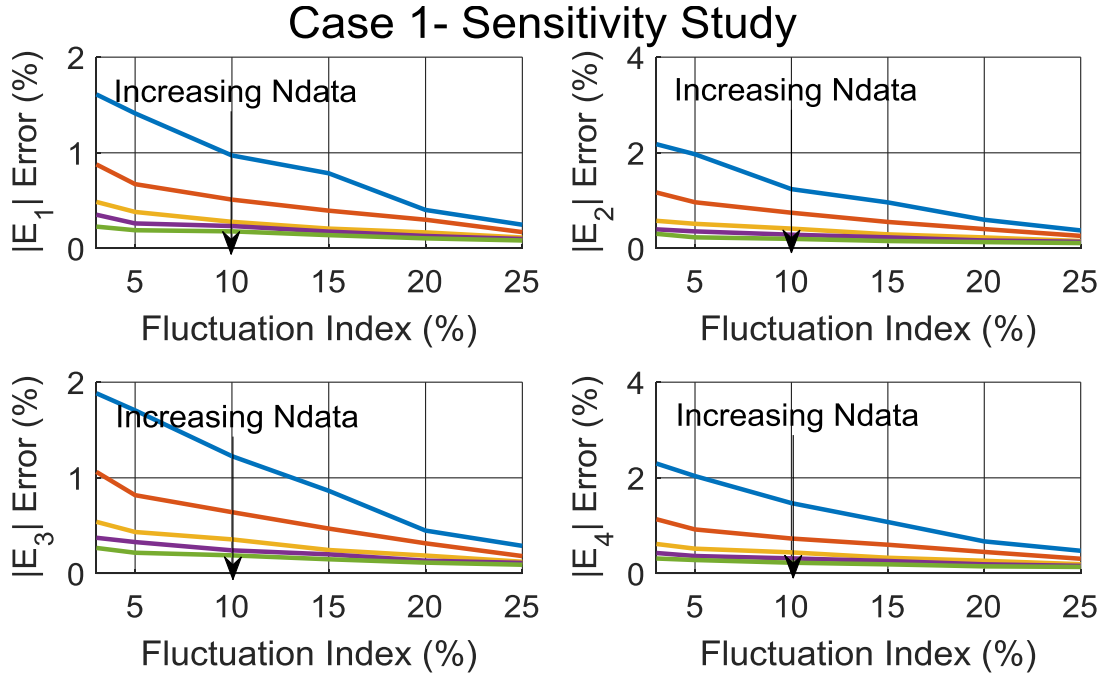


Figure 2.11 Equivalent voltage sources errors for different numbers of data points ($N_{data}=7, 9, 11, 13, 15$) and different fluctuation levels

As it can be seen in Figure 2.10 and Figure 2.11, having more data points and higher fluctuation level improves the accuracy of the results. But, having too many data points does not noticeably improve the accuracy. Also, if enough data points are available, fluctuation index does not have a significant impact on the accuracy. Considering these points, eleven data points with 5% fluctuation level is considered and the results of each of the 1000 cases for these parameters are compared with the actual values in Figure 2.12 and Figure 2.13. As it can be seen, the estimated parameters are close to the actual values.

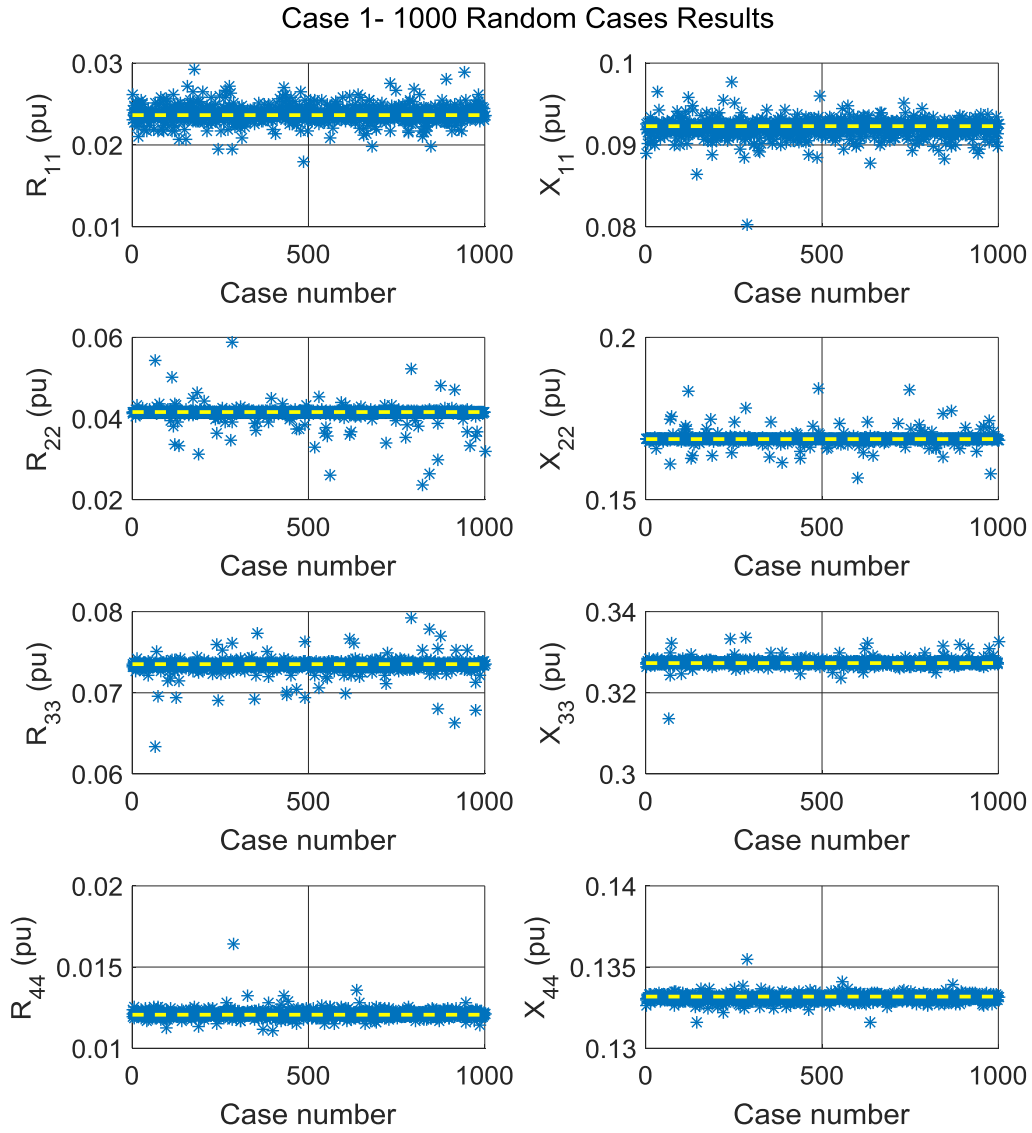


Figure 2.12 Comparison of the equivalent impedances from 1000 random cases (stars) with actual values (dashed line) for eleven data points and 5% fluctuation level for case one

Case 1- 1000 Random Cases Results

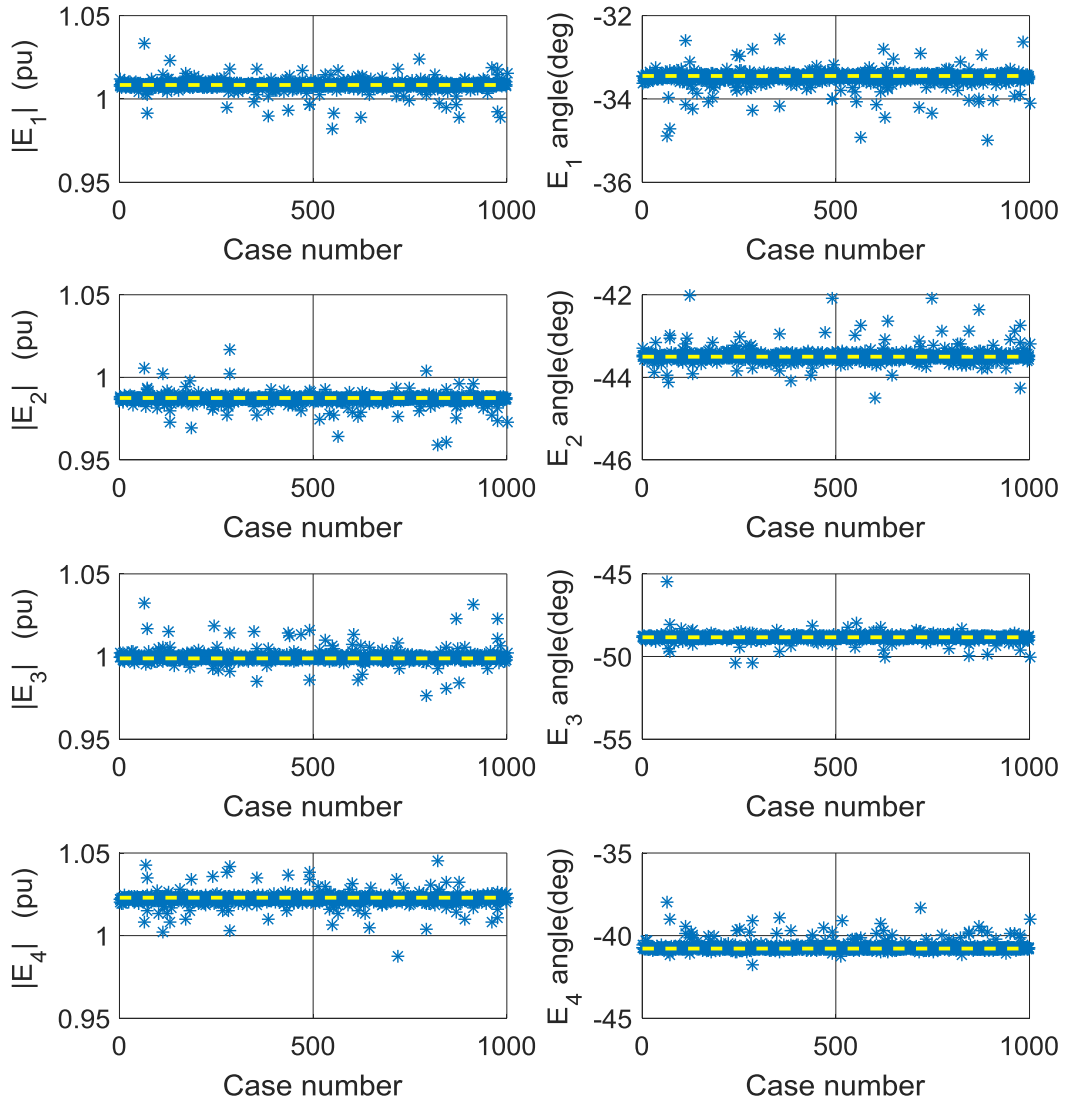


Figure 2.13 Comparison of the equivalent voltage sources magnitudes and phase angles from 1000 random cases (stars) with actual values (dashed line) for eleven data points and 5% fluctuation level for case one

To summarize the results shown in Figure 2.12 and Figure 2.13, the accurate value, mean value, and standard deviation of the parameters are presented in TABLE 2.1.

TABLE 2.1 The results obtained by the proposed method for case one

| Parameter | Accurate value | Mean value | Standard deviation |
|-----------------|----------------|------------|--------------------|
| R_{11} (pu) | 2.3645E-2 | 2.3763E-2 | 9.4056E-4 |
| R_{22} (pu) | 4.1595E-2 | 4.1457E-2 | 1.6773E-3 |
| R_{33} (pu) | 7.3528E-2 | 7.3394E-2 | 7.8012E-4 |
| R_{44} (pu) | 1.2063E-2 | 1.2097E-2 | 2.2922E-4 |
| X_{11} (pu) | 9.2299E-2 | 9.2072E-2 | 9.8144E-4 |
| X_{22} (pu) | 1.6866E-1 | 1.6870E-1 | 1.4703E-3 |
| X_{33} (pu) | 3.2732E-1 | 3.2740E-1 | 7.9477E-4 |
| X_{44} (pu) | 1.3318E-1 | 1.3310E-1 | 2.0031E-4 |
| $ E_1 $ (pu) | 1.0084 | 1.0083 | 0.0029 |
| $ E_2 $ (pu) | 0.9875 | 0.9870 | 0.0028 |
| $ E_3 $ (pu) | 0.9989 | 0.9995 | 0.0032 |
| $ E_4 $ (pu) | 1.0230 | 1.0223 | 0.0032 |
| E_1 ang (deg) | -33.4487 | -33.4850 | 0.1620 |
| E_2 ang (deg) | -43.5002 | -43.4886 | 0.1439 |
| E_3 ang (deg) | -48.8368 | -48.8408 | 0.1920 |
| E_4 ang (deg) | -40.7851 | -40.7144 | 0.2561 |

To analyze the performance of the disturbance direction detection method with 5% fluctuation level, 250 random cases are created. For each case, four disturbances are used to find the equivalent impedance matrix using (2.4)- (2.6). Voltage sags and generation changes are the disturbance types used for these cases. The equivalent impedance matrices are found and compared with the actual values in Figure 2.14.

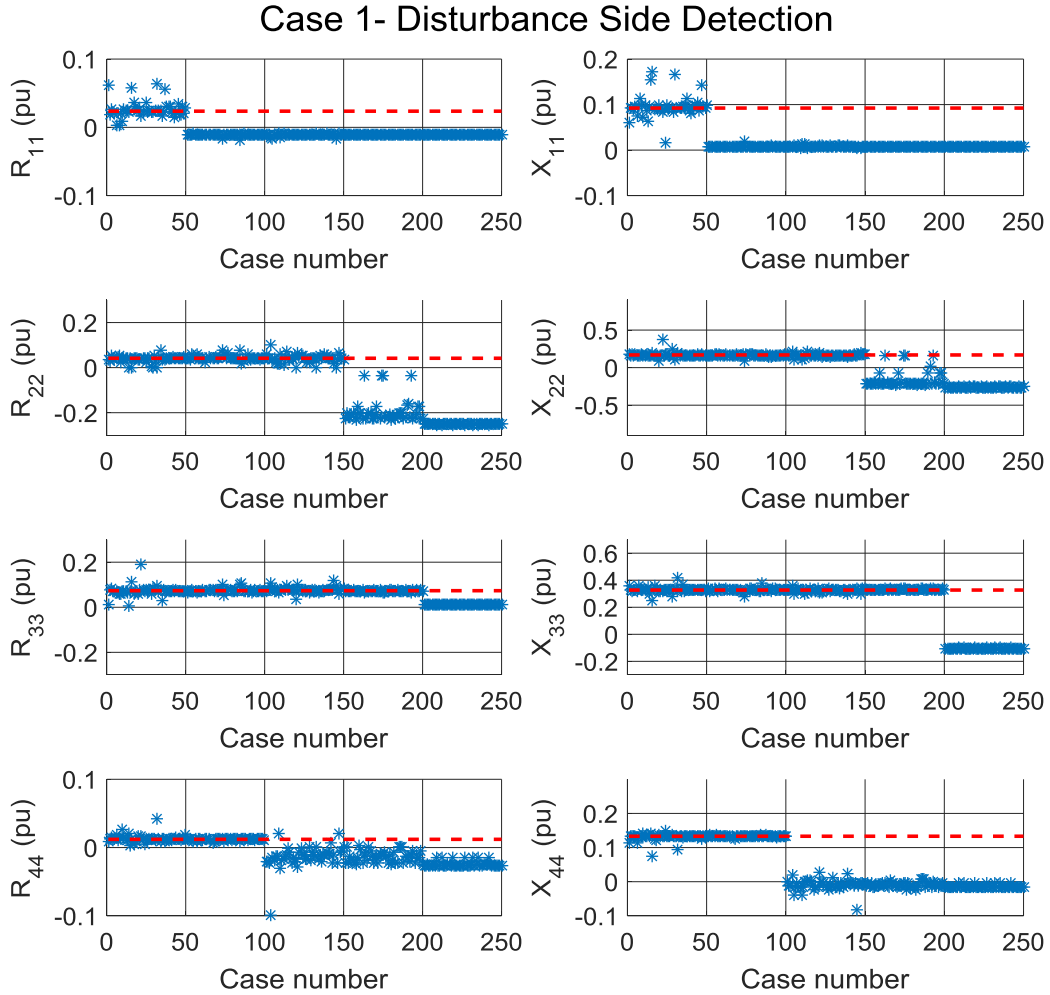


Figure 2.14 Real and imaginary parts of the diagonal elements of Z_e from the proposed method (stars) compared with the actual values (dashed line)

As it can be seen in Figure 2.14, in cases 1-50 all disturbances are from the internal system and all of the values are positive. In cases 51-100, a random disturbance occurs near bus 23 in the external system while three other disturbances occur in the internal system. R_{11} and X_{11} are near zero. Considering that node 24 is a PV bus, these zero values reveal that the disturbance is occurred in the external system. In cases 101-150, two random disturbances occur near buses 23 and 38 in the external system while two other disturbances occur in the internal system. R_{11} , X_{11} , R_{44} , and X_{44} are near zero (node 49 is also a PV bus). In cases 151-200, three disturbances occur near buses 23, 38, and 34 in the external

system while the fourth one occurs in the internal system. R_{11} , X_{11} , R_{44} , and X_{44} , are near zero while R_{22} and X_{22} are negative. Therefore, in all cases it is possible to detect that the external system has not remained constant. Finally, in cases 201-250, all of the values are either negative or close to zero which shows that all of the disturbances are coming from the external system.

2.4.2 Case 2: Modified IEEE 118 Bus System

To further evaluate the performance of the proposed method, IEEE 118 bus system is modified and considered as the second case. The external system is replaced by an equivalent found by the method and the contingency analysis results are compared. First a sensitivity analysis is conducted to study the performance of the method in this case. Similar to the previous case, 1000 random cases are created for each fluctuation level and number of data points. To summarize the results, the average error is shown in Figure 2.15. It should be mentioned that when mutual impedance between two nodes is close to zero, a small error leads to a huge percentage error. Therefore, small impedances are not considered in calculating the average percentage error.

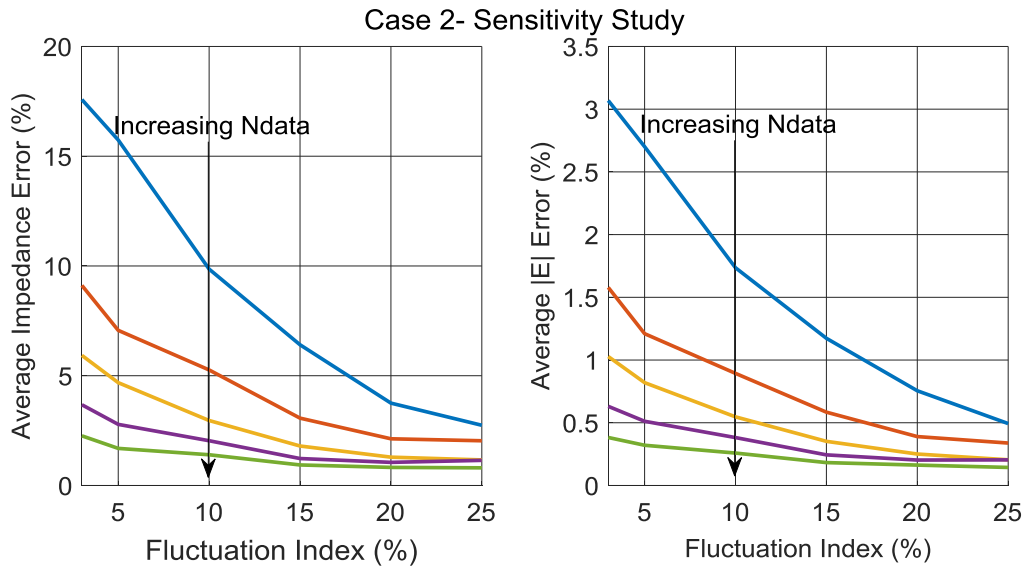


Figure 2.15 Average error of non-zero equivalent impedance values and voltage sources with different numbers of data points ($N_{data}=7, 9, 11, 13, 15$) and different fluctuation levels

As it can be seen, if eleven data points with 5% fluctuation level are chosen, the average error for impedance and voltage source magnitudes will be around 4% and 0.6%, respectively. The equivalent impedance and voltage source values obtained by the method are compared with the actual values in Figure 2.16 to Figure 2.18.

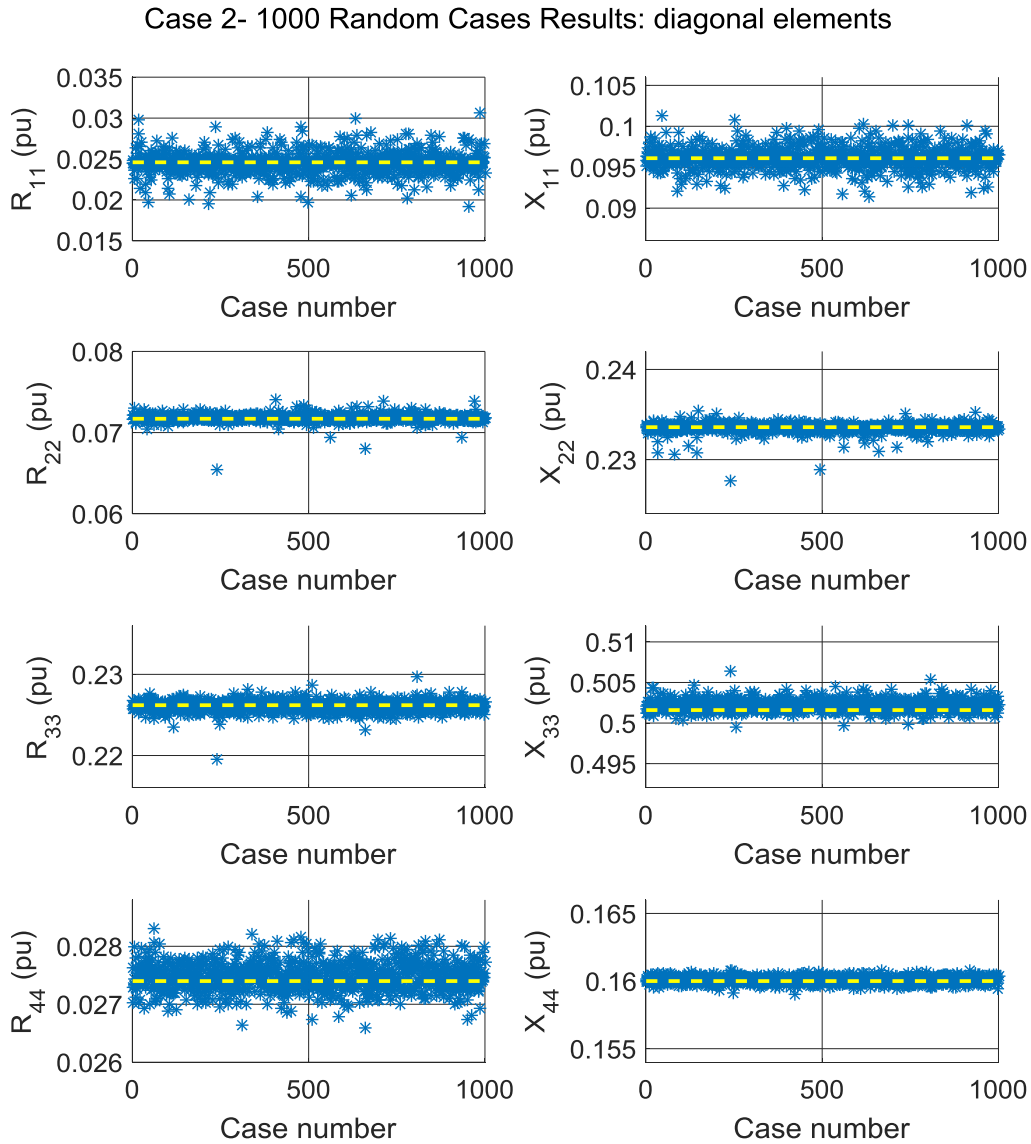


Figure 2.16 Comparison of the diagonal elements of the equivalent impedance matrix from 1000 random cases (stars) with actual values (dashed line) for eleven data points and 5% fluctuation level for case two

Case 2- 1000 Random Cases Results: non-diagonal elements

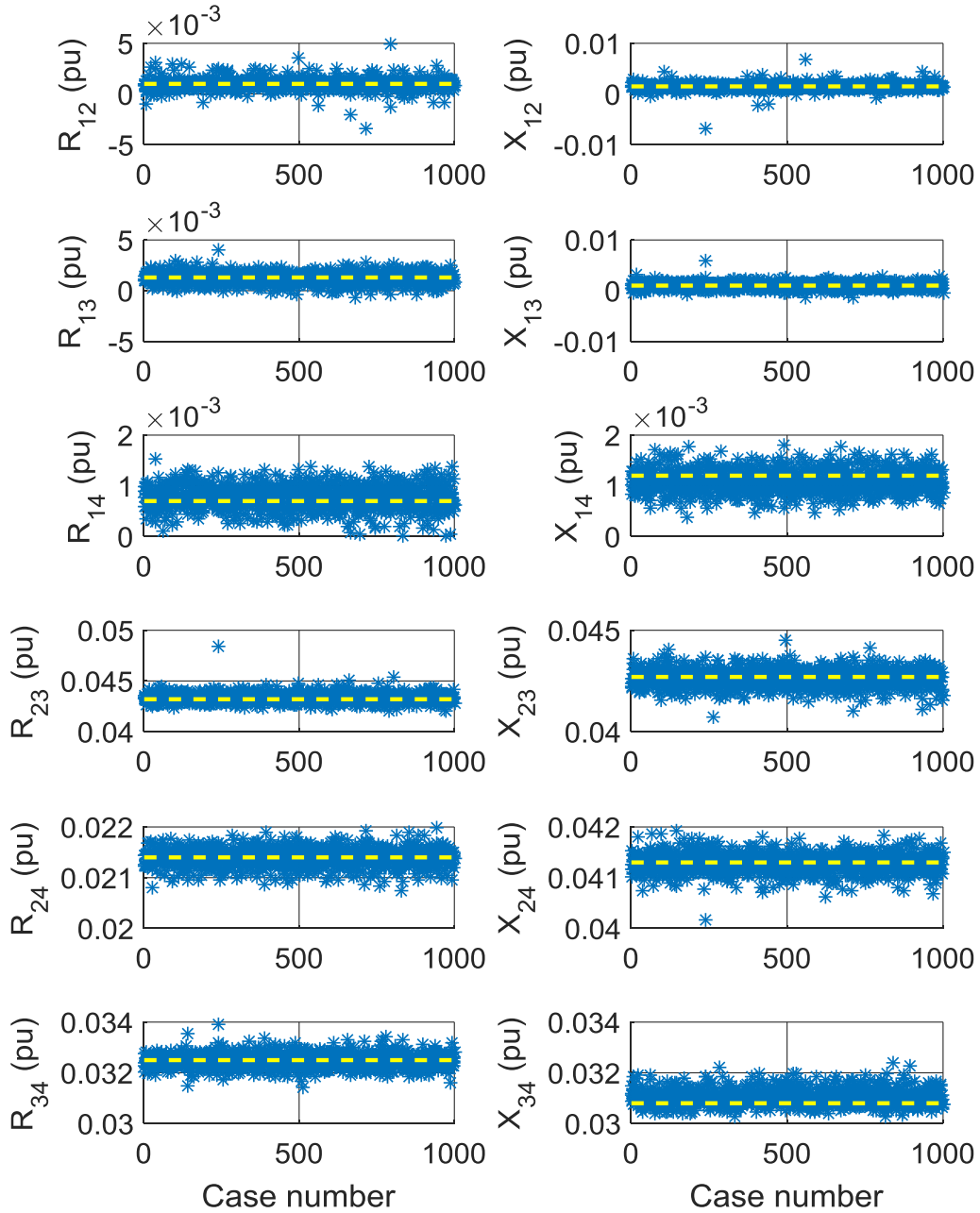


Figure 2.17 Comparison of the non-diagonal elements of the equivalent impedance matrix from 1000 random cases (stars) with actual values (dashed line) for eleven data points and 5% fluctuation level for case two

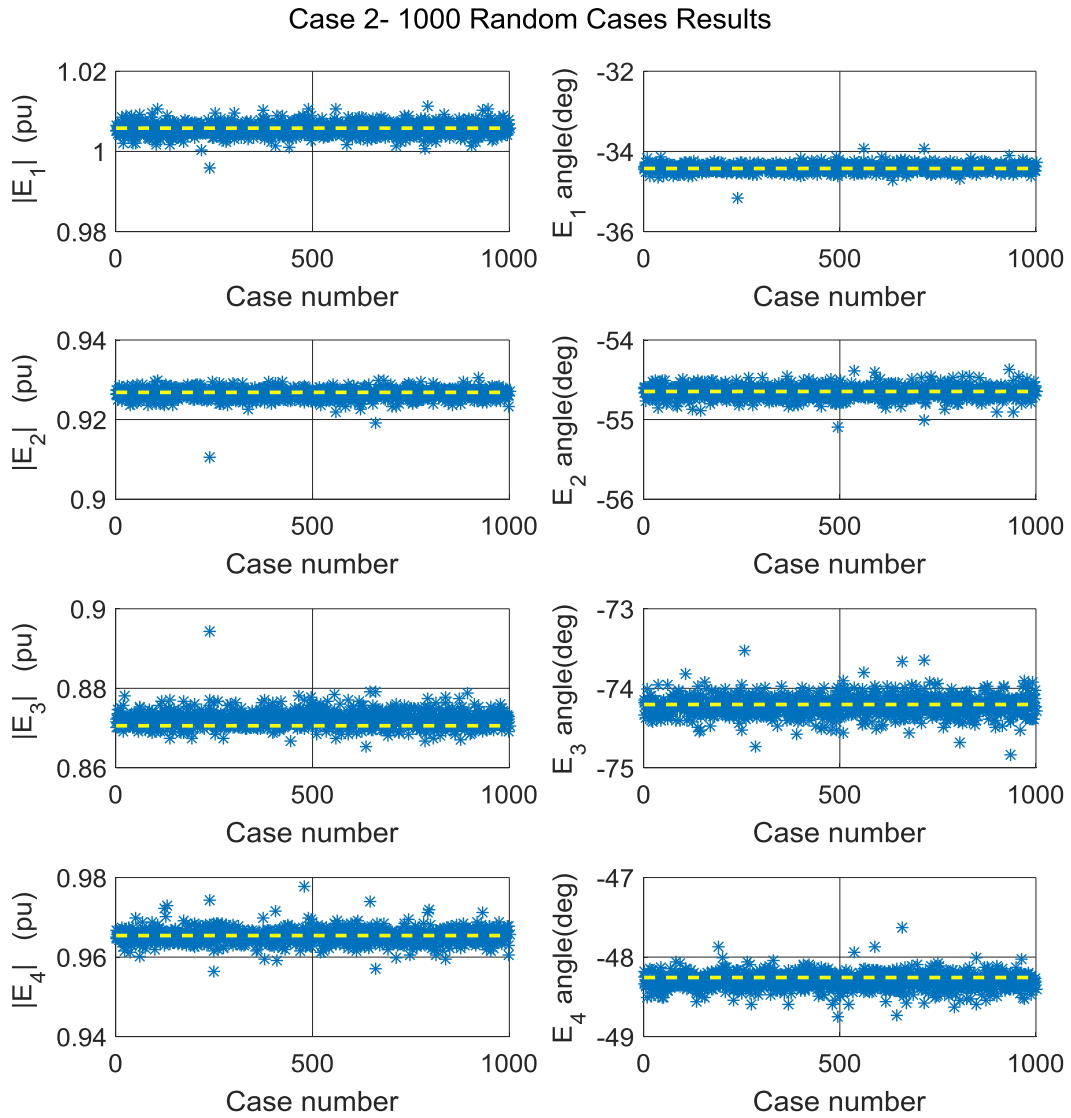


Figure 2.18 Comparison of the equivalent voltage sources from 1000 random cases (stars) with actual values (dashed line) for eleven data points and 5% fluctuation level

As it can be seen in Figure 2.16 to Figure 2.18, the equivalent parameters are close to their actual values. To summarize the results shown in Figure 2.16 to Figure 2.18, the accurate value, mean value, and standard deviation of the parameters are presented in TABLE 2.2 and TABLE 2.3.

TABLE 2.2 The results obtained by the proposed method for case two, resistance and impedance values

| Parameter | Accurate value | Mean value | Standard deviation |
|----------------------|----------------|------------|--------------------|
| R ₁₁ (pu) | 2.4600E-2 | 2.4504E-2 | 1.2358E-3 |
| R ₂₂ (pu) | 7.1700E-2 | 7.1806E-2 | 4.1991E-4 |
| R ₃₃ (pu) | 2.2620E-1 | 2.2607E-1 | 6.3482E-4 |
| R ₄₄ (pu) | 2.7400E-2 | 2.7476E-2 | 2.3964E-4 |
| R ₁₂ (pu) | 1.0000E-3 | 9.6889E-4 | 5.0390E-4 |
| R ₁₃ (pu) | 1.3000E-3 | 1.2309E-3 | 5.3064E-4 |
| R ₁₄ (pu) | 7.0000E-4 | 7.7514E-4 | 2.2781E-4 |
| R ₂₃ (pu) | 4.3200E-2 | 4.3347E-2 | 4.3786E-4 |
| R ₂₄ (pu) | 2.1400E-2 | 2.1398E-2 | 1.7187E-4 |
| R ₃₄ (pu) | 3.2500E-2 | 3.2477E-2 | 2.7032E-4 |
| X ₁₁ (pu) | 9.6100E-2 | 9.6117E-2 | 1.1803E-3 |
| X ₂₂ (pu) | 2.3360E-1 | 2.3353E-1 | 4.6400E-4 |
| X ₃₃ (pu) | 5.0160E-1 | 5.0218E-1 | 6.5227E-4 |
| X ₄₄ (pu) | 1.6000E-1 | 1.6008E-1 | 2.2959E-4 |
| X ₁₂ (pu) | 1.5000E-3 | 1.4969E-3 | 5.7725E-4 |
| X ₁₃ (pu) | 1.0000E-3 | 9.9029E-4 | 5.5396E-4 |
| X ₁₄ (pu) | 1.2000E-3 | 1.0934E-3 | 2.1206E-4 |
| X ₂₃ (pu) | 4.2700E-2 | 4.2654E-2 | 4.2947E-4 |
| X ₂₄ (pu) | 4.1300E-2 | 4.1286E-2 | 1.8629E-4 |
| X ₃₄ (pu) | 3.0800E-2 | 3.1034E-2 | 3.0540E-4 |

TABLE 2.3 The results obtained by the proposed method for case two, equivalent voltage sources

| Parameter | Accurate value | Mean value | Standard deviation |
|-----------------|----------------|------------|--------------------|
| $ E_1 $ (pu) | 1.0058 | 1.0057 | 0.0015 |
| $ E_2 $ (pu) | 0.9268 | 0.9265 | 0.0013 |
| $ E_3 $ (pu) | 0.8706 | 0.8722 | 0.0020 |
| $ E_4 $ (pu) | 0.9654 | 0.9653 | 0.0018 |
| E_1 ang (deg) | -34.4241 | -34.4128 | 0.0852 |
| E_2 ang (deg) | -54.6473 | -54.6552 | 0.0733 |
| E_3 ang (deg) | -74.2035 | -74.2193 | 0.1197 |
| E_4 ang (deg) | -48.2572 | -48.3021 | 0.0978 |

To evaluate the accuracy of the reduced model for contingency analysis, one of the equivalents found with eleven data points and 5% fluctuation level is randomly selected and converted to a network in PSS/E. The external system is replaced with the reduced one and the contingency analysis is done for both full and reduced external networks. Internal system transmission lines and transformers outages are considered and eighty six N-1 contingencies are simulated.

The accuracy of the contingency analysis results using the reduced system is presented in TABLE 2.4. As it can be seen, the average errors are very small for both bus voltage and apparent power flow errors. The maximum bus voltage error is also very small. Only the maximum MVA flow error is relatively large. To better analyse the results, the maximum voltage magnitude and apparent power flow error for each case is shown in Figure 2.19.

TABLE 2.4 Accuracy of the contingency analysis results

| | Largest Error (%) | Average Error (%) |
|--------------|-------------------|-------------------|
| Bus Voltages | 0.11 | 0.00 |
| MVA Flows | 7.22 | 0.04 |

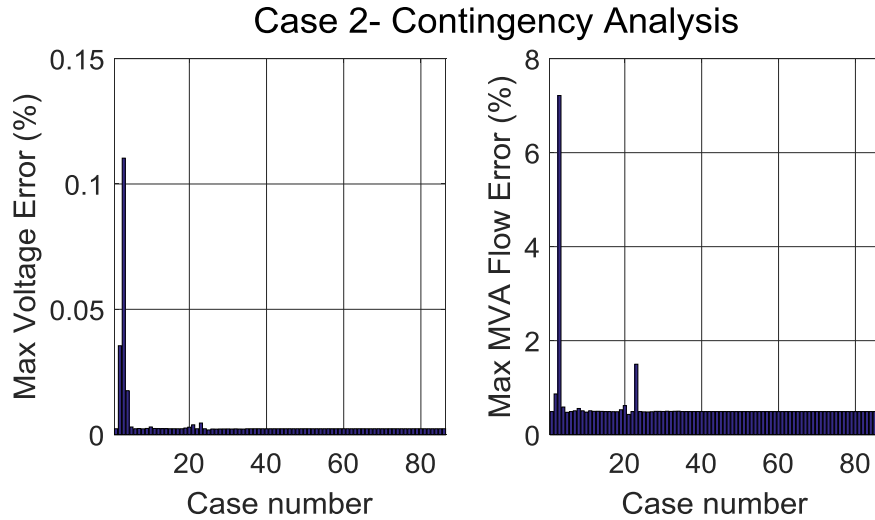


Figure 2.19 Accuracy of the reduced model for contingency analysis

The accuracy requirements in the model reduction may be different in different utilities. For example, according to the accuracy criteria adopted in [6], the maximum allowed error for contingency analysis is 1% for bus voltage magnitudes and MVA flows. According to these criteria, as it can be seen in Figure 2.19, the bus voltage error is always below the limit. In addition, the MVA flow is also below the limit except for two cases. Further investigation of the results reveals that the reason of having large errors in these cases is that the contingencies happened near bus 65 in the internal system. As it is shown in Figure 2.9, there is a transmission line between bus 65 of the internal system and bus 38 of the external system. Therefore, replacing the external system with the equivalent model caused a relatively large error for contingencies near bus 65. This reveals that to get accurate results, it is important to have a boundary zone between the internal and external systems. More accurate results could be

obtained by selecting a better boundary zone. It should be mentioned that when determining the boundary zone, there is always a trade-off between the accuracy and computational burden. Having a bigger boundary zone improves the accuracy but it increases the computational burden.

2.5 Conclusion

A measurement-based method for determining an equivalent model for external power systems at multiple boundary nodes has been proposed in this paper. The main contributions of this chapter were 1) proposing a multiport Thevenin equivalent circuit to model external systems, 2) developing a method for online estimation of the circuit parameters, 3) introducing a disturbance direction detection method to select valid disturbances. The availability of PMU data at the boundary buses has made the proposed method practical.

The method has been applied to the IEEE 118 bus system and the performance of the disturbance side detection method was evaluated. The results proved that the origin of the disturbances could be determined by evaluating the signs of the real and imaginary parts of the diagonal elements of the equivalent impedance matrix. The accuracy of the method with different numbers of data points and different fluctuation levels were analyzed. The results proved that the method could accurately find the equivalent Thevenin parameters even in the presence of measurement error. Finally, comparing the contingency analysis results obtained by the full external system and the reduced model found by the proposed method proved the efficacy of the method in representing the external system with good accuracy.

Chapter 3

Frequency Dependent Network

Equivalent

To study high frequency transients, all of the component of the system should be replaced with appropriate models to reflect frequency dependent effects. Detailed modeling of the entire power system, including the neighboring system, leads to a very high computational burden which might not be possible to handle. Therefore, only the internal system or study area is modelled in details whereas the rest of the system is replaced with a simpler equivalent model. Such equivalent is estimated from the network frequency-response data which can be obtained by field measurements or simulation studies. A method is then required to convert this data to a time-domain equivalent circuit which can be implemented in electromagnetic transients program (EMTP) software [42].

This chapter proposes a new method to find frequency dependent network equivalent of a power system. The equivalent model consists of a number of parallel branches. To find the parameters of these branches, a new coding scheme is proposed and a proper optimization approach is found by comparing different methods. The equivalent model is guaranteed to be passive which in turn ensures the stability of time-domain simulation. For the multi-port case, a new equivalent model is proposed with branches with all-positive or all-negative elements which guarantee the stability of each branch and consequently, the stability of the whole equivalent model. The elements of the admittance matrix can be fitted one by one

using the proposed method and the equivalent model for each element can be directly implemented in EMTP software.

3.1 Literature Review

The frequency-dependent terminal response of the external network, which is usually represented by the admittance matrix, is modeled using either a lumped parameter circuit model or a rational function model which can be converted to a lumped parameter circuit to be implemented in EMTP software.

Time domain approaches including ARMA modeling [27] ,[28], z-domain vector fitting [29], and time domain vector fitting [30] have been proposed. A comparison of these approaches is presented in [31]. However, the frequency domain approach is the natural choice because the terminal characterization of components is usually performed by frequency sweep measurements [31].

The rational function approximation can be used to estimate the known frequency response of the external system

$$f(s) \approx \sum_{n=1}^N \frac{c_n}{s - a_n} + d + sh \quad (3.1)$$

where the residues c_n and poles a_n are either real quantities or complex conjugate pairs, while d and h are real numbers.

The problem is to find the unknown parameters c_n , a_n , d , and h to obtain a least square approximation of $f(s)$ over a given frequency range. This is an overdetermined nonlinear problem as the unknown poles appear in the denominator. Various methods have been proposed to solve this problem. In [61], [62] the problem is solved by partitioning the whole frequency range into several sections and applying rational fitting to each section.

One of the most well-known approaches is vector fitting (VF) [32]- [34] in which the nonlinear problem is converted into two linear problems which are solved sequentially as follows [32]. Specifying a set of initial poles \bar{a}_n , an unknown rational function is introduced and an augmented problem is formed

$$\begin{bmatrix} \sigma(s)f(s) \\ \sigma(s) \end{bmatrix} \approx \begin{bmatrix} \sum_{n=1}^N \frac{c_n}{s - \bar{a}_n} + d + sh \\ \sum_{n=1}^N \frac{\tilde{r}}{s - \bar{a}_n} \end{bmatrix} \quad (3.2)$$

Multiplying the second row of (3.2) by $f(s)$ gives

$$\sum_{n=1}^N \frac{c_n}{s - \bar{a}_n} + d + sh \approx \left(\sum_{n=1}^N \frac{\tilde{r}}{s - \bar{a}_n} \right) f(s) \quad (3.3)$$

Equation (3.3) is an overdetermined linear problem which can be solved as a least-squares problem. The improved set of poles for approximating $f(s)$ is equal to the zeros of σ which can be calculated as the eigenvalues of the matrix

$$H = A - b\tilde{r} \quad (3.4)$$

where A is a diagonal matrix containing the starting poles, b is a column vector of ones, and \tilde{r} is a row vector containing the residues of σ calculated in the previous step. Replacing the newly found poles as the specified poles for σ , this process is repeated until convergence is met. Then, the residues of $f(s)$ can be calculated from another overdetermined linear problem.

The identified rational function can be represented by an equivalent electric circuit model consisting of inductors (L), capacitors (C), and resistors (R) [35] as shown in Figure 3.1.

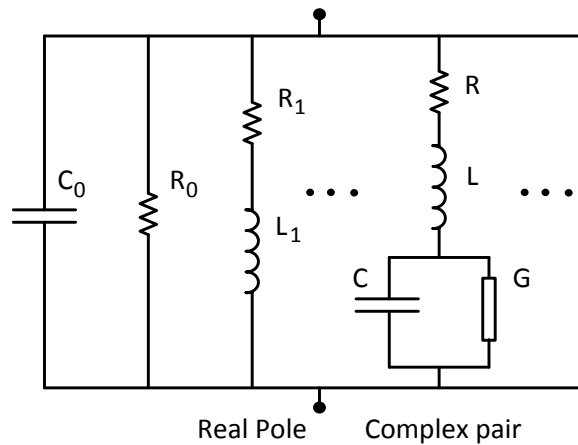


Figure 3.1 Synthesizing the equivalent obtained by VF method

An important problem is that the model may not be passive which may lead to unstable time domain simulation. Therefore, the parameters of the model have to be perturbed to enforce passivity [36]. Several passivity enforcement methods have been proposed in the literature. A comparative study is conducted in [37] which shows that all of the passivity enforcement methods have some limitations and disadvantages. For example, the iterative passivity enforcement methods [38]-[40], which are the most popular type of passivity enforcement methods, are only suboptimal and sometime fail [37]. Therefore, enforcing passivity is still a main concern in VF approaches.

Methods that directly find the parameters of an equivalent circuit of lumped elements have also been proposed. In [60] the external system is modeled by a number of modules consisting of RLC branches as shown in Figure 3.2. An initial module is generated to match the frequency characteristics at series resonance frequencies only. Then an optimization is done to minimize the mean square of the error over the given frequency range. The parameters of the module are adjusted one branch at a time through an iterative method. The iterations continue until the error falls within an acceptable limit or until the maximum number of iterations is reached. Since only the parameters of one branch are adjusted at a time, this method is prone to trap in local minima.

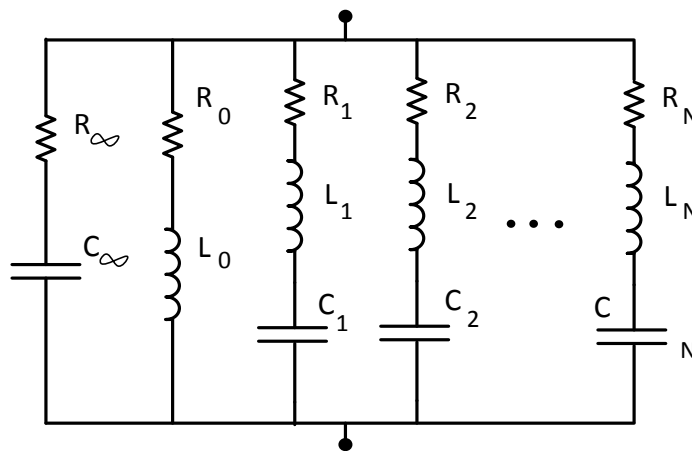


Figure 3.2 Structure of a single module used in [60]

In [41] a genetic algorithm (GA) approach is proposed for single-port problem which models the external system with an electric circuit shown in Figure 3.3 [41]. The parameters of the elements are found using GA. Since the equivalent circuit consists of only passive elements, the equivalent model is always passive. Another approach with guaranteed passivity is proposed in [42] which tries to find the optimal configuration of the equivalent circuit as well as the corresponding optimal values using genetic programming (GP). These methods have good accuracy, but they are not applicable for multi-port problems.

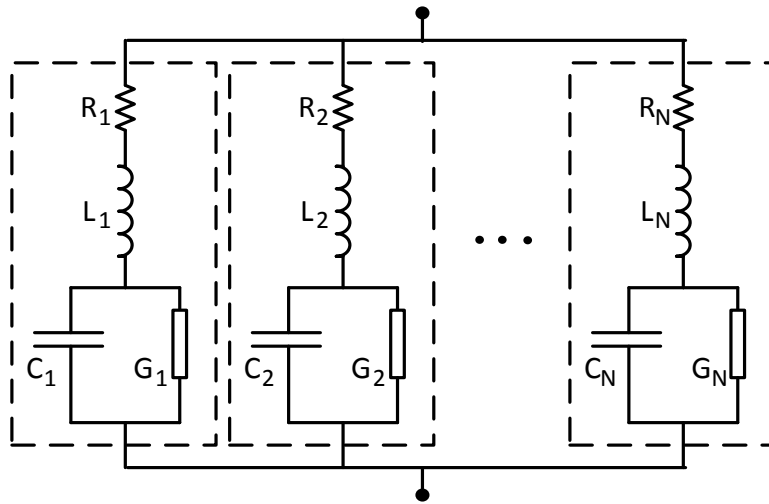


Figure 3.3 Configuration of the equivalent circuit in [41]

In this chapter, a new method for finding FDNE of external systems is proposed. For the single-port case, the equivalent model shown in Figure 3.3 is assumed and a new coding scheme is introduced to solve the problem using heuristic optimization methods. The population-based nature of these methods reduces the probability of getting trapped in local optima and sensitivity to the initial guess. A proper optimization method is then chosen by applying different optimization methods and comparing the results. For the multi-port case, a new equivalent model is proposed with all-positive and all-negative branches which guarantee the stability of each branch and consequently, the stability of the whole equivalent model.

3.2 Problem Definition

For the single-port problem, usually the admittance of the external network at different frequencies is given as the input of the problem. The desired output is an equivalent electrical circuit which can be implemented in EMTP software. For example, the admittance amplitude and phase angle of a transformer at different frequencies is shown in Figure 3.4 [41], [85].

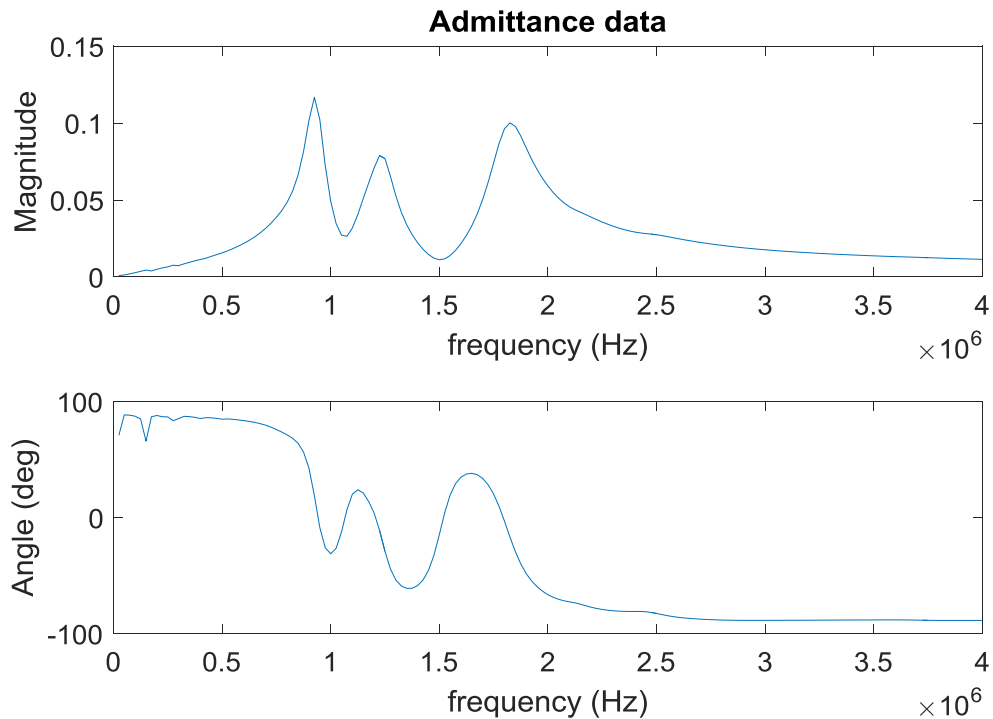


Figure 3.4 Actual admittance data of a transformer

The goal is to find an equivalent circuit to fit both the amplitude and phase angle of the actual frequency response. Therefore, the difference between the actual response and the response of the equivalent circuit should be minimized. In addition, if the equivalent network is passive, meaning that it absorbs power for any applied voltages at any frequency, the stability of the time domain simulation is ensured. For a single-port problem, the passivity criterion is that the real part of its frequency response should be always positive.

For the multi-port problem, the input is an admittance matrix found by multi-port frequency scan and the desired output is a network interconnecting the boundary nodes. Similar to the single-port case, the equivalent network (excluding the voltage sources) should be passive. To define passivity, an admittance matrix Y is considered as

$$I = YV \quad (3.5)$$

where I is the injected current vector and V is the voltage vector of the selected nodes.

The absorbed power for this network can be found by

$$P_{absorbed} = \text{Re}\{V^* YV\} = \text{Re}\{V^* (G + jB)V\} = \text{Re}\{V^* GV\} \quad (3.6)$$

where G and B are the conductance and susceptance of the admittance matrix.

From (3.6), it can be deduced that $P_{absorbed}$ will always be positive only if G is positive semidefinite. In other words, all of the eigenvalues of G should be positive. It should be mentioned that G is a real, symmetric matrix. Therefore, its eigenvalues are all real [38].

3.3 Proposed FDNE method

3.3.1 Single-port FDNE

The proposed approach for finding the equivalent circuit for single-port problems is presented in this section. First, the problem will be formulated as a minimization problem and the objective function and the constraints will be defined. Then, the heuristic optimization-based optimization scheme for single-port FDNE will be presented.

3.3.1.1 Mathematical Formulation

The equivalent circuit configuration considered in this paper consists of parallel RLCG branches shown in Figure 3.3 [41]. This model is in fact a more general version of the model obtained by rational function approximation [32]. Comparing Figure 3.3 with Figure 3.1 reveals that the branches dedicated to real

poles in Figure 3.1 could be represented by RLCG branches with G equal to infinity (i.e. short circuit) and C equal to zero (i.e. open circuit). The R branch in Figure 3.1 could be obtained by L and C equal to zero and G equal to infinity. Finally, The C branch in Figure 3.1 could be obtained by R, L, and G equal to zero. The RLCG model of Figure 3.3 can also represent the equivalent model used in [60] shown in Figure 3.2. Therefore, this equivalent model is considered in this thesis as the more general version of the equivalent models proposed in the literature.

Similar to [41], in order to guarantee the passivity, only passive elements are used in the equivalent circuit. The problem can be mathematically formulated as

$$\min_{R,L,C,G \geq 0} e = \sqrt{\frac{1}{N_F} \sum_{f \in S_F} w_f |Y_{actual}^f - \hat{Y}^f|^2} \quad (3.7)$$

where

$$\hat{Y}^f = \sum_{u \in S_U} \frac{1}{R_u + j2\pi fL_u + \frac{1}{j2\pi fC_u + G_u}} \quad (3.8)$$

where N_F is the number of frequency samples. u and f denote branch number and frequency, respectively. S_U and S_f denote the set of branches and frequencies, respectively. Y_{actual}^f , \hat{Y}^f represent the actual and equivalent admittance at frequency f . w_f is a weighting factor that helps the convergence of the optimization method. More discussion about the weighting factor can be found in [41], [35], and [85]. Two weighting factors are used in this thesis which are [14]

- Strong inverse weight $w_f = 1/|Y_{actual}^f|^2$
- Weak inverse weight $w_f = 1/\sqrt{|Y_{actual}^f|}$

3.3.1.2 Optimization Scheme

The optimization problem formulated in the previous section is an overdetermined non-linear non-convex problem. None of the methods proposed for solving this problem, including the famous VF method, can guarantee the global optimality of the solution. Heuristic optimization methods could be an alternative option for solving these kinds of problems.

Three heuristic optimization approach including particle swarm optimization (PSO), shuffled frog-leaping algorithm (SFLA), and differential evolution (DE), which have been successfully applied for other power system applications [80]-[84], are used to solve the problem defined in (3.7). These algorithms are briefly explained in Appendix B. The performance of these methods will be compared in a case study to be able to choose the proper one for the problem.

According to (3.7), the optimization parameters that need to be tuned are R , L , C , and G of the branches. In order to accelerate the convergence rate, the resonance frequency of each branch is used as the optimization parameter instead of L . Therefore, each individual is defined as

$$Ind^i = [\omega_1^i, R_1^i, C_1^i, G_1^i, \dots, \omega_N^i, R_N^i, C_N^i, G_N^i] \quad (3.9)$$

where N is the maximum number of the branches.

The advantages of using ω_{res} instead of L is that the major resonant frequencies can be easily found from the admittance data and can be directly used in the optimization process. To find L_u from ω_{res} , the admittance of a single branch is rewritten as (3.10) by separating the real and imaginary parts of the denominator

$$\hat{Y}(\omega) = \frac{1}{R_u + \frac{G_u}{G_u^2 + \omega^2 C_u^2} + j\omega L_u - \frac{j\omega C_u}{G_u^2 + \omega^2 C_u^2}} \quad (3.10)$$

The (approximate) resonance frequency could be found by

$$\omega_{res,u} L_u - \frac{\omega_{res,u} C_u}{G_u^2 + \omega_{res,u}^2 C_u^2} = 0 \quad (3.11)$$

Finally, L could be found by

$$L_u = \frac{C_u}{G_u^2 + \omega_{res,u}^2 C_u^2} \quad (3.12)$$

It should be noted that the above formula is an approximation and the actual resonance frequency of the branch is slightly different from the resonant frequency used as the optimization parameter. However, the optimization process adjusts the parameters so that the frequency response of the final solution matches with that of the actual data with highest possible accuracy.

In order to find the optimal number of branches and optimal values of ω , R , C , G of each branch simultaneously, the process shown in flowchart of Figure 3.5 is used. The process is shown for only SFLA. PSO and DE are also implemented in the same manner.

The first step is to set the initial number of branches. It can be set to the number of (major) peaks of the frequency response. Then, the parameters of each branch are initialized using the approach similar to the method proposed in [41]. The only difference is that here the frequency of the peak is directly used as the branch parameter instead of L . Then, a heuristic optimization method is applied to find the optimal parameters of the branches. These parameters are stored as the optimal parameters for the respective number of branches.

Then the stopping criterion is checked. If the maximum number of the branches is reached, the algorithm will stop. Otherwise, the number of branches is increased and the heuristic optimization method is applied to find the optimal parameters. A point worth mentioning is that the two optimization loops have to be coordinated which means that the inner loop should reach its final solution before the number of branches is increased in the outer loop. After the algorithm is stopped, a matrix consisting of optimal parameters of each branch is returned. The operator can then pick up the desired equivalent circuit considering the required accuracy and available computational capability.

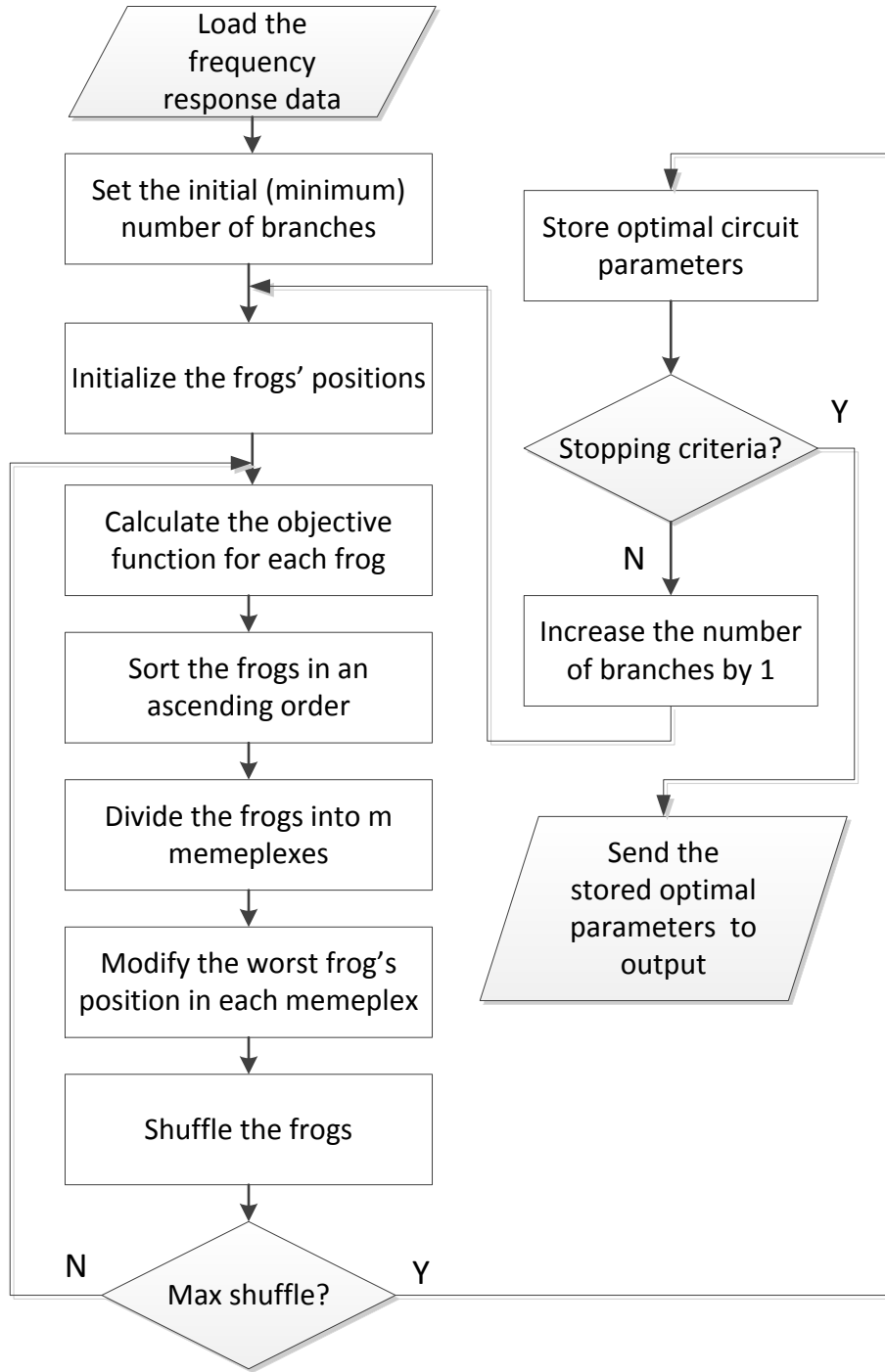


Figure 3.5 Flowchart of the proposed approach for single-port FDNE problem

3.3.2 Multi-port FDNE

For the multi-port problem, some of the mutual admittance data might have negative real parts. It is obvious that such data cannot be approximated by using only positive elements. Therefore, the single-port approach presented in the previous subsection cannot be applied directly and some modifications are required.

To overcome the aforementioned problem, RLCG branches with negative values are added to the equivalent circuit as shown in Figure 3.6. It should be noted that if all of the R, L, C, and G values are negative at the same time, the branch will have a stable response. Since each branch has a stable response, the overall response of the whole circuit will be stable as well [60]. The model is a more general version of the model proposed in [60].

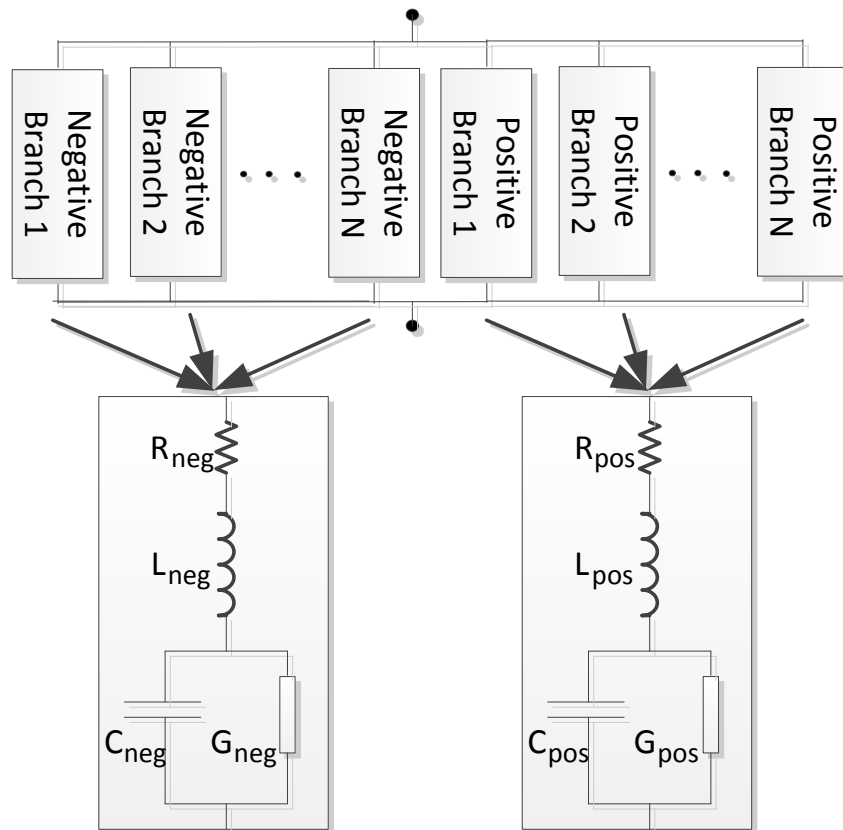


Figure 3.6 The proposed equivalent circuit configuration for frequency responses with negative real parts

To apply the approach for multi-port case, the first step is to determine the initial number of positive and negative branches. This can be realized by observing the real part as well as magnitude of the admittance data. To better explain the initialization method, a sample mutual admittance data is shown in Figure 3.7 [85].

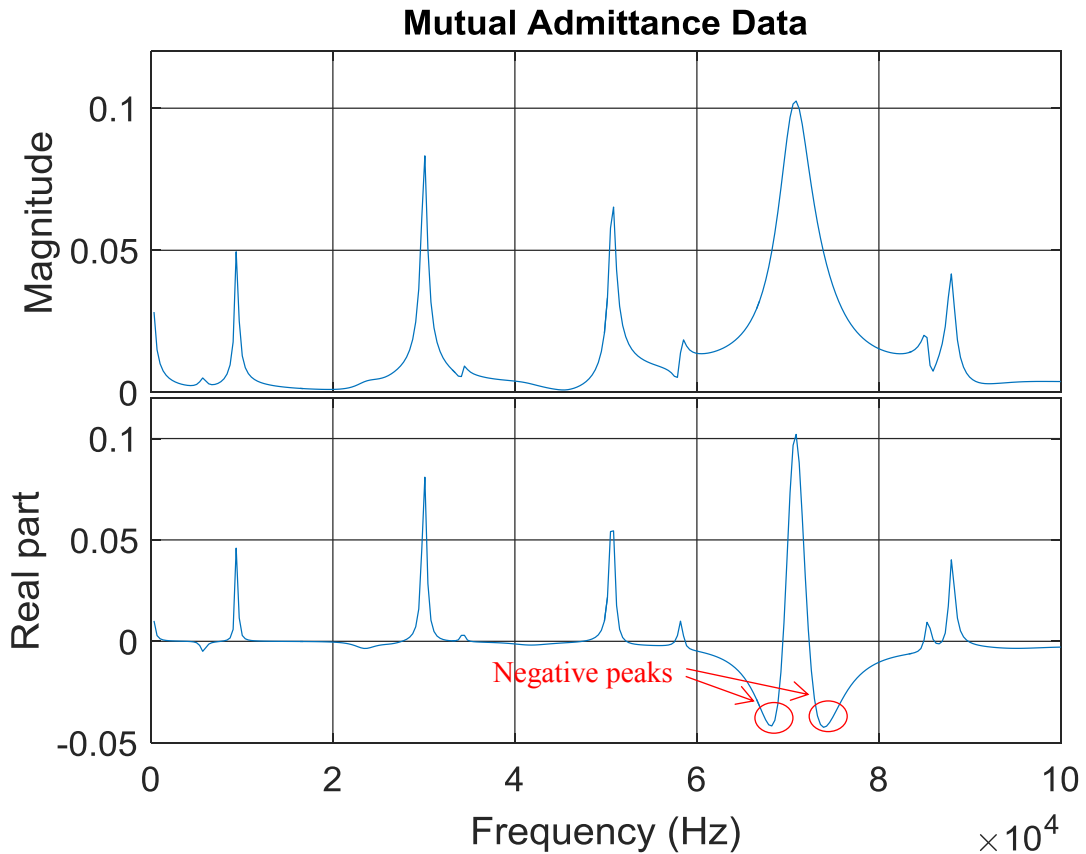


Figure 3.7 Sample magnitude and real part of a mutual admittance data

Similar to the single-port approach, the first step of initialization is to find the resonance frequencies. To do this, the peaks of the admittance magnitude are identified. The next step is to locate the peaks of negative branches. Some of these negative peaks might not be visible in the admittance magnitude. Two of such negative peaks are shown in Figure 3.7. Therefore, the real part of the admittance

is used to identify the frequencies of negative peaks. The resonance frequencies obtained using magnitudes and real parts of the admittance are then unified. An approach similar to the single port case is used to initialize the rest of the parameters (i.e. R , C , and G of the branches). The only difference is that these values are all set to be negative for negative peaks.

To ensure the stability of each branch during the optimization process, whenever the R parameter of each branch switches signs, L , C and G of the corresponding branch will also be forced to follow the sign of R . In this way, all of the elements of each branch will always have the same sign.

3.4 Case Studies

Several case studies are considered to evaluate the performance of the method for single-port and multi-port applications. The algorithm is implemented in MATLAB on a system with an Intel Core i5-3450 CPU and 8 GB of RAM.

3.4.1 Case One: Sample Electrical Circuit

The first case is a sample electrical circuit consisting eight RLCG branches to compare the performances of the optimization methods and choose the proper one. The parameters of the circuit are given in TABLE 3.1. The frequency response of the circuit is shown in Figure 3.8.

TABLE 3.1 Circuit parameters for case one

| Branch no. | R(ohm) | L(mH) | C(uF) | G(Mho) |
|------------|---------|---------|---------|-----------|
| 1 | 2.3173 | 81.6177 | 94.5378 | 0.030687 |
| 2 | 12.8754 | 13.2632 | 1.3410 | 9.5007e-6 |
| 3 | 1.4850 | 3.1842 | 3.0850 | 5.3547e-5 |
| 4 | 4.5540 | 12.1748 | 0.6467 | 1.9187e-4 |
| 5 | 33.5430 | 1.9202 | 1.3580 | 2.4893e-5 |
| 6 | 25.542 | 0.5579 | 19.8560 | 3.2110e-5 |
| 7 | 0.9708 | 2.9254 | 0.8273 | 4.4098e-4 |
| 8 | 43.1230 | 18.8058 | 0.3583 | 4.5874e-6 |

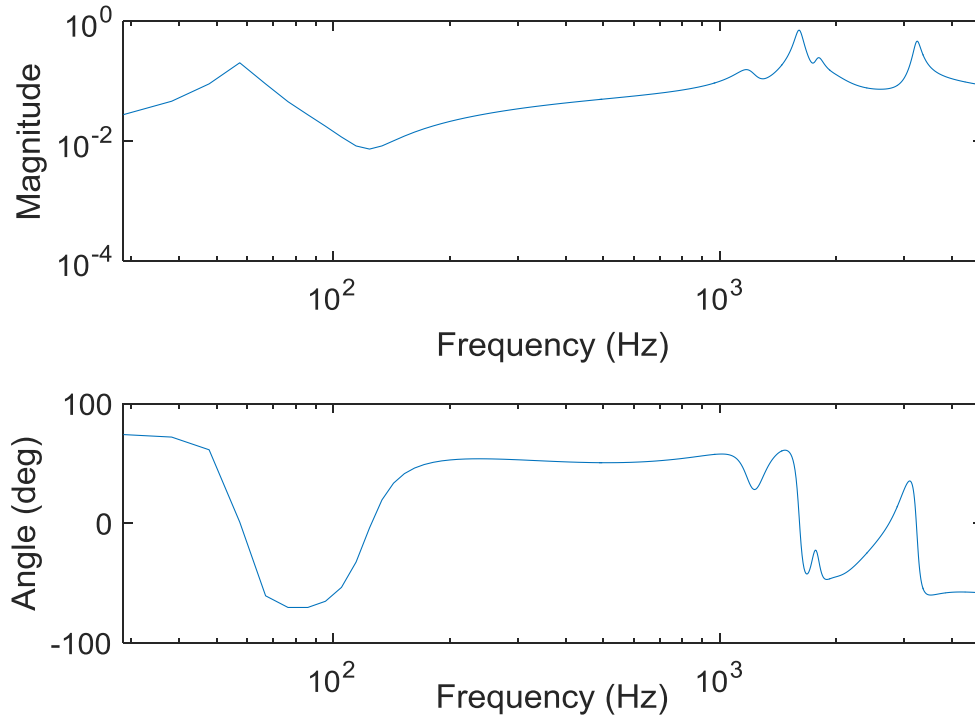


Figure 3.8 Admittance data of case one

3.4.1.1 Comparison of different methods

PSO, DE, and SFLA are implemented to find the optimal parameters. For all of them the number of branches, population size, and maximum iteration number is set to 8, 400, and 1000, respectively. Weak inverse weight is used as the weighting factor for this case. For SFLA, 100 memplexes are considered. The results of ten independent run for each method is summarized in TABLE 3.2. Also the average convergence rates are compared in Figure 3.9.

TABLE 3.2 Comparison of the results of PSO, DE, and SFLA for case one

| Method | Best OF | Mean OF | Worst OF | Mean execution time (s) |
|--------|----------|----------|----------|-------------------------|
| PSO | 4.392e-3 | 1.030e-2 | 2.092e-2 | 1302 |
| DE | 3.777e-3 | 4.056e-3 | 4.550e-3 | 1345 |
| SFLA | 6.425e-4 | 3.087e-3 | 4.545e-3 | 425 |

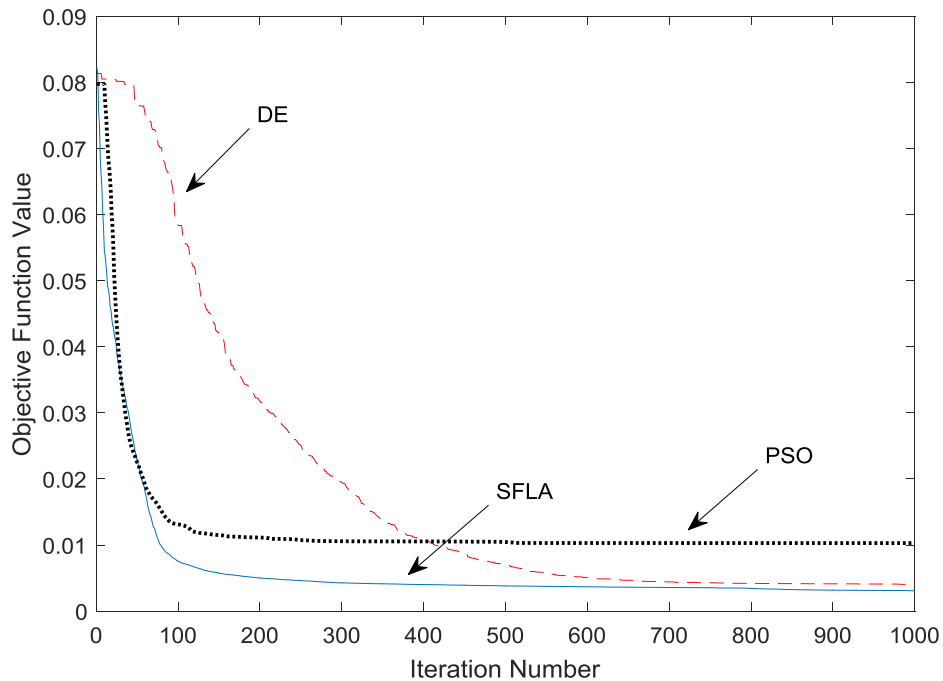


Figure 3.9 Convergence rates of different methods for case one

As it can be seen, SFLA has the best performance in terms of accuracy, convergence rate, and execution time. Therefore, SFLA is chosen as the desired method. It should be mentioned that all of the results presented from this point forward are obtained by SFLA.

3.4.1.2 Number of branches

As it can be seen in Figure 3.8, five peaks are visible in the frequency response. Therefore, the initial number of branches is set to five. The maximum is set to ten to observe the effect of additional branches. The objective function value for different number of branches is shown in Figure 3.10. As it can be seen, from five branches to eight branches the accuracy improves fast, but after eight branches there is not much improvement in the accuracy. Therefore, eight is considered as the optimal number of branches for this case.

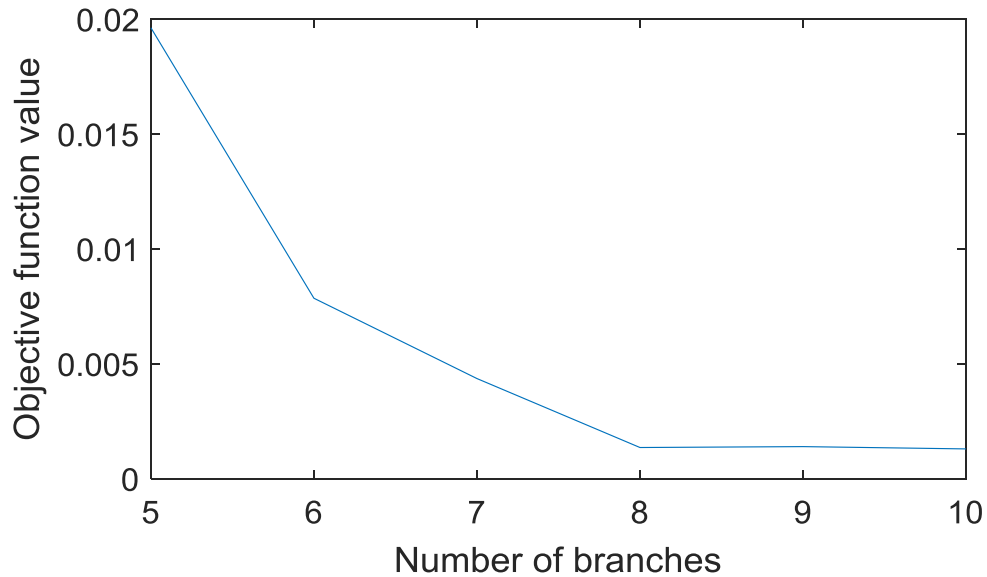


Figure 3.10 The effect of increasing the number of branches on the objective function value for case one

3.4.1.3 Accuracy

The accurate admittance data calculated using the parameters given in TABLE 3.1 and the admittance of the optimal configuration with eight branches found by SFLA are compared in Figure 3.11. As it can be seen, the response of the optimal circuit matches with that of the sample circuit with a very high accuracy. The objective function is equal to $6.425e-4$ for the optimal circuit.

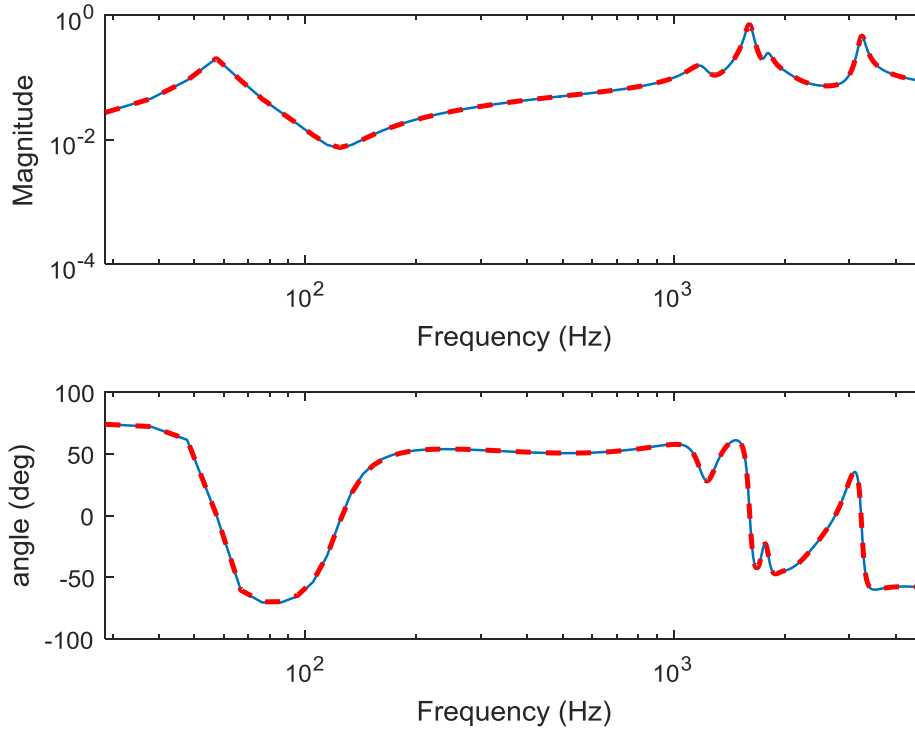


Figure 3.11 Comparison of the actual admittance (solid line) with the admittance of the equivalent circuit (dashed-line) for case one

3.4.2 Case Two: Transformer

The second case is the transformer frequency response previously shown in Figure 3.4. As it can be seen in the figure, there are three major peaks in the admittance magnitude curve. Therefore, the minimum number of branches is set to three. The maximum is set to eight to see the effect of having more branches. Strong inverse weight is used as the weight factor for this case. The population size is set to 200 with 50 memplexes. The maximum iteration number is equal to 500.

3.4.2.1 Number of branches

The objective function value versus number of branches is shown in Figure 3.12. As it can be seen, after five branches, the value of objective function does not improve that much. Therefore, five is considered as the optimal number of branches for this case.

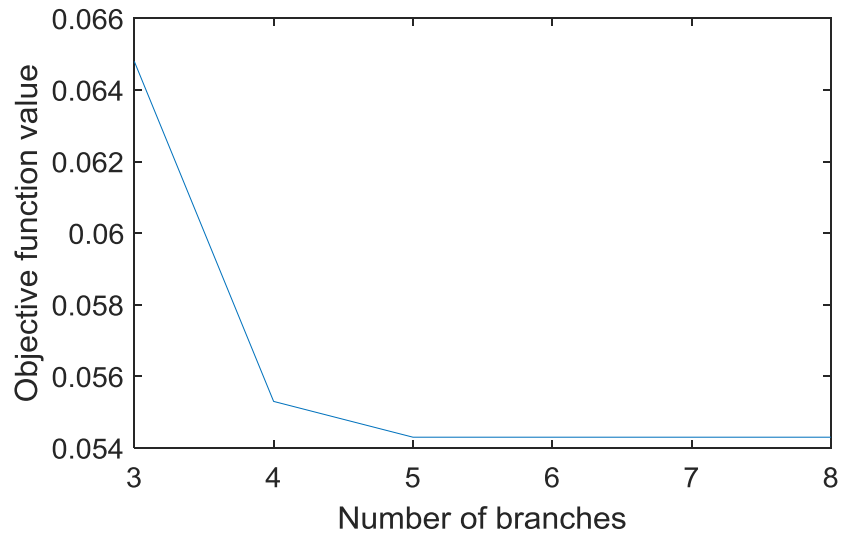


Figure 3.12 The effect of increasing the number of branches on the objective function value for case two

3.4.2.2 Convergence characteristics

The convergence rate of the method with five branches is shown in Figure 3.13. As it can be seen, the method nearly reaches the optimal solution after about 250 iterations. The total simulation time is 23 seconds for this case.

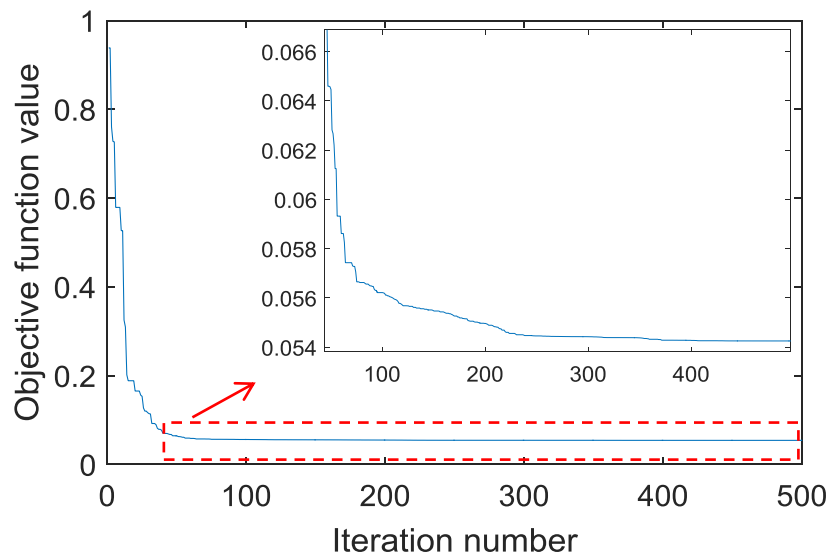


Figure 3.13 Convergence rate of the method for case two

3.4.2.3 Accuracy

The admittance response of the optimal configuration with five branches found by SFLA is compared to the actual admittance data in Figure 3.14. The optimal parameters are given in TABLE 3.3.

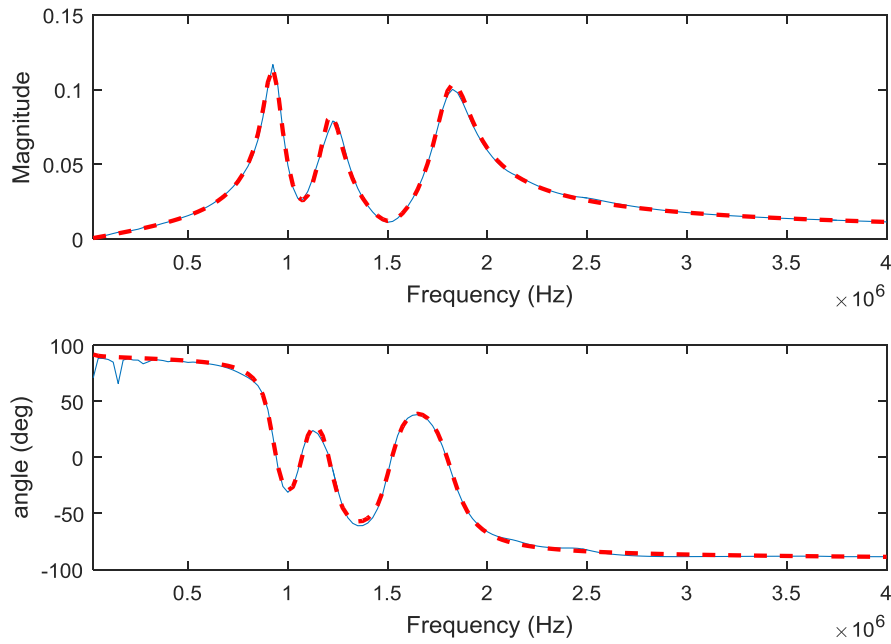


Figure 3.14 Comparison of the actual admittance (solid line) with the admittance of the equivalent circuit (dashed-line) for case two

The objective function value of the optimal circuit found by SFLA is compared with those of GA [41] and VF with passivity enforcement [85] in TABLE 3.4. It can be seen that the proposed SFLA method gives better results with fewer number of branches compared to the other methods.

TABLE 3.3 Optimal Equivalent circuit parameters for case two

| Branch no. | R(ohm) | L(mH) | C(nF) | G(Mho) |
|------------|----------|--------|--------|------------|
| 1 | 594.4958 | 6.0352 | 0.1831 | 3.1501e-20 |
| 2 | 767.7740 | 8.9535 | 0.0350 | 0 |
| 3 | 9.2621 | 0.0149 | 1.9615 | 0 |
| 4 | 9.3355 | 0.0169 | 1.0181 | 2.1960e-4 |
| 5 | 9.9993 | 0.0083 | 0.9239 | 7.2131e-19 |

TABLE 3.4 Comparison of SFLA, GA, and VF with passivity enforcement for case two

| Method | GA | VF | SFLA |
|-----------------|--------|--------|--------|
| OF value | 0.0849 | 0.0608 | 0.0543 |
| No. of branches | 7 | 7 | 5 |

3.4.3 Case Three: Distribution System Terminals

This case is the network equivalent seen at two three-phase terminals of a distribution system [85]. The input is a 6 by 6 admittance matrix. The multi-port equivalencing method with positive and negative RLCG branches is applied to the first column of the admittance matrix to evaluate the efficacy of the proposed equivalent model. First, the non-diagonal elements are fitted one by one. The responses of these elements are added together and the total is subtracted from the diagonal admittance element to get the equivalent shunt between the first node and the ground using (3.13). The obtained response is then fitted similar to a single-port problem.

$$Y_{01} = Y_{11} - \sum_{j=2}^6 \hat{Y}_{j,1} \quad (3.13)$$

Weak inverse weight is used as the weighting factor for this case. The population size is set to 400 with 100 memplexes. The maximum iteration number is set to 2000.

3.4.3.1 Number of branches

To determine the required number of branches the strategy explained before is used for each of the admittance matrix elements. The number of branches for each admittance matrix elements is presented in TABLE 3.5.

TABLE 3.5 Number of branches used for creating the equivalent circuit for each element of the admittance matrix

| Element | Y_{01} | Y_{21} | Y_{31} | Y_{41} | Y_{51} | Y_{61} |
|--------------------|----------|----------|----------|----------|----------|----------|
| Number of branches | 10 | 18 | 22 | 18 | 17 | 20 |

3.4.3.2 Convergence characteristics

The convergence rate of the method is shown in Figure 3.15. As it can be seen, except for Y_{31} , in all cases the algorithm converges to the optimal solution way before 2000 iterations. For Y_{31} , it is found that after 2000 iterations there is not any noticeable improvement in the objective function value. Therefore, 2000 iterations are shown to be consistent with the other results.

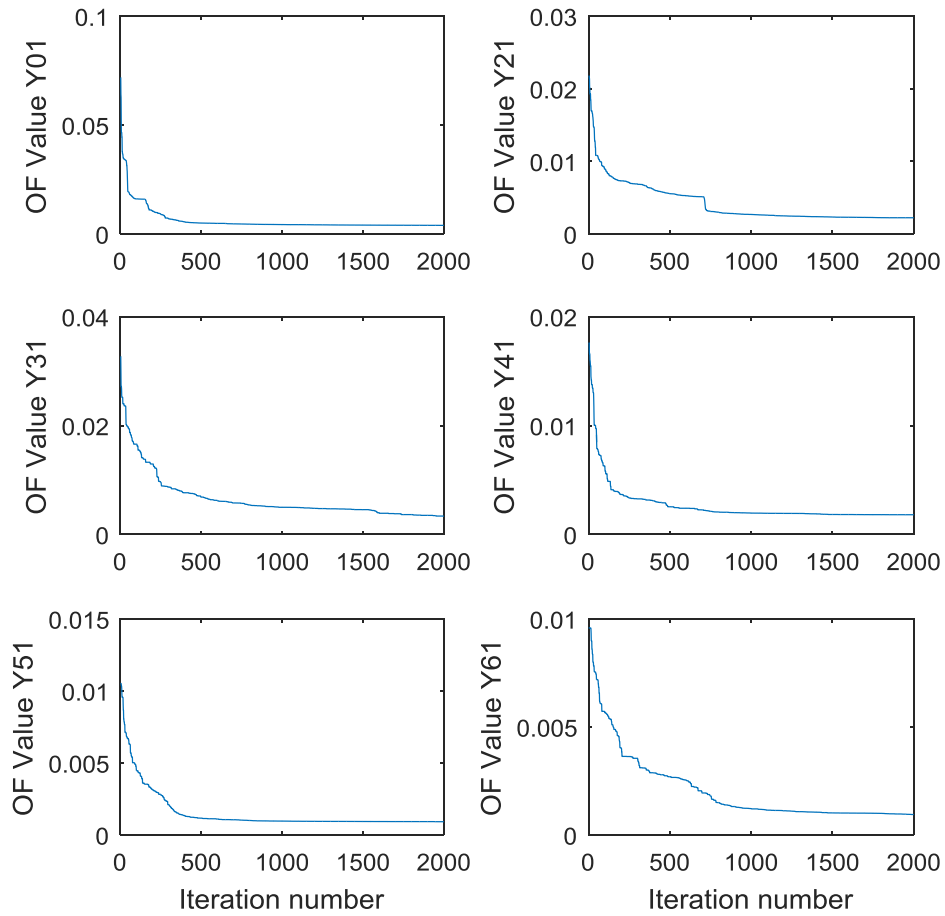


Figure 3.15 Convergence rate of the method for case three

3.4.3.3 Accuracy

The frequency responses of the equivalent circuits found by the proposed method are compared with the actual data in Figure 3.16 and Figure 3.17.

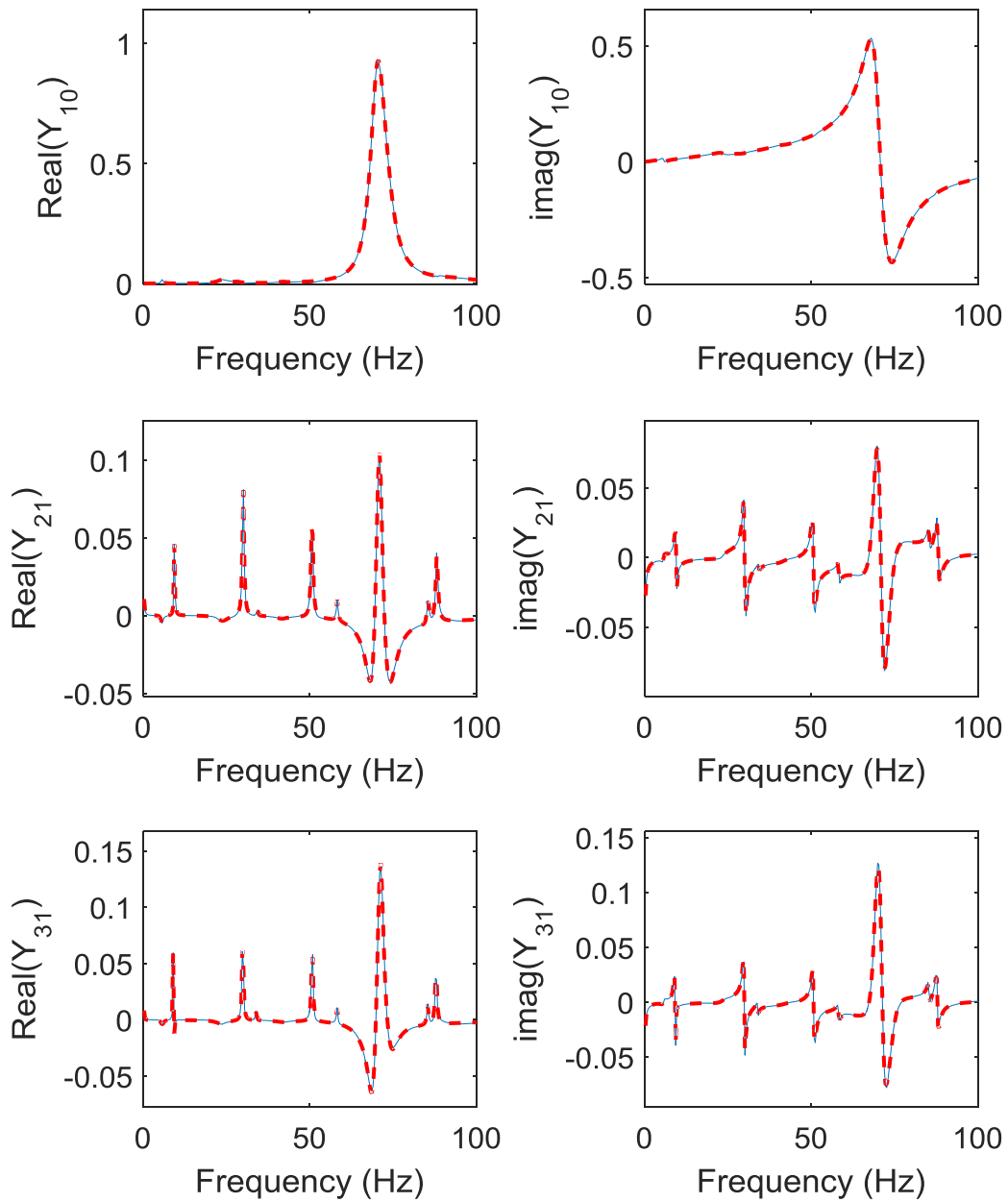


Figure 3.16 Comparison of the actual value (solid line) with the value of the equivalent circuit (dashed-line) for the first three elements of the first column of the admittance matrix in case three

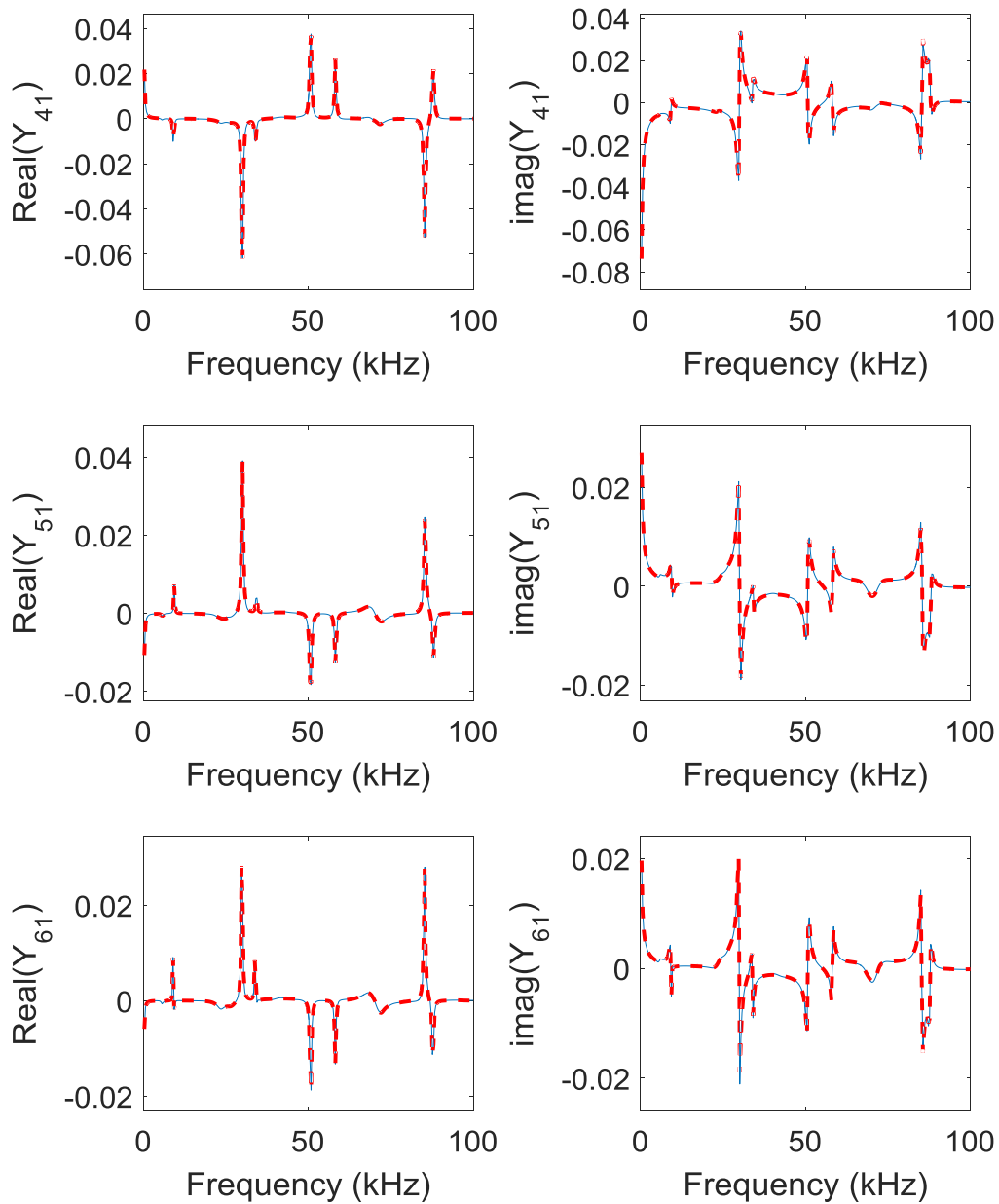


Figure 3.17 Comparison of the actual value (solid line) with the value of the equivalent circuit (dashed-line) for the last three elements of the first column of the admittance matrix in case three

As it can be seen, in all cases the response of the equivalent circuit matches with the actual one with good accuracy. The objective function values for this case are given in TABLE 3.6.

TABLE 3.6 Objective function value of fitting each element of the first column of the admittance matrix in case three

| Element | Y_{11} | Y_{21} | Y_{31} | Y_{41} | Y_{51} | Y_{61} |
|-----------------|----------|----------|----------|----------|----------|----------|
| Objective Value | 0.0039 | 0.0022 | 0.0034 | 0.0018 | 0.0009 | 0.0009 |

3.4.4 Case Four: IEEE 118 Bus System

For this case, a modified version of the IEEE 118 bus system is built in EMTDC/PSCAD and an external network with three boundary nodes is considered as shown in Figure 3.18. Frequency scan is done to get the positive sequence frequency responses seen from the boundary nodes. The frequency scan tool developed in EMTDC/PSCAD is discussed in more details in Appendix C. The elements of the Y_{bus} matrix of the external network are fitted using the proposed multi-port approach. The weak inverse weight is used for this case. Since the external network is an active network with voltage sources at fundamental frequency, the equivalent voltage sources are added to the equivalent network to build the full network. For finding the voltage sources, current injections at boundary nodes are found similar to the method used in Ward-type equivalents [11]. Then the current source in parallel with the shunt admittance is converted to a voltage source in series with the impedance. It should be mentioned that if the external system had some harmonic sources, the equivalent voltage sources at corresponding harmonic frequencies could be found using a similar approach. The external network circuit configuration is shown in Figure 3.19.

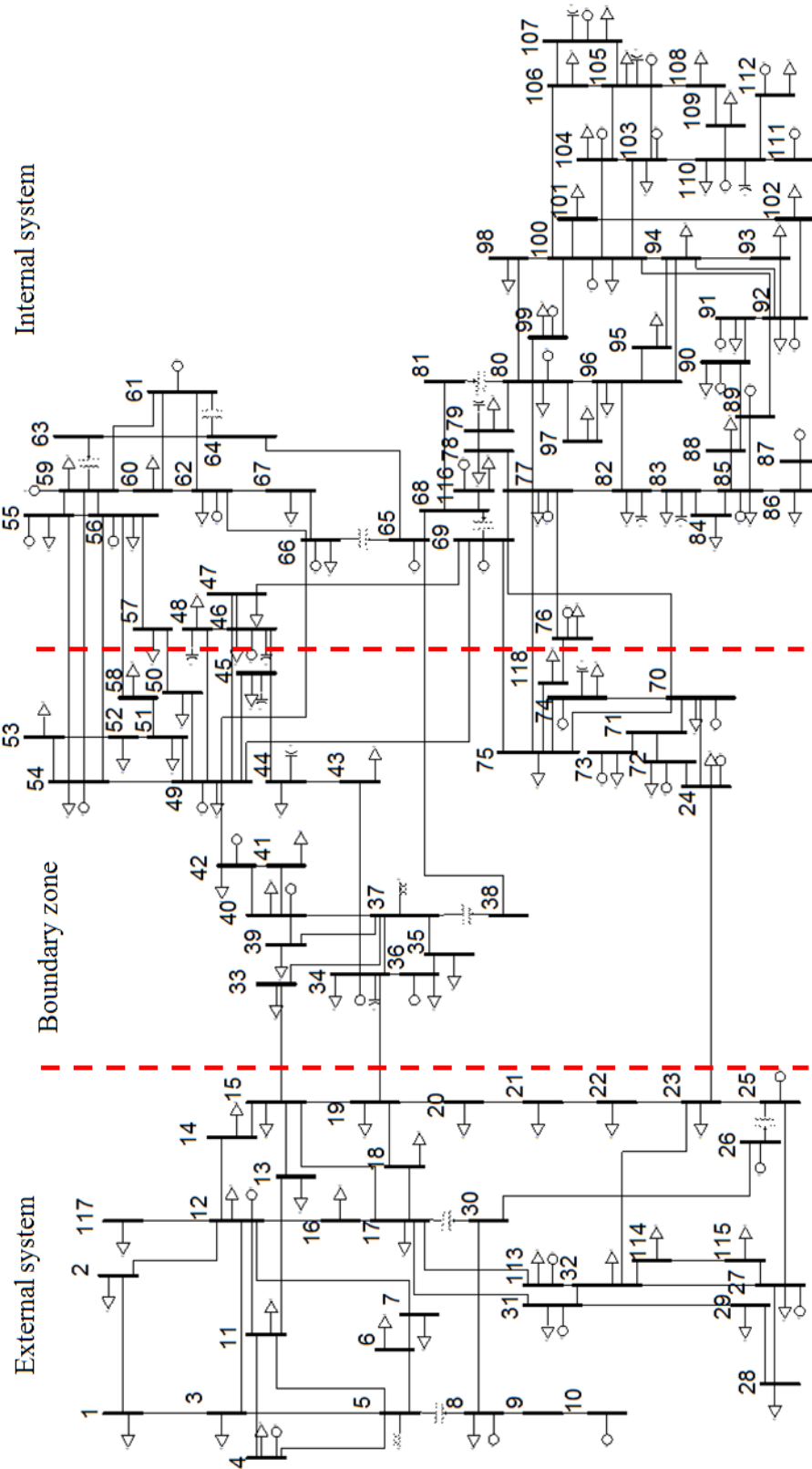


Figure 3.18 Internal, boundary, and external systems

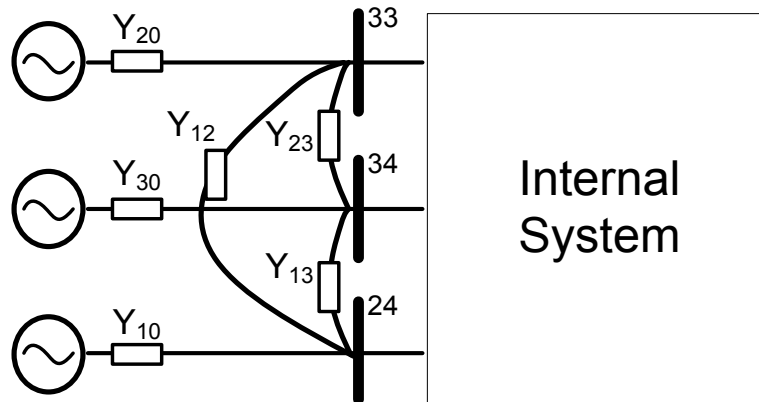


Figure 3.19 External system equivalent circuit configuration

3.4.4.1 Number of branches

As the system size is larger than the previous cases, there are many peaks in the frequency data. Considering all of these peaks for building the equivalent network leads to a very large number of branches which is not desirable. To limit the number of branches, only the significant peaks are considered. Similar to previous cases, for each admittance matrix element, the optimal number of branches is found by a few trial and errors. The maximum number of branches is set to 30 and after the optimization the equivalent circuits have between 10 to 28 branches.

3.4.4.2 Convergence characteristics

The convergence rate of the method for the first column of the admittance matrix is shown in Figure 3.20. In all cases the algorithm reaches the optimal solution after about 400 iterations but extra iterations are allowed to fine-tune the optimal parameters.

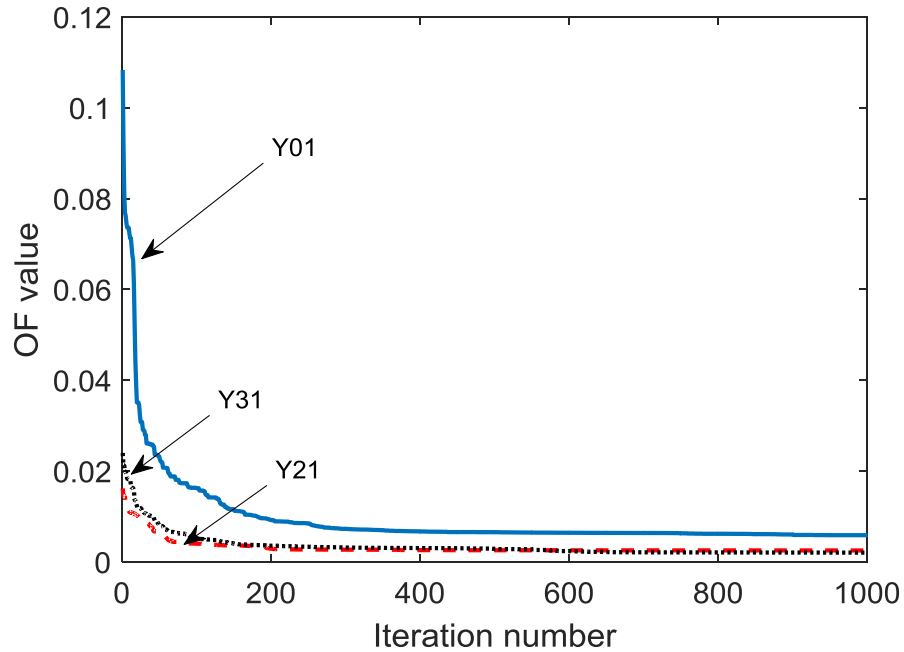


Figure 3.20 Convergence rate of the method for case four

3.4.4.3 Accuracy

The frequency responses of the equivalent circuits found by the proposed method are compared with the actual data in Figure 3.21 and Figure 3.22. In all cases, the response of the equivalent circuit matches with the actual one with good accuracy. The objective function values for this case are given in TABLE 3.7.

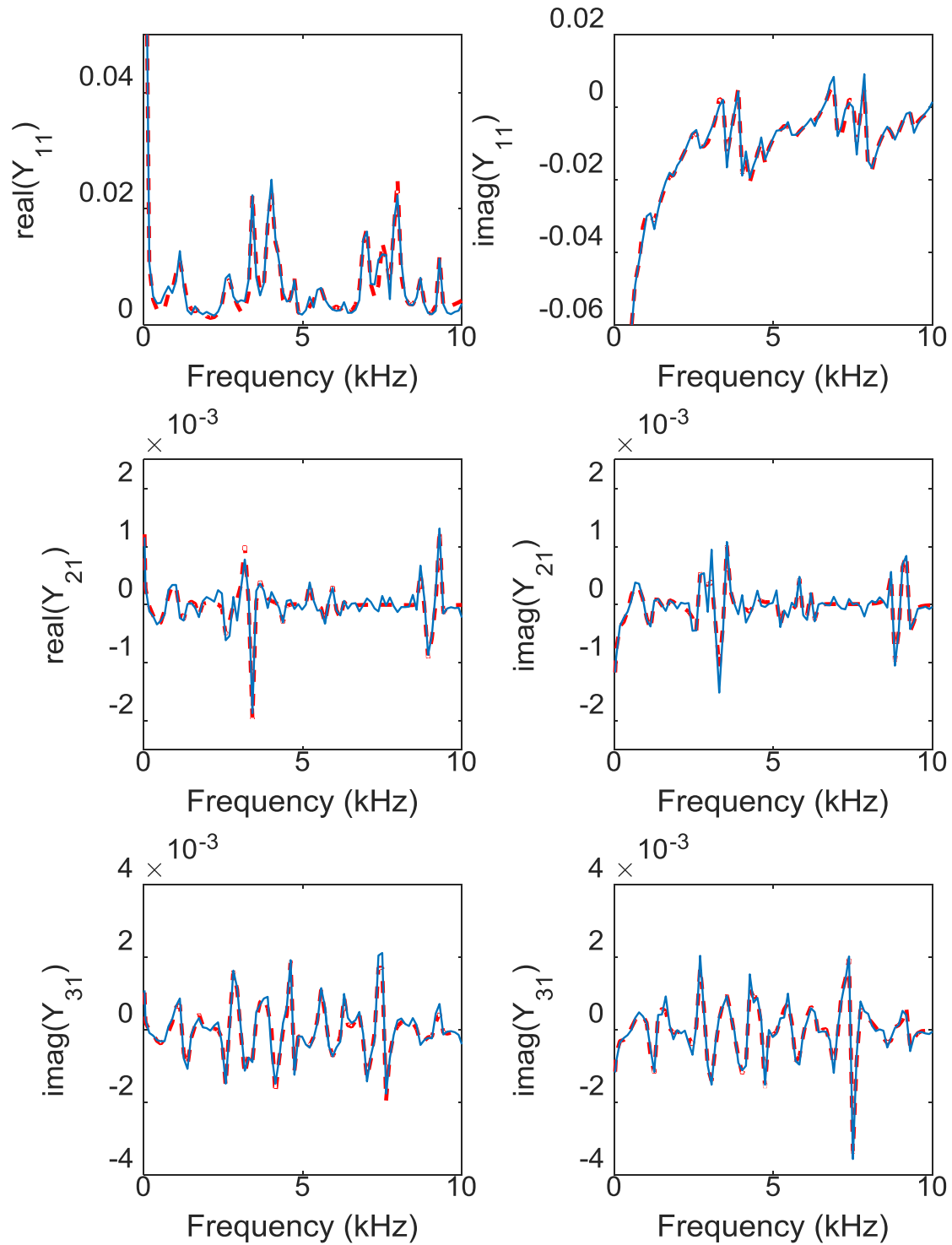


Figure 3.21 Comparison of the actual admittance (solid line) with the admittance of the equivalent circuit (dashed-line) for the first column of the admittance matrix in case four

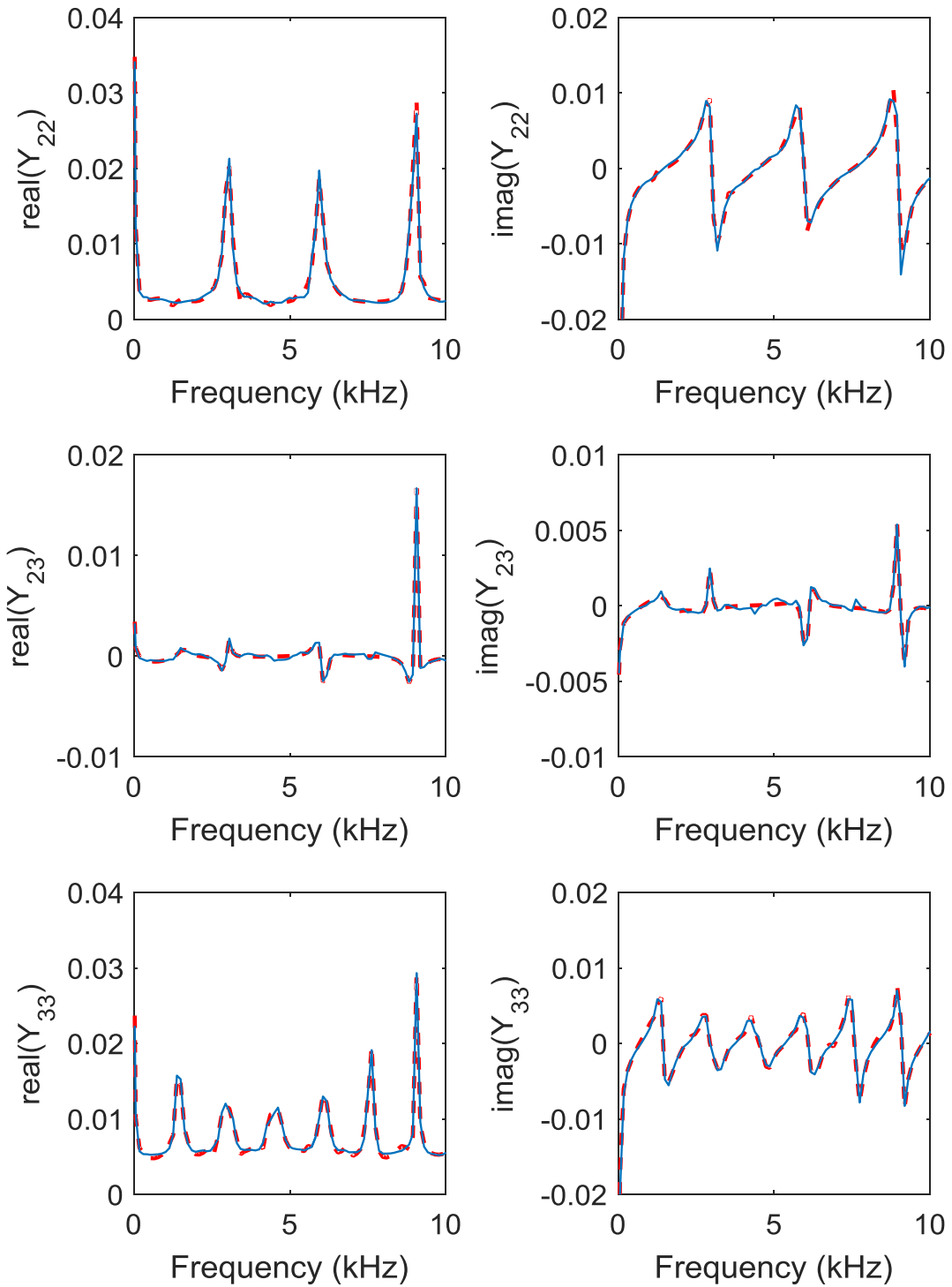


Figure 3.22 Comparison of the actual admittance (solid line) with the admittance of the equivalent circuit (dashed-line) for the rest of the lower triangle elements of the admittance matrix in case four

TABLE 3.7 Objective function value of fitting admittance elements for case four

| Element | Y_{01} | Y_{21} | Y_{31} | Y_{02} | Y_{32} | Y_{03} |
|-----------------|----------|----------|----------|----------|----------|----------|
| Objective Value | 0.0059 | 0.0012 | 0.0013 | 0.0025 | 0.0015 | 0.0020 |

3.4.4.4 Time-domain simulation results

To further evaluate the performance of the method, the equivalent network is simulated in EMTDC/PSCAD and time domain simulations are done to compare the results obtained from the full network and the reduced one. The process of replacing the external network with the reduced one is presented in Appendix C. A balanced three-phase to ground fault is applied at bus 76 and the fault current at this bus is monitored. The results are shown in Figure 3.23. As it can be seen, the results of the full and reduced networks match with a very good accuracy.

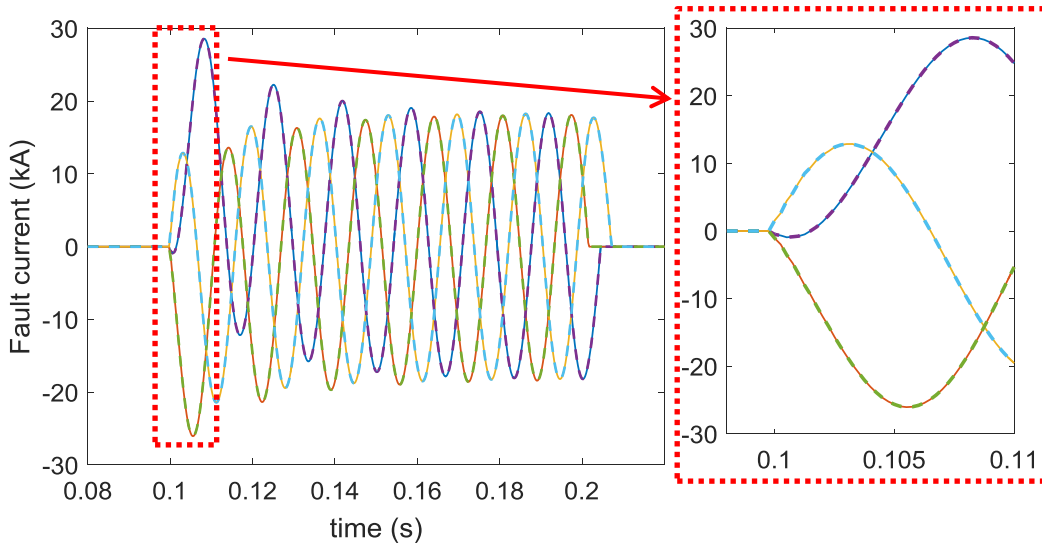


Figure 3.23 Fault current of the full (solid lines) and reduced (dashed-lined) networks

3.4.4.5 Passivity

As mentioned in the introduction, the equivalent model should be passive to ensure the stability of the time domain simulations. For the multi-port case, the real part of the admittance matrix should be semi-positive definite (i.e. the eigenvalues should be non-negative). The eigenvalues of the admittance matrix of the equivalent are shown in Figure 3.24.

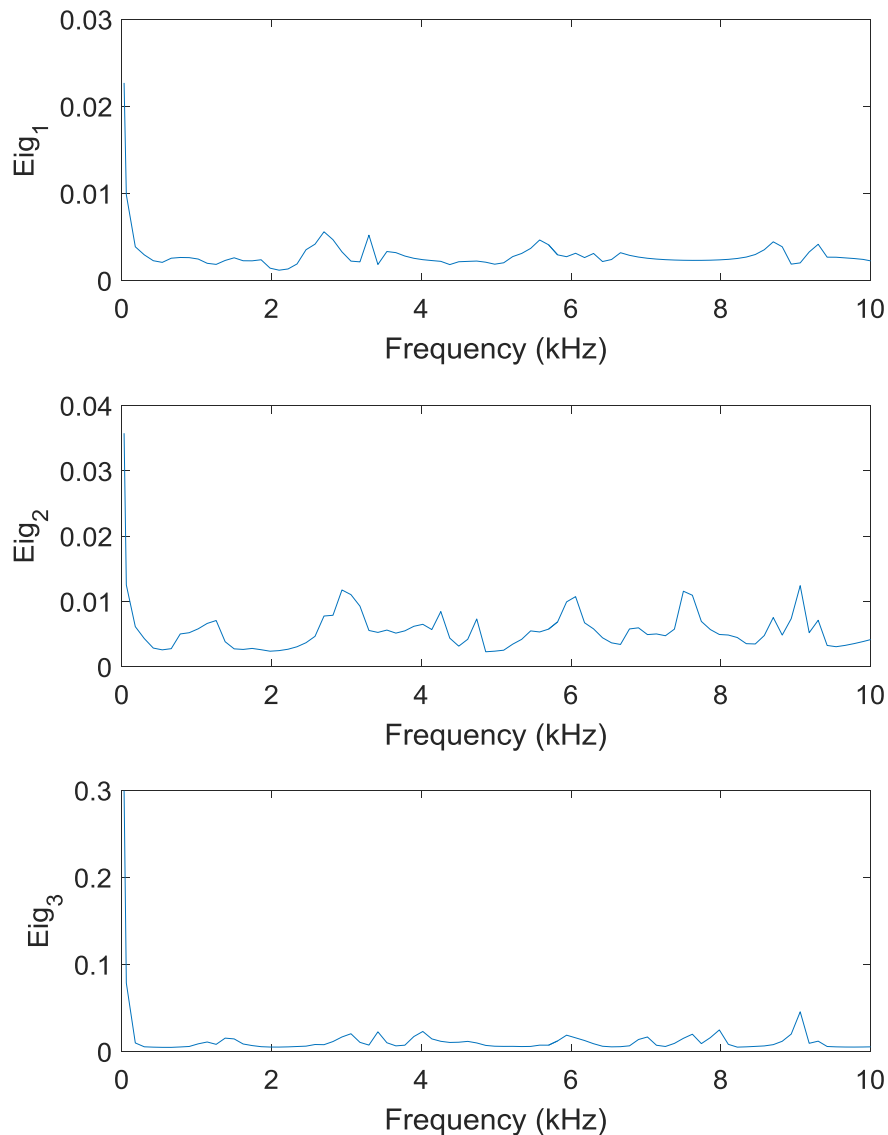


Figure 3.24 The eigenvalues of the equivalent network admittance matrix in case four

As it can be seen, the eigenvalues are all positive and as a result, the equivalent circuit found by the proposed method in case 4 is indeed passive. Therefore, the stability of time domain simulations is guaranteed. In general, additional constraints should be added to the optimization problem to ensure the passivity of the equivalent. It should be noticed that the actual frequency response is passive, because the sources are modeled separately. Therefore, any passivity violation comes from equivalencing error. As a result, if the equivalent is modeled with good accuracy, the passivity violation, if there is any, should be small. Increasing the number of branches in the equivalent model, which in turn increases the accuracy, might be a possible solution to fix the passivity violation.

The other point worth mentioning is that in power system application, there is usually a boundary zone between the study system and the external system, similar to case 4. This boundary zone provides additional damping and needs to be considered in passivity enforcement. Therefore, even if the external system slightly violates the passivity requirement, because of having this boundary zone, the overall response seen from the internal system might still be stable.

3.5 Conclusion

A new method for finding the FDNE of a power system has been proposed in this chapter. The optimization problem has been formulated and additional constraints have been added to ensure that the equivalent is stable. The main contributions of this chapter are a) proposing a new coding scheme to improve the convergence rate of the optimization methods, b) applying different heuristics methods to choose the proper method for finding the optimal parameters, and c) proposing a new equivalent model consisting of all-positive and all-negative branches for multi-port FDNE.

Four case studies have been considered to evaluate the performance of the proposed methods. For the single-port cases, the simulation results proved that the method was able to find accurate equivalent circuits while the stability was guaranteed by utilizing only passive elements in the equivalent circuit. For the

Chapter 3: Frequency Dependent Network Equivalent

multi-port case, the simulation results verified that the method could successfully find accurate equivalent circuits for all of the elements of the given multi-port admittance data while only stable branches were used in the equivalent circuits.

Chapter 4

Transmission Line Parameter

Measurement

Before a new line is put in service, it is always necessary to find the electrical parameters of this line for applications like protective relay settings. Rapid development of power systems has resulted in increased number of transmission lines sharing the same corridor. In this case, there is a strong electromagnetic coupling between the two lines [63] which lead to high induced voltages which make the parameter measurement of the new line a challenging task.

In this chapter, a new method for measuring the electrical parameters of parallel transmission lines is proposed. The method is meant for measuring the parameters of a line disconnected from the grid in parallel with an energized line. The key idea of the method is to consider the induced voltages as an excitation source rather than an interference source to avoid. A proper data collection method is proposed to improve the accuracy of the method. A set of data points obtained at different load conditions with different connections of the conductors of the new line is used to find the line parameters. The unknowns are found in two steps by applying the least-squares method.

4.1 Literature Review

Parameters of transmission lines are commonly calculated based on geometric parameters of tower and conductors, conductor type, soil characteristics, etc. [43], [44]. The results can have large errors due to the fact that

values for the input data may differ from the actual values [47]. Reference [2] discusses some sources of inaccuracies in the calculated line parameters including environmental factors like temperature and soil resistance [48], modeling inaccuracies like neglecting parallel lines coupling, and human factors.

As a result, it is a common industry practice that line parameters must be measured before a new line is put in service. For instance, in China after a transmission line is constructed, upgraded, or maintained, it is required by industry regulations that the line parameters have to be measured [49]. Transmission line measurement is also recommended by North American Electric Reliability Corporation for transmission line as-built verification practices [50]. This has resulted in the development of off-line methods for line parameter measurement. These methods require the transmission line to be disconnected from the grid. In recent years, progresses have also been made in online measurement of line parameters. Different parameter estimation methods are categorized in Figure 4.1.

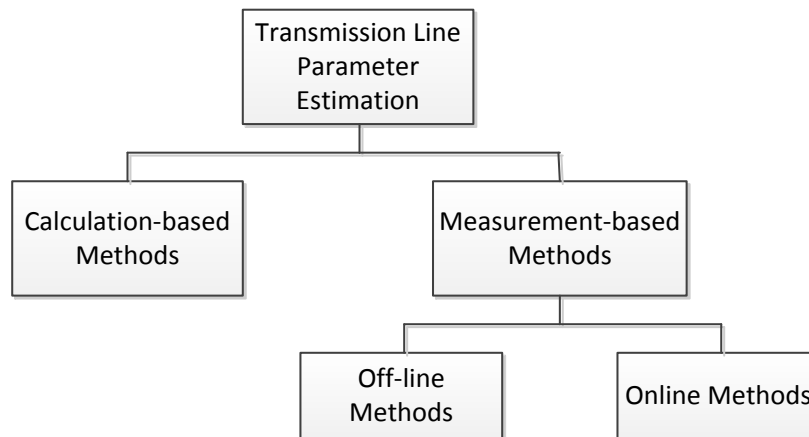


Figure 4.1 Transmission line parameter estimation methods

Various online approaches based on SCADA and/or PMU data have been developed in the literature [51]- [56]. Regardless of these developments, the need to measure the line parameters before it is energized always exists. There is little challenge for this task when a single line is involved and commercial products are already available to do the measurement [57]. However, the problem is more

complicated when parallel transmission lines are considered due to mutual couplings between the two transmission lines. In fact, parallel transmission lines sharing the same corridor or tower are one of the main power-frequency interference sources [58].

A method for estimating the zero-sequence parameters of double-circuit transmission lines is proposed in [59]. The method assumes that both lines are offline; therefore there is no interference problem. The method has a good accuracy but it is not applicable to the case when one of the lines is already in service.

Conventional methods for measuring the parameters of an offline transmission line assume grounded tail end and then apply an external voltage source at the head end to measure line impedance. To deal with power-frequency interference, these methods usually perform the measurements at different frequencies, e.g. ± 10 Hz around the fundamental frequency [45].

Methods based on analysing the frequency response of the line have also been proposed. The method proposed in [46] uses the impedances measured at the head end of the line with the tail end open- and short-circuited at a wide frequency range to calculate the line propagation constant and characteristic impedance. Another frequency response based approach is proposed in [45]. The measurement scheme used in this method is shown in Figure 4.2.

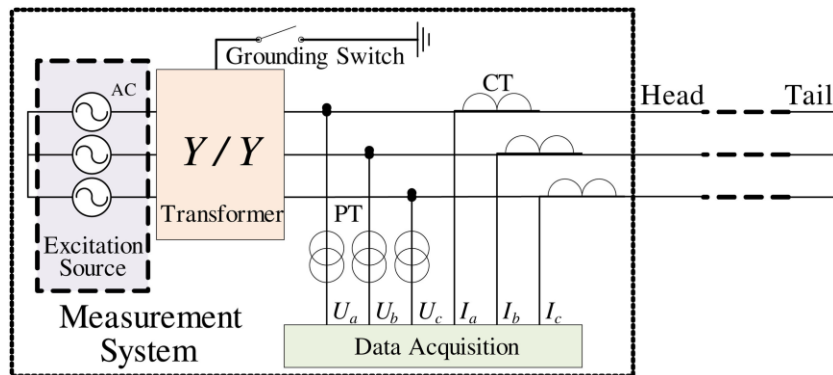


Figure 4.2 Measurement scheme used in [45]

These methods require a variable frequency excitation source that has to withstand a high voltage induced by the other transmission line. For instance, the induced voltage for a case reported in [45] can reach 14.48 kV which is high enough to cause insulation problems. Therefore, high voltage equipment is required to implement these methods which increases the overall implementation cost of these methods.

In view of these considerations, a new method for measuring the electrical parameters of parallel transmission lines is proposed in this chapter. The method is meant for off-line measurement of the parameters of a line not connected to the grid which shares the same corridor with a parallel energized line. The key advantage of the method is that it utilizes the induced voltage as an excitation source instead of considering it as an interference source which has to be avoided. Therefore, it does not require an additional excitation source which reduces the hardware cost. A proper data collection method is also proposed to improve the accuracy.

4.2 Proposed Method

In this section, the proposed method for estimating the π -circuit parameters of a newly constructed transmission line in parallel with an existing transmission line will be presented. First, the line model is briefly reviewed and the case of parallel transmission line is discussed. The problem is mathematically formulated and the proposed method will be presented. Finally, the measurement scheme to collect the required data is presented.

4.2.1 Transmission Line Model

Representation of the transmission line for power system studies depends on the type of study and the length of the line. Generally, a transmission line can be represented by series resistance R , series inductance L , shunt capacitance C , and shunt conductance G . However, shunt conductance is usually neglected. The π -circuit model with half of the whole capacitance of the transmission line lumped

at each end and the series resistance and inductance lumped in between as shown in Figure 4.3 is commonly used for many power system studies [86].

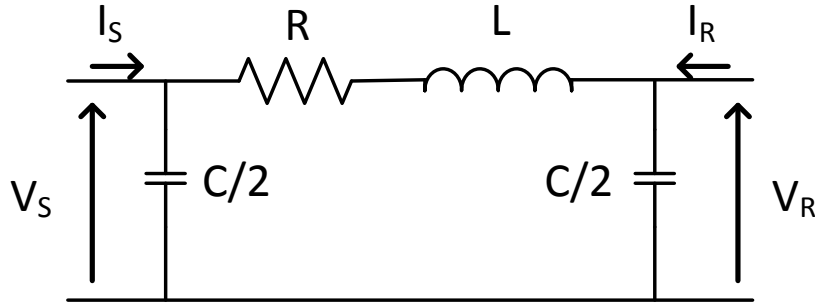


Figure 4.3 Equivalent π -circuit model of a transmission line

The following equation can be written for the circuit shown in Figure 4.3

$$V_S - V_R = (I_S - \frac{jB}{2} V_S) Z \quad (4.1)$$

$$I_S + I_R = (V_S + V_R) \frac{jB}{2} \quad (4.2)$$

where Z and B are the series impedance and shunt susceptance of the transmission line, respectively, found by

$$Z = R + j2\pi fL = R + jX \quad (4.3)$$

$$B = 2\pi fC \quad (4.4)$$

Equations (4.1) and (4.2) are also valid for multi-phase systems where V_S , V_R , I_S , and I_R are represented by vectors and Z and B are represented by matrices.

4.2.2 Parallel Transmission Lines

As mentioned before, the case considered in this thesis is a new transmission line that is built in the same corridor with an existing parallel transmission line as shown in Figure 4.4.

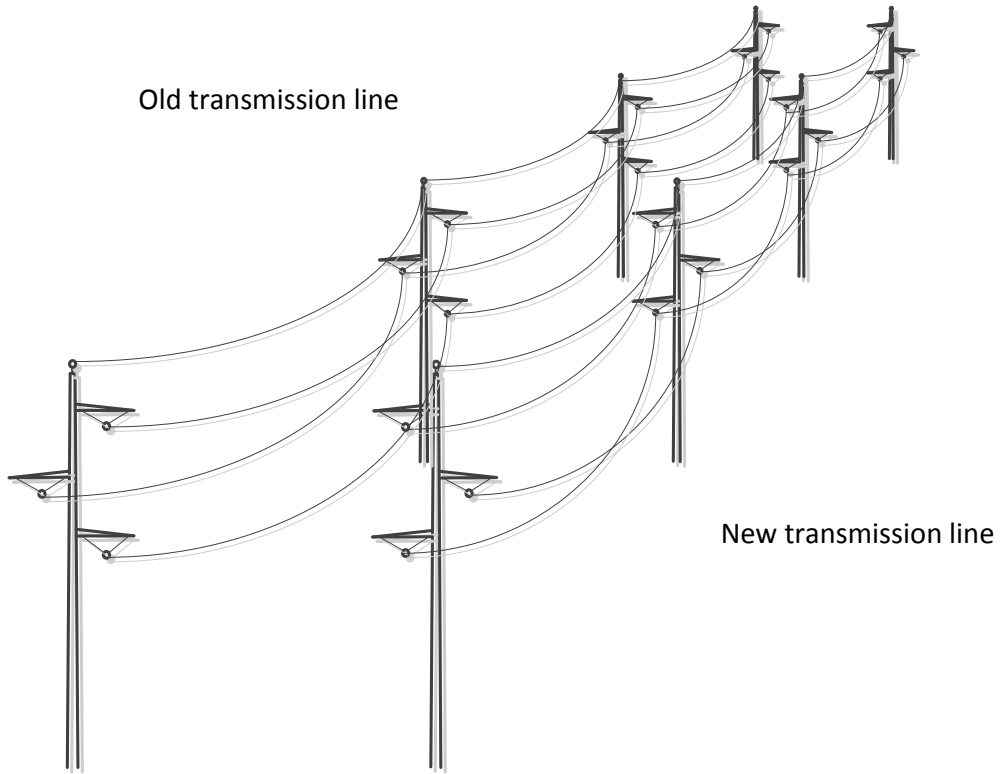


Figure 4.4 The old (connected to the grid) and new (not connected to the grid) transmission lines

The parameters of the two parallel transmission lines could be represented by the series impedance matrix and shunt susceptance matrix as

$$Z = \begin{bmatrix} Z_{a1} & Z_{a1b1} & Z_{a1c1} & Z_{a1a2} & Z_{a1b2} & Z_{a1c2} \\ Z_{a1b1} & Z_{b1} & Z_{b1c1} & Z_{b1a2} & Z_{b1b2} & Z_{b1c2} \\ Z_{a1c1} & Z_{b1c1} & Z_{c1} & Z_{c1a2} & Z_{c1b2} & Z_{c1c2} \\ Z_{a1a2} & Z_{b1a2} & Z_{c1a2} & Z_{a2} & Z_{a2b2} & Z_{a2c2} \\ Z_{a1b2} & Z_{b1b2} & Z_{c1b2} & Z_{a2b2} & Z_{b2} & Z_{b2c2} \\ Z_{a1c2} & Z_{b1c2} & Z_{c1c2} & Z_{a2c2} & Z_{b2c2} & Z_{c2} \end{bmatrix} \quad (4.5)$$

$$B = \begin{bmatrix} B_{a1} & B_{a1b1} & B_{a1c1} & B_{a1a2} & B_{a1b2} & B_{a1c2} \\ B_{a1b1} & B_{b1} & B_{b1c1} & B_{b1a2} & B_{b1b2} & B_{b1c2} \\ B_{a1c1} & B_{b1c1} & B_{c1} & B_{c1a2} & B_{c1b2} & B_{c1c2} \\ B_{a1a2} & B_{b1a2} & B_{c1a2} & B_{a2} & B_{a2b2} & B_{a2c2} \\ B_{a1b2} & B_{b1b2} & B_{c1b2} & B_{a2b2} & B_{b2} & B_{b2c2} \\ B_{a1c2} & B_{b1c2} & B_{c1c2} & B_{a2c2} & B_{b2c2} & B_{c2} \end{bmatrix} \quad (4.6)$$

If the symmetry of these matrices is considered, there are forty two unknowns in Z including twenty one resistances and twenty one inductances. Also, there are twenty one unknowns in B . Therefore, in total, there are sixty three unknown parameters. However, the main focus is on the parameters of the new transmission line and the mutual couplings between the phase conductors of the two transmission lines. Therefore, only the lower halves of these matrices are needed to be found.

The circuit diagram of the two lines is shown in Figure 4.5. It should be mentioned that only mutually coupled susceptances and impedances connected to phase-A of the new line are shown in this figure. The rest of the coupled elements are not shown, but they have been considered in the calculations. The terminals on the left side are considered as the sending end and the terminals on the right side are considered as the receiving end in the formulation. The shunt element connected between phase-A of the new line and the ground is found by

$$B_{a20} = B_{a2} + B_{b2a2} + B_{c2a2} + B_{a1a2} + B_{b1a2} + B_{c1a2} \quad (4.7)$$

Similar formula could be applied to find the values of the shunt susceptances between the other phase conductors of the two lines and the ground.

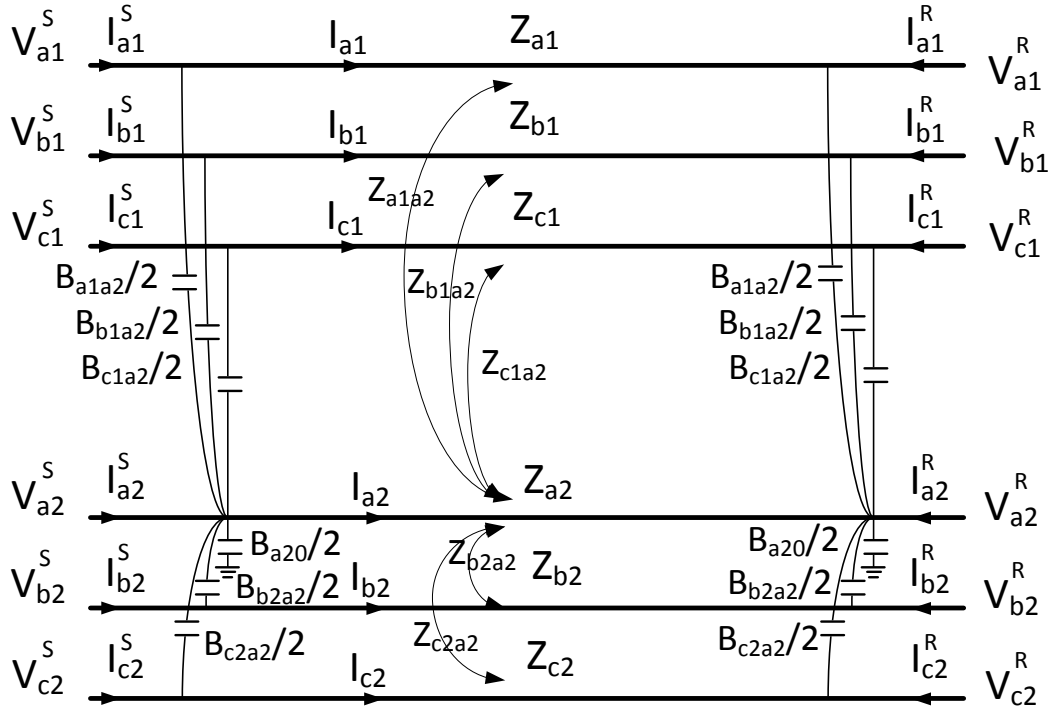


Figure 4.5 The circuit diagram showing the mutual couplings between phase A of the new line and other phase conductors

4.2.3 Mathematical Formulation

As mentioned before, (4.1) and (4.2) could be written for multi-phase transmission lines. Since the parameters of the new line are of interest, the voltage difference equation presented in (4.1) is written for each phase of the new line as

$$V_{a2}^S - V_{a2}^R = I_{a1}Z_{a1a2} + I_{b1}Z_{b1a2} + I_{c1}Z_{c1a2} + I_{a2}Z_{a2} + I_{b2}Z_{b2a2} + I_{c2}Z_{c2a2} \quad (4.8)$$

$$V_{b2}^S - V_{b2}^R = I_{a1}Z_{a1b2} + I_{b1}Z_{b1b2} + I_{c1}Z_{c1b2} + I_{a2}Z_{a2b2} + I_{b2}Z_{b2} + I_{c2}Z_{c2b2} \quad (4.9)$$

$$V_{c2}^S - V_{c2}^R = I_{a1}Z_{a1c2} + I_{b1}Z_{b1c2} + I_{c1}Z_{c1c2} + I_{a2}Z_{a2c2} + I_{b2}Z_{b2c2} + I_{c2}Z_{c2} \quad (4.10)$$

where V_{a2}^S and V_{a2}^R are the voltage phasors of phase A of the new line at the sending and receiving ends, respectively. I_{a2} , I_{b2} , ..., I_{c1} are the currents passing through the coupled impedances found by

Chapter 4: Transmission Line Parameter Measurement

$$I = I^S - jB / 2 \times V^S \quad (4.11)$$

where

$$I = [I_{a1}, I_{b1}, I_{c1}, I_{a2}, I_{b2}, I_{c2}]^T \quad (4.12)$$

$$I^S = [I_{a1}^S, I_{b1}^S, I_{c1}^S, I_{a2}^S, I_{b2}^S, I_{c2}^S]^T \quad (4.13)$$

$$V^S = [V_{a1}^S, V_{b1}^S, V_{c1}^S, V_{a2}^S, V_{b2}^S, V_{c2}^S]^T \quad (4.14)$$

where V_{a1}^S and I_{a1}^S are the voltage and current phasors of phase A of the old line at the sending end, respectively. I_{a2}^S is the current phasors of phase A of the new line at the sending end.

Equation (4.8) is expanded to better see the unknowns involved in it

$$\begin{aligned} V_{a2}^S - V_{a2}^R = & [I_{a1}^S - j(B_{a1}V_{a1}^S + B_{a1b1}V_{b1}^S + B_{a1c1}V_{c1}^S + B_{a1a2}V_{a2}^S + B_{a1b2}V_{b2}^S + B_{a1c2}V_{c2}^S) / 2]Z_{a1a2} \\ & + [I_{b1}^S - j(B_{a1b1}V_{a1}^S + B_{b1}V_{b1}^S + B_{b1c1}V_{c1}^S + B_{b1a2}V_{a2}^S + B_{b1b2}V_{b2}^S + B_{b1c2}V_{c2}^S) / 2]Z_{b1a2} \\ & + [I_{c1}^S - j(B_{a1c1}V_{a1}^S + B_{b1c1}V_{b1}^S + B_{c1}V_{c1}^S + B_{c1a2}V_{a2}^S + B_{c1b2}V_{b2}^S + B_{c1c2}V_{c2}^S) / 2]Z_{c1a2} \\ & + [I_{a2}^S - j(B_{a1a2}V_{a1}^S + B_{b1a2}V_{b1}^S + B_{c1a2}V_{c1}^S + B_{a2}V_{a2}^S + B_{a2b2}V_{b2}^S + B_{a2c2}V_{c2}^S) / 2]Z_{a2} \\ & + [I_{b2}^S - j(B_{a1b2}V_{a1}^S + B_{b1b2}V_{b1}^S + B_{c1b2}V_{c1}^S + B_{a2b2}V_{a2}^S + B_{b2}V_{b2}^S + B_{b2c2}V_{c2}^S) / 2]Z_{b2a2} \\ & + [I_{c2}^S - j(B_{a1c2}V_{a1}^S + B_{b1c2}V_{b1}^S + B_{c1c2}V_{c1}^S + B_{a2c2}V_{a2}^S + B_{b2c2}V_{b2}^S + B_{c2}V_{c2}^S) / 2]Z_{c2a2} \end{aligned} \quad (4.15)$$

It can be seen that (4.8)-(4.10) are nonlinear equations with fifty one unknowns including fifteen unknown resistances, fifteen unknown reactances, and twenty one unknown shunts. It should be mentioned that similar equations could be written for the three phases of the old line, but they are ignored as the parameters of the old line are not of interest in the proposed method.

Additional equations can be obtained for the unknown shunts by writing the sum of currents at the sending and receiving ends of the lines, similar to (4.2).

Chapter 4: Transmission Line Parameter Measurement

$$I^S + I^R = \frac{jB}{2}(V^S + V^R) \quad (4.16)$$

where

$$I^R = [I_{a1}^R, I_{b1}^R, I_{c1}^R, I_{a2}^R, I_{b2}^R, I_{c2}^R]^T \quad (4.17)$$

$$V^R = [V_{a1}^R, V_{b1}^R, V_{c1}^R, V_{a2}^R, V_{b2}^R, V_{c2}^R]^T \quad (4.18)$$

V_{a1}^R and I_{a1}^R are the voltage and current phasors of phase A of the old line at the receiving end, respectively. I_{a2}^R is the current phasors of phase A of the new line at the receiving end.

Equation (4.16) is a linear equation with twenty one unknown shunts.

To sum up, there are fifty one unknown parameters that need to be found. In addition, for each measurement sample, there are eighteen equations available, which are in fact the three equations presented in (4.8)- (4.10) and the six equations presented in (4.16), separated to real and imaginary parts. The problem is finding the parameters that minimize the following function

$$\min_{R,X,B} e = \sum_{d=1}^{N_{data}} (|r_1^d|^2 + |r_2^d|^2 + \dots + |r_9^d|^2) \quad (4.19)$$

where

$$r_1^d = I_{a2}^d Z_{a2} + I_{b2}^d Z_{b2a2} + I_{c2}^d Z_{c2a2} + I_{a1}^d Z_{a1a2} + I_{b1}^d Z_{b1a2} + I_{c1}^d Z_{c1a2} - V_{a2}^{S,d} + V_{a2}^{R,d} \quad (4.20)$$

$$r_2^d = I_{a2}^d Z_{a2b2} + I_{b2}^d Z_{b2} + I_{c2}^d Z_{c2b2} + I_{a1}^d Z_{a1b2} + I_{b1}^d Z_{b1b2} + I_{c1}^d Z_{c1b2} - V_{b2}^{S,d} + V_{b2}^{R,d} \quad (4.21)$$

$$r_3^d = I_{a2}^d Z_{a2c2} + I_{b2}^d Z_{b2c2} + I_{c2}^d Z_{c2} + I_{a1}^d Z_{a1c2} + I_{b1}^d Z_{b1c2} + I_{c1}^d Z_{c1c2} - V_{c2}^{S,d} + V_{c2}^{R,d} \quad (4.22)$$

$$r_4^d = j[B_{a1}(V_{a1}^S + V_{a1}^R) + B_{a1b1}(V_{b1}^S + V_{b1}^R) + B_{a1c1}(V_{c1}^S + V_{c1}^R) + B_{a1a2}(V_{a2}^S + V_{a2}^R) + B_{a1b2}(V_{b2}^S + V_{b2}^R) + B_{a1c2}(V_{c2}^S + V_{c2}^R)] / 2 - (I_{a1}^S + I_{a1}^R) \quad (4.23)$$

$$r_5^d = j[B_{a1b1}(V_{a1}^S + V_{a1}^R) + B_{b1}(V_{b1}^S + V_{b1}^R) + B_{b1c1}(V_{c1}^S + V_{c1}^R) + B_{b1a2}(V_{a2}^S + V_{a2}^R) + B_{b1b2}(V_{b2}^S + V_{b2}^R) + B_{b1c2}(V_{c2}^S + V_{c2}^R)] / 2 - (I_{b1}^S + I_{b1}^R) \quad (4.24)$$

$$r_6^d = j[B_{a1c1}(V_{a1}^S + V_{a1}^R) + B_{b1c1}(V_{b1}^S + V_{b1}^R) + B_{c1}(V_{c1}^S + V_{c1}^R) + B_{c1a2}(V_{a2}^S + V_{a2}^R) + B_{c1b2}(V_{b2}^S + V_{b2}^R) + B_{c1c2}(V_{c2}^S + V_{c2}^R)] / 2 - (I_{c1}^S + I_{c1}^R) \quad (4.25)$$

$$r_7^d = j[B_{a1a2}(V_{a1}^S + V_{a1}^R) + B_{b1a2}(V_{b1}^S + V_{b1}^R) + B_{c1a2}(V_{c1}^S + V_{c1}^R) + B_{a2}(V_{a2}^S + V_{a2}^R) + B_{a2b2}(V_{b2}^S + V_{b2}^R) + B_{a2c2}(V_{c2}^S + V_{c2}^R)] / 2 - (I_{a2}^S + I_{a2}^R) \quad (4.26)$$

$$r_8^d = j[B_{a1b2}(V_{a1}^S + V_{a1}^R) + B_{b1b2}(V_{b1}^S + V_{b1}^R) + B_{c1b2}(V_{c1}^S + V_{c1}^R) + B_{a2b2}(V_{a2}^S + V_{a2}^R) + B_{b2}(V_{b2}^S + V_{b2}^R) + B_{b2c2}(V_{c2}^S + V_{c2}^R)] / 2 - (I_{b2}^S + I_{b2}^R) \quad (4.27)$$

$$r_9^d = j[B_{a1c2}(V_{a1}^S + V_{a1}^R) + B_{b1c2}(V_{b1}^S + V_{b1}^R) + B_{c1c2}(V_{c1}^S + V_{c1}^R) + B_{a2c2}(V_{a2}^S + V_{a2}^R) + B_{b2c2}(V_{b2}^S + V_{b2}^R) + B_{c2}(V_{c2}^S + V_{c2}^R)] / 2 - (I_{c2}^S + I_{c2}^R) \quad (4.28)$$

where d is the measurement point number and N_{data} is the total number of available measurements.

4.2.4 Solution Approach

In the previous part, the problem was formulated using nine complex equations. Each of these equations can be separated to real and imaginary part to obtain eighteen equations in total. Considering that there are fifty one unknowns, three measurements should be enough to obtain the unknowns. However, to deal with measurement error and noise, extra measurements are necessary. Therefore, the problem becomes an overdetermined nonlinear minimization problem.

Based on analyzing the equations mentioned in the previous section, a two-step method is applied to divide the nonlinear problem into two linear problems [56]. The advantage of this method is that in each step we are dealing with an overdetermined linear problem which can be solved using linear least-squares method.

Chapter 4: Transmission Line Parameter Measurement

First, (4.11) is manipulated and rewritten in the following form

$$\begin{bmatrix} A^{S,1} + A^{R,1} \\ A^{S,2} + A^{R,2} \\ \vdots \\ A^{S,N} + A^{R,N} \end{bmatrix} \mathbf{V} = \begin{bmatrix} B^1 \\ B^2 \\ \vdots \\ B^N \end{bmatrix} \quad (4.29)$$

where

$$X_B = [B_{a2}, B_{a2b2}, B_{a2c2}, B_{a2a1}, B_{a2b1}, B_{a2c1}, B_{b2}, B_{b2c2}, B_{b2a1}, B_{b2b1}, B_{b2c1}, B_{c2}, B_{c2a1}, B_{c2a2}, B_{c2c1}, B_{a1}, B_{a1b1}, B_{a1c1}, B_{b1}, B_{b1c1}, B_{c1}] \quad (4.30)$$

$$B^i = [I_{a2,i,real}^S + I_{a2,i,real}^R, I_{a2,i,imag}^S + I_{a2,i,imag}^R, I_{b2,i,real}^S + I_{b2,i,real}^R, I_{b2,i,imag}^S + I_{b2,i,imag}^R, I_{c2,i,real}^S + I_{c2,i,real}^R, I_{c2,i,imag}^S + I_{c2,i,imag}^R, I_{a1,i,real}^S + I_{a1,i,real}^R, I_{a1,i,imag}^S + I_{a1,i,imag}^R, I_{b1,i,real}^S + I_{b1,i,real}^R, I_{b1,i,imag}^S + I_{b1,i,imag}^R, I_{c1,i,real}^S + I_{c1,i,real}^R, I_{c1,i,imag}^S + I_{c1,i,imag}^R]^T \quad (4.31)$$

$$A^{S,i} = [A_{Left}^{S,i} \quad A_{Mid}^{S,i} \quad A_{Right}^{S,i}] \quad (4.32)$$

where

$$A_{Left}^{S,i} = \begin{bmatrix} V_{a2,i,re}^S & V_{b2,i,re}^S & V_{c2,i,re}^S & V_{a1,i,re}^S & V_{b1,i,re}^S & V_{c1,i,re}^S & 0 \\ V_{a2,i,im}^S & V_{b2,i,im}^S & V_{c2,i,im}^S & V_{a1,i,im}^S & V_{b1,i,im}^S & V_{c1,i,im}^S & 0 \\ 0 & V_{a2,i,re}^S & 0 & 0 & 0 & 0 & V_{b2,i,re}^S \\ 0 & V_{a2,i,im}^S & 0 & 0 & 0 & 0 & V_{b2,i,im}^S \\ 0 & 0 & V_{a2,i,re}^S & 0 & 0 & 0 & 0 \\ 0 & 0 & V_{a2,i,im}^S & 0 & 0 & 0 & 0 \\ 0 & 0 & 0 & V_{a2,i,re}^S & 0 & 0 & 0 \\ 0 & 0 & 0 & V_{a2,i,im}^S & 0 & 0 & 0 \\ 0 & 0 & 0 & 0 & V_{a2,i,re}^S & 0 & 0 \\ 0 & 0 & 0 & 0 & V_{a2,i,im}^S & 0 & 0 \\ 0 & 0 & 0 & 0 & 0 & V_{a2,i,re}^S & 0 \\ 0 & 0 & 0 & 0 & 0 & V_{a2,i,im}^S & 0 \end{bmatrix} \quad (4.33)$$

$$A_{Mid}^{S,i} = \begin{bmatrix} 0 & 0 & 0 & 0 & 0 & 0 & 0 \\ 0 & 0 & 0 & 0 & 0 & 0 & 0 \\ V_{c2,i,re}^S & V_{a1,i,re}^S & V_{b1,i,re}^S & V_{c1,i,re}^S & 0 & 0 & 0 \\ V_{c2,i,im}^S & V_{a1,i,im}^S & V_{b1,i,im}^S & V_{c1,i,im}^S & 0 & 0 & 0 \\ V_{b2,i,re}^S & 0 & 0 & 0 & V_{c2,i,re}^S & V_{a1,i,re}^S & V_{b1,i,re}^S \\ V_{b2,i,im}^S & 0 & 0 & 0 & V_{c2,i,im}^S & V_{a1,i,im}^S & V_{b1,i,im}^S \\ 0 & V_{b2,i,re}^S & 0 & 0 & 0 & V_{c2,i,re}^S & 0 \\ 0 & V_{b2,i,im}^S & 0 & 0 & 0 & V_{c2,i,im}^S & 0 \\ 0 & 0 & V_{b2,i,re}^S & 0 & 0 & 0 & V_{c2,i,re}^S \\ 0 & 0 & V_{b2,i,im}^S & 0 & 0 & 0 & V_{c2,i,im}^S \\ 0 & 0 & 0 & V_{b2,i,re}^S & 0 & 0 & 0 \\ 0 & 0 & 0 & V_{b2,i,im}^S & 0 & 0 & 0 \end{bmatrix} \quad (4.34)$$

$$A_{Right}^{S,i} = \begin{bmatrix} 0 & 0 & 0 & 0 & 0 & 0 & 0 \\ 0 & 0 & 0 & 0 & 0 & 0 & 0 \\ 0 & 0 & 0 & 0 & 0 & 0 & 0 \\ 0 & 0 & 0 & 0 & 0 & 0 & 0 \\ V_{c1,i,re}^S & 0 & 0 & 0 & 0 & 0 & 0 \\ V_{c1,i,im}^S & 0 & 0 & 0 & 0 & 0 & 0 \\ 0 & V_{a1,i,re}^S & V_{b1,i,re}^S & V_{c1,i,re}^S & 0 & 0 & 0 \\ 0 & V_{a1,i,im}^S & V_{b1,i,im}^S & V_{c1,i,im}^S & 0 & 0 & 0 \\ 0 & 0 & V_{a1,i,re}^S & 0 & V_{b1,i,re}^S & V_{c1,i,re}^S & 0 \\ 0 & 0 & V_{a1,i,im}^S & 0 & V_{b1,i,im}^S & V_{c1,i,im}^S & 0 \\ V_{c2,i,re}^S & 0 & 0 & V_{a1,i,re}^S & 0 & V_{b1,i,re}^S & V_{c1,i,re}^S \\ V_{c2,i,im}^S & 0 & 0 & V_{a1,i,im}^S & 0 & V_{b1,i,im}^S & V_{c1,i,im}^S \end{bmatrix} \quad (4.35)$$

$A^{R,i}$ is formed in a similar way, using the receiving end voltages instead of the sending end voltages.

Equation (4.29) represents a linear overdetermined problem which can be solved by applying the least-squares method. At this step, the unknown parameters that minimize the following function are found

$$\min_B e_B = \sum_{d=1}^{N_{data}} (|r_4^d|^2 + |r_5^d|^2 + \dots + |r_9^d|^2) \quad (4.36)$$

Chapter 4: Transmission Line Parameter Measurement

After finding shunt elements, the series impedance elements have to be found. First, the currents passing through the coupled impedances are found using (4.11). Then, the voltage drop equations mentioned in (4.8)- (4.10) are manipulated and rewritten as

$$\begin{bmatrix} C^1 \\ C^2 \\ \vdots \\ C^N \end{bmatrix} \mathbf{v} = \begin{bmatrix} D^1 \\ D^2 \\ \vdots \\ D^N \end{bmatrix} \quad (4.37)$$

where

$$X_Z = [Z_{a2}, Z_{a2b2}, Z_{a2c2}, Z_{a2a1}, Z_{a2b1}, Z_{a2c1}, Z_{b2}, Z_{b2c2}, Z_{b2a1}, Z_{b2b1}, Z_{b2c1}, Z_{c2}, Z_{c2a1}, Z_{c2b1}, Z_{c2c1}] \quad (4.38)$$

$$C^i = \begin{bmatrix} I'_{a2,i} & I'_{b2,i} & I'_{c2,i} & I'_{a1,i} & I'_{b1,i} & I'_{c1,i} & 0 & 0 & 0 & 0 & 0 & 0 & 0 & 0 \\ 0 & I'_{a2,i} & 0 & 0 & 0 & 0 & I'_{b2,i} & I'_{c2,i} & I'_{a1,i} & I'_{b1,i} & I'_{c1,i} & 0 & 0 & 0 \\ 0 & 0 & I'_{a2,i} & 0 & 0 & 0 & 0 & I'_{b2,i} & 0 & 0 & 0 & I'_{c2,i} & I'_{a1,i} & I'_{b1,i} & I'_{c1,i} \end{bmatrix} \quad (4.39)$$

$$D^i = [V_{a2,i}^S - V_{a2,i}^R \quad V_{b2,i}^S - V_{b2,i}^R \quad V_{c2,i}^S - V_{c2,i}^R]^T \quad (4.40)$$

Equation (4.37) represents another linear overdetermined problem which can be solved by applying the least-squares method. At this step, the unknown parameters which minimize the following function are found

$$\min_{R,X} e_Z = \sum_{d=1}^{N_{data}} (|r_1^d|^2 + |r_2^d|^2 + |r_3^d|^2) \quad (4.41)$$

4.2.5 Measurement Scheme

According to the formulation presented in the previous section, voltage and current phasors at the sending and receiving ends of both lines are required. Therefore, measurement devices should be installed at these locations as shown in Figure 4.6. It should be noted that since the measurements are taken at different

locations, it is necessary that they are synchronized. Power Quality monitoring devices with GPS signal time tagging capability can be utilized for this purpose. After collecting measurement data at different locations, the time tags can be used to synchronize the collected data.

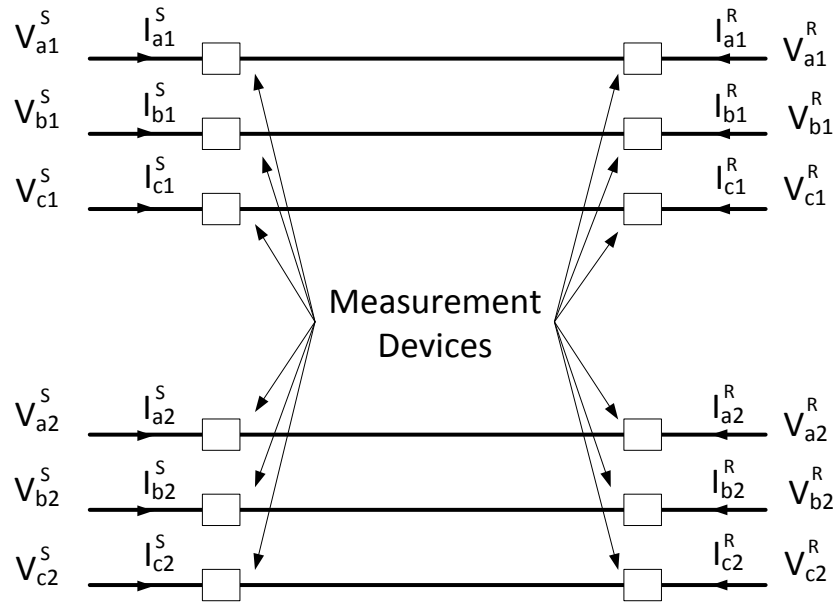


Figure 4.6 The measurement scheme for the proposed method

To collect the required data points, different connections of the secondary transmission line are used. The reason of using different connections is to collect data points with enough differences to be able to find the parameters with good accuracy. Otherwise, the collected data would be too similar, since the method only relies on the normal load variations in the old line. Each of the three phases of the new line could be either open circuit or short circuit at each end. Therefore, each phase could have four different connections shown in TABLE 4.1.

TABLE 4.1 Different connections for phase-A of the new line

| | Connection | | Connection |
|---|------------|---|------------|
| 1 | | 3 | |
| 2 | | 4 | |

Having more connections leads to having a better accuracy, but it requires more effort in practical implementation. Therefore, an optimal number of connections should be determined. A sensitivity study will be conducted in the next section to determine the desired number of connections.

4.2.6 Implementation Summary

The implementation process of the proposed method is summarized in the following steps:

- Step 1) Connect the conductors of the new lines according to the first defined connection.
- Step 2) Record measurement data points at defined time intervals.
- Step 3) Modify the connection of the conductors of the new line. If all of the desired connections are applied, continue to step 4. Otherwise, return to step 2.
- Step 4) Form the linear equations according to (4.29) and find the unknown shunt susceptances by applying the least-squares method.

Step 5) For each recorded measurement point, apply (4.11) and find the corresponding currents passing through the coupled impedances.

Step 6) Form the linear equations according to (4.37) and find the unknown series resistances and inductances by applying the least-squares method.

Step 7) Return the found shunt susceptances and series impedances as the output of the method.

4.3 Case Study

To evaluate the performance of the proposed method, two parallel transmission lines as shown in Figure 4.7 are considered. The parameters for these transmission lines are given in TABLE 4.2 and TABLE 4.3.

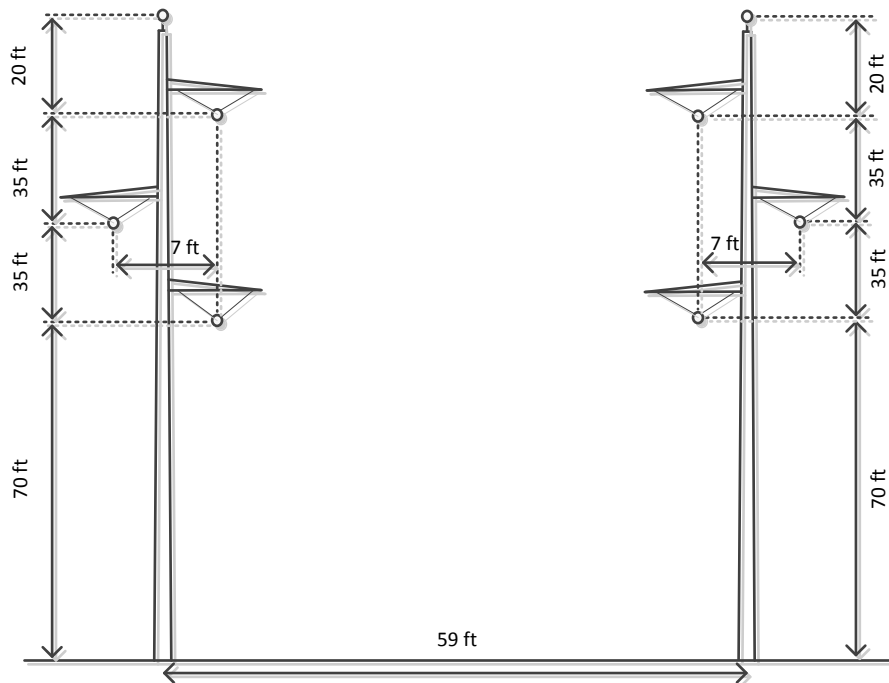


Figure 4.7 The diagram of the two parallel transmission line

TABLE 4.2 Case study parameters

| | |
|-----------------------|---------------|
| Frequency | 60 Hz |
| Line length | 160 km |
| Earth resistivity | 100 Ohm.Meter |
| Nominal line voltage | 350 kV |
| Nominal phase current | 2.600 kA |

TABLE 4.3 Conductor data for the case study

| Conductor name | X (ft) | Y tower (ft) | Y min (ft) | Outside diameter (inches) | T/D ratio | DC resistance (ohm/mi) | Number of conductors per bundle | Bundle diameter (inches) |
|----------------|--------|--------------|------------|---------------------------|-----------|------------------------|---------------------------------|--------------------------|
| Line1-phase1 | 7.75 | 140 | 110 | 1.465 | 0.04938 | 0.0657 | 2 | 18 |
| Line1-phase2 | 0.75 | 105 | 75 | 1.465 | 0.04938 | 0.0657 | 2 | 18 |
| Line1-phase3 | 7.75 | 70 | 40 | 1.465 | 0.04938 | 0.0657 | 2 | 18 |
| Line2-phase1 | 59.25 | 140 | 110 | 1.465 | 0.04938 | 0.0657 | 2 | 18 |
| Line2-phase2 | 66.25 | 105 | 75 | 1.465 | 0.04938 | 0.0657 | 2 | 18 |
| Line2-phase3 | 59.25 | 70 | 40 | 1.465 | 0.04938 | 0.0657 | 2 | 18 |
| Line1-shield | 2 | 160 | 130 | 0.5770 | 0.01852 | 0.5880 | 1 | - |
| Line2-shield | 65 | 160 | 130 | 0.5770 | 0.01852 | 0.5880 | 1 | - |

First, to get the equivalent R, L, and C matrices, RLC Line Parameters block of Matlab/Simulink is used. The obtained parameters are

$$r = \begin{bmatrix} 0.0872 & 0.0600 & 0.0566 & 0.0621 & 0.0581 & 0.0558 \\ 0.0600 & 0.0761 & 0.0535 & 0.0581 & 0.0549 & 0.0532 \\ 0.0566 & 0.0535 & 0.0724 & 0.0558 & 0.0532 & 0.0518 \\ 0.0621 & 0.0581 & 0.0558 & 0.0872 & 0.0600 & 0.0566 \\ 0.0581 & 0.0549 & 0.0532 & 0.0600 & 0.0761 & 0.0535 \\ 0.0558 & 0.0532 & 0.0518 & 0.0566 & 0.0535 & 0.0724 \end{bmatrix} \text{ (ohm / km)} \quad (4.42)$$

$$l = 1e-4 \times \begin{bmatrix} 14 & 4.7455 & 3.7858 & 3.5000 & 3.5361 & 3.3862 \\ 4.7455e & 15 & 5.6530 & 3.5361 & 4.1556 & 4.3733 \\ 3.7858 & 5.6530 & 16 & 3.3862 & 4.3733 & 5.2086 \\ 3.5000 & 3.5361 & 3.3862 & 14 & 4.7455 & 3.7858 \\ 3.5361 & 4.1556 & 4.3733 & 4.7455 & 15 & 5.6530 \\ 3.3862 & 4.3733 & 5.2086 & 3.7858 & 5.6530 & 16 \end{bmatrix} (H / km) \quad (4.43)$$

$$c = 1e-10 \times \begin{bmatrix} 102.02 & -17.979 & -5.4944 & -11.179 & -6.3144 & -3.2748 \\ -17.979 & 101.15 & -16.956 & -6.3144 & -6.4880 & -5.3986 \\ -5.4944 & -16.956 & 103.39 & -3.2748 & -5.3986 & -8.8413 \\ -11.179 & -6.3144 & -3.2748 & 102.02 & -17.979 & -5.4944 \\ -6.3144 & -6.4880 & -5.3986 & -17.979 & 101.15 & -16.956 \\ -3.2748 & -5.3986 & -8.8413 & -5.4944 & -16.956 & 103.39 \end{bmatrix} (F / km) \quad (4.44)$$

Using these parameters, a model is built in Matlab/Simulink to get the measurement data required for applying the method. To account for the measurement error, 1% noise is added to the data and the obtained data is considered as the measurement data. Load variations are considered to create the whole data set. It should be mentioned that the three-phase load is considered to be balanced. The model created in Matlab/Simulink is shown in Appendix D.

At the first step, the data set created using the Simulink model is used for finding the elements of B . To determine the optimal number of connections, 3, 6, 9, and 15 connections are considered. For each of them, one hundred independent data sets are generated and the average of the absolute relative percentage errors is shown in Figure 4.8.

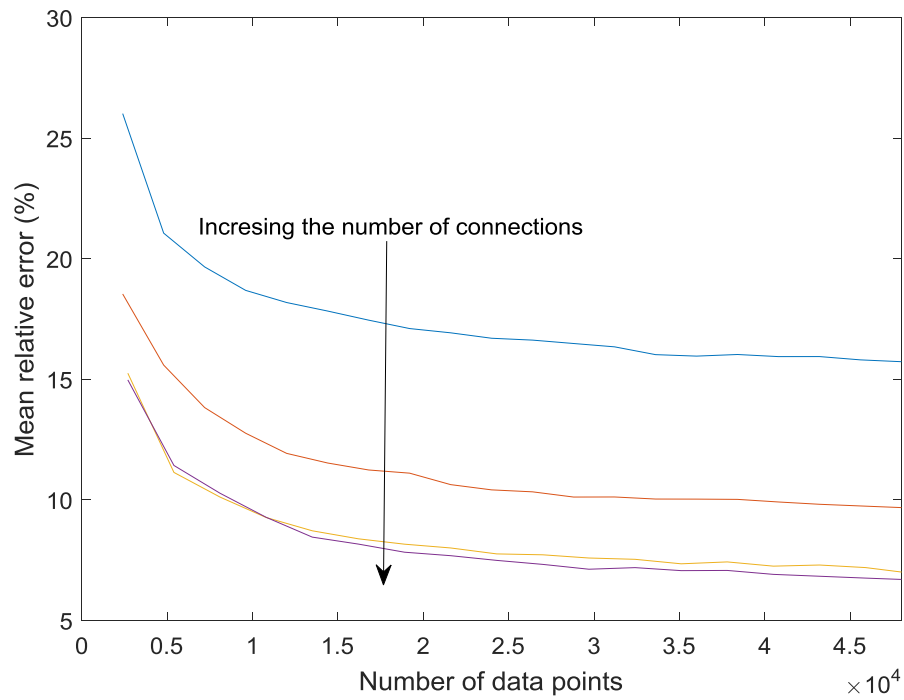


Figure 4.8 Mean error for different numbers of data points for 3, 6, 9, and 15 connections of the new line

As it can be seen in Figure 4.8, a better accuracy could be obtained by having more connections. But after nine connections, there is not much improvement in the accuracy. Therefore, the desired number of connections is chosen to be nine. The individual connections are shown in TABLE 4.4.

TABLE 4.4 Different connections of the new line conductors for collecting data

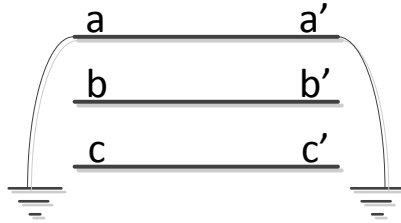
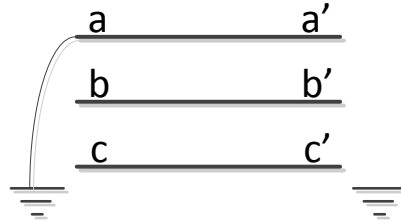
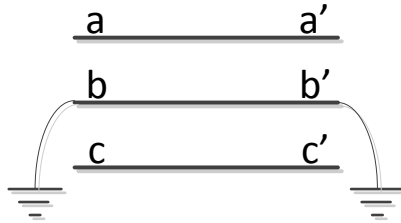
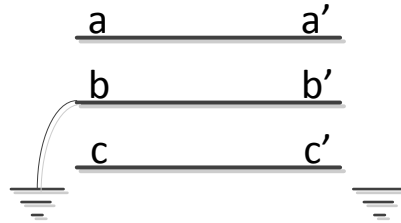
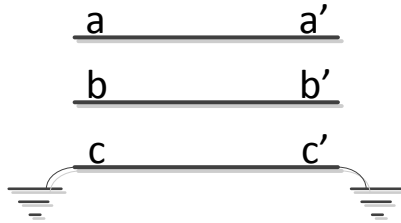
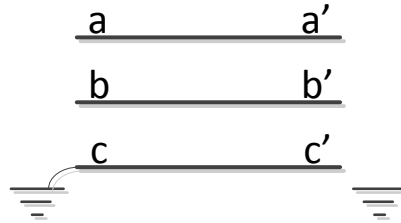
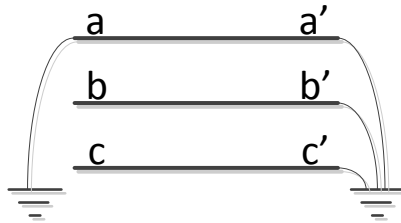
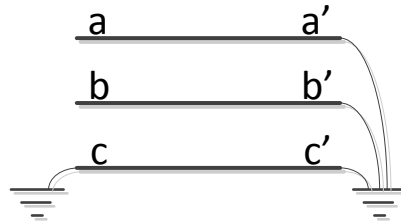
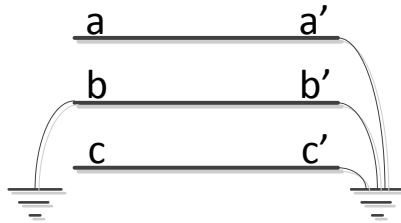
| | Connection | | Connection |
|---|---|---|--|
| 1 |  | 6 |  |
| 2 |  | 7 |  |
| 3 |  | 8 |  |
| 4 |  | 9 |  |
| 5 |  | | |

Figure 4.8 shows that having 3000 measurements per connection for each of the nine connections shown in TABLE 4.4 leads to less than eight percent mean error. To better show the results, 100 independent cases are created and the

obtained susceptances are compared with the actual values in Figure 4.9 and Figure 4.10.

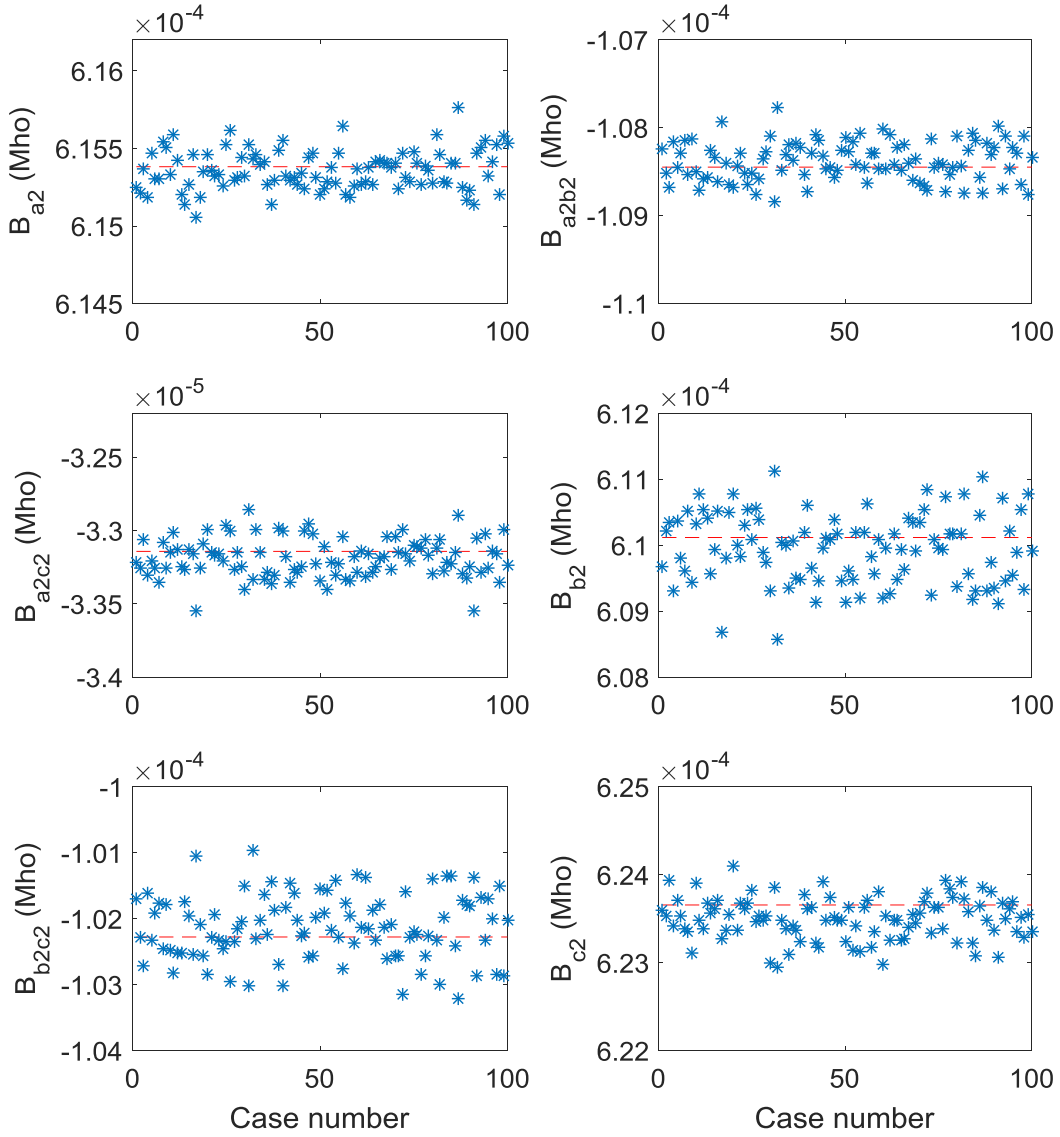


Figure 4.9 Comparison between the susceptances of the new line obtained by the method (blue stars) and the actual values (red dashed-line)

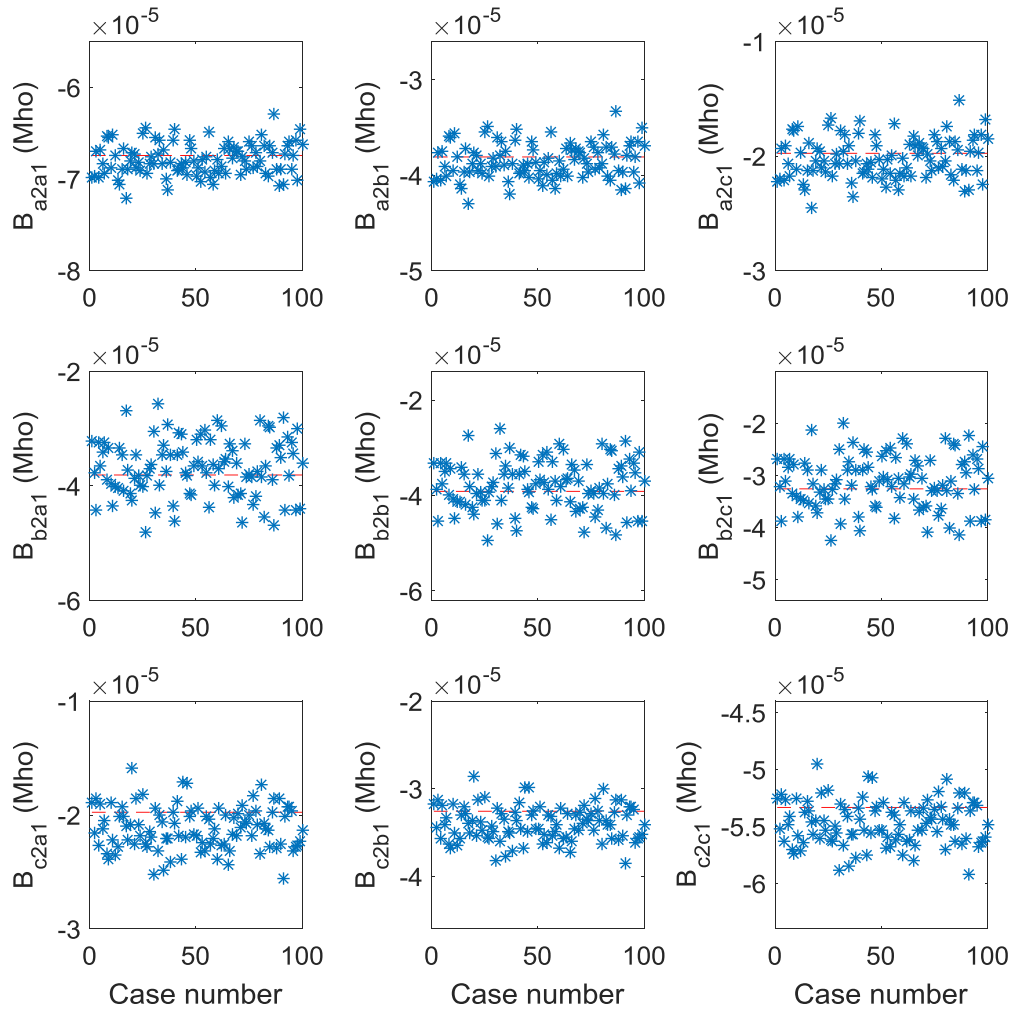


Figure 4.10 Comparison of the mutual susceptances between the two lines obtained by the method (blue stars) and the actual values (red dashed-line)

As it can be seen, the values obtained by the proposed method are close to the actual values. The next step is to apply the second least-squares method to get the series impedance values. For each of the 100 cases mentioned above, the obtained susceptance values are used to find the corresponding series impedances. The parameters obtained by the method are compared with the actual values in Figure 4.11 to Figure 4.14.

Chapter 4: Transmission Line Parameter Measurement

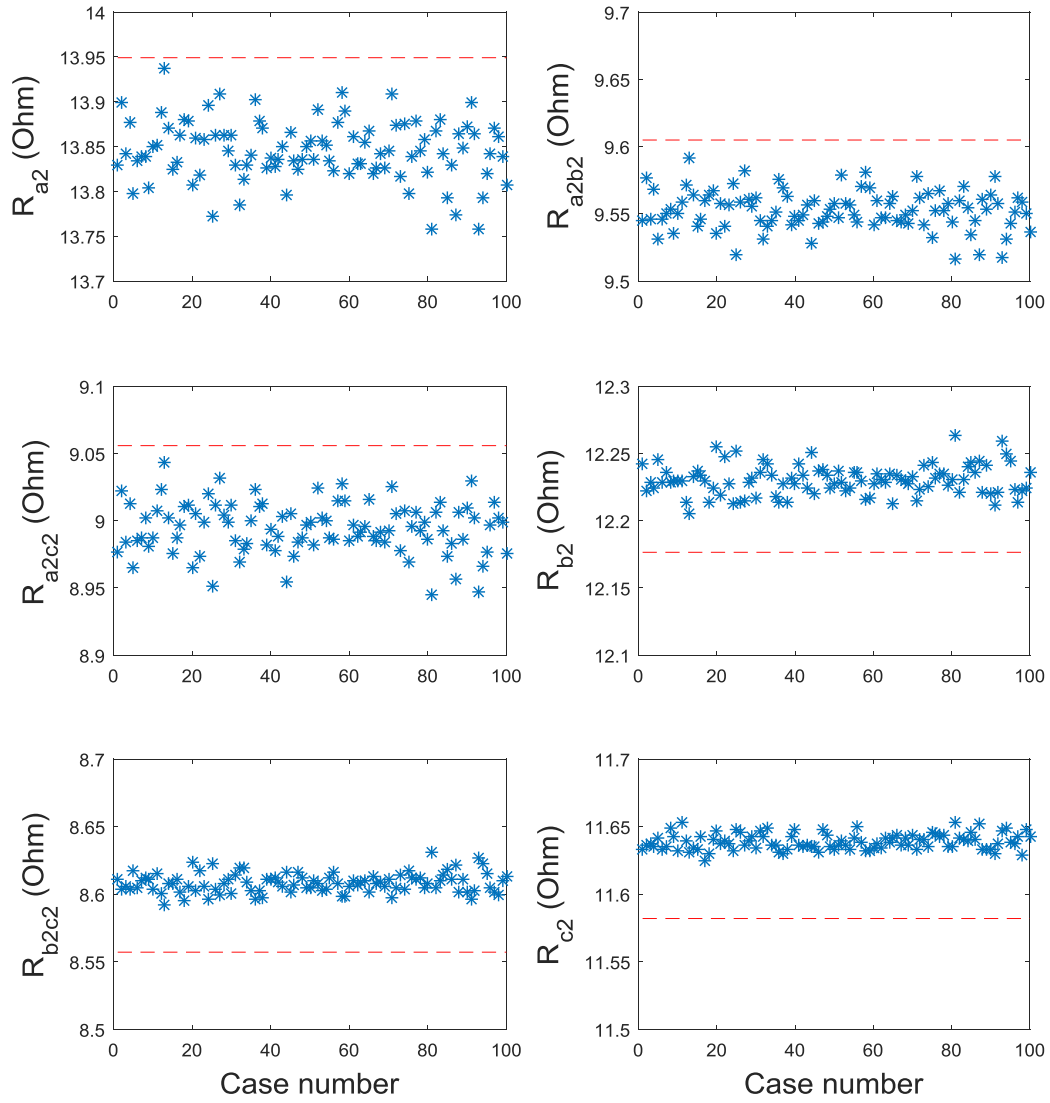


Figure 4.11 The resistance values obtained by the method (blue stars) and the actual values (red dashed-line)

Chapter 4: Transmission Line Parameter Measurement

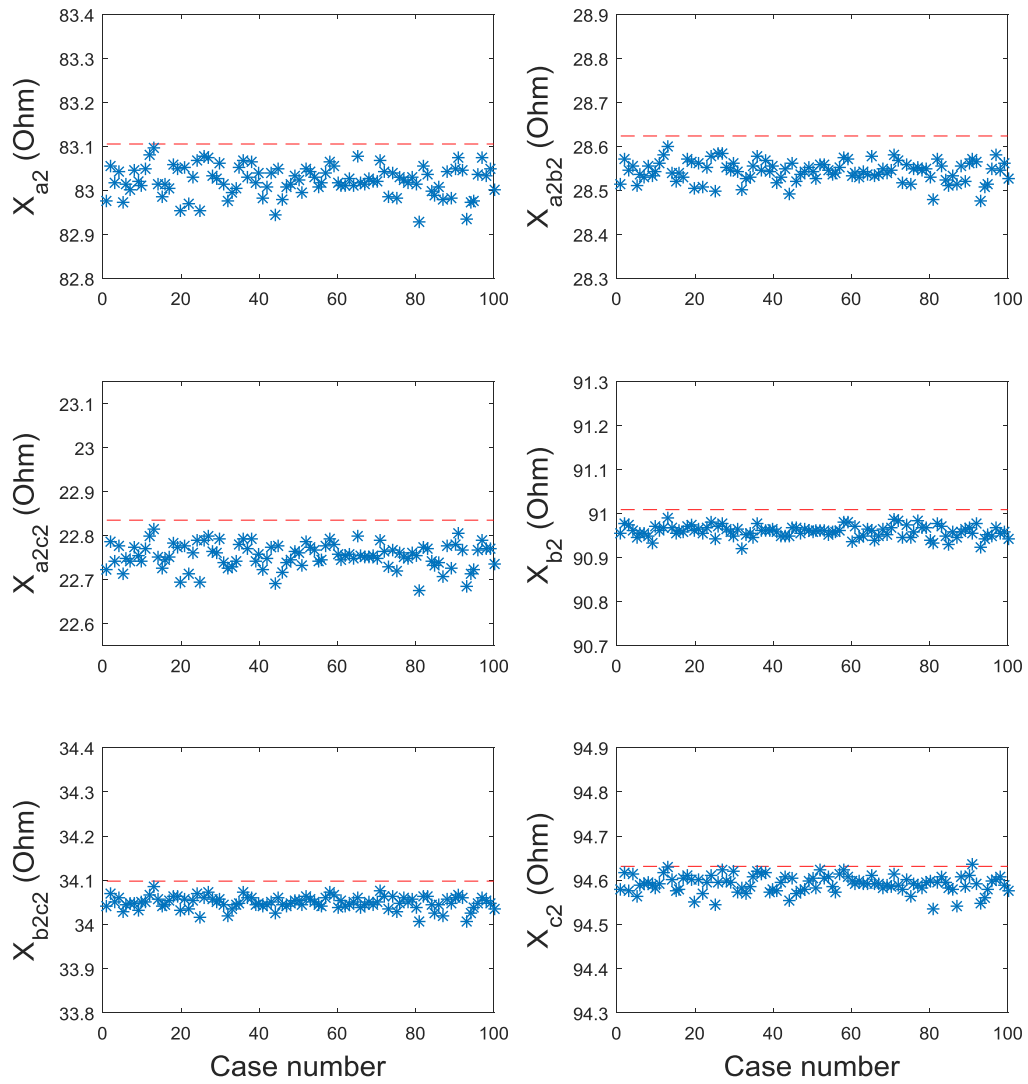


Figure 4.12 The inductance values obtained by the method (blue stars) and the actual values (red dashed-line)

Chapter 4: Transmission Line Parameter Measurement

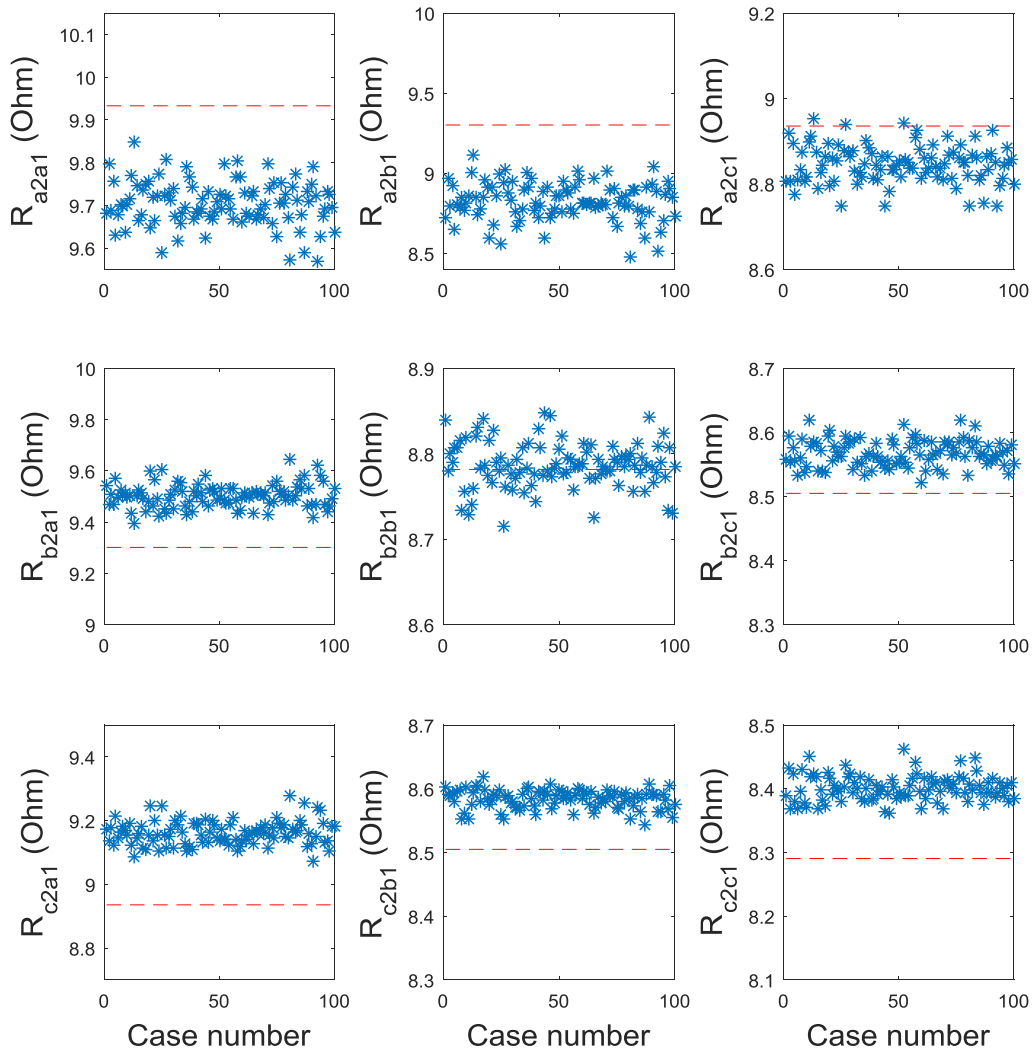


Figure 4.13 The mutual resistance values between the two lines obtained by the proposed method (blue stars) and the actual values (red dashed-line)

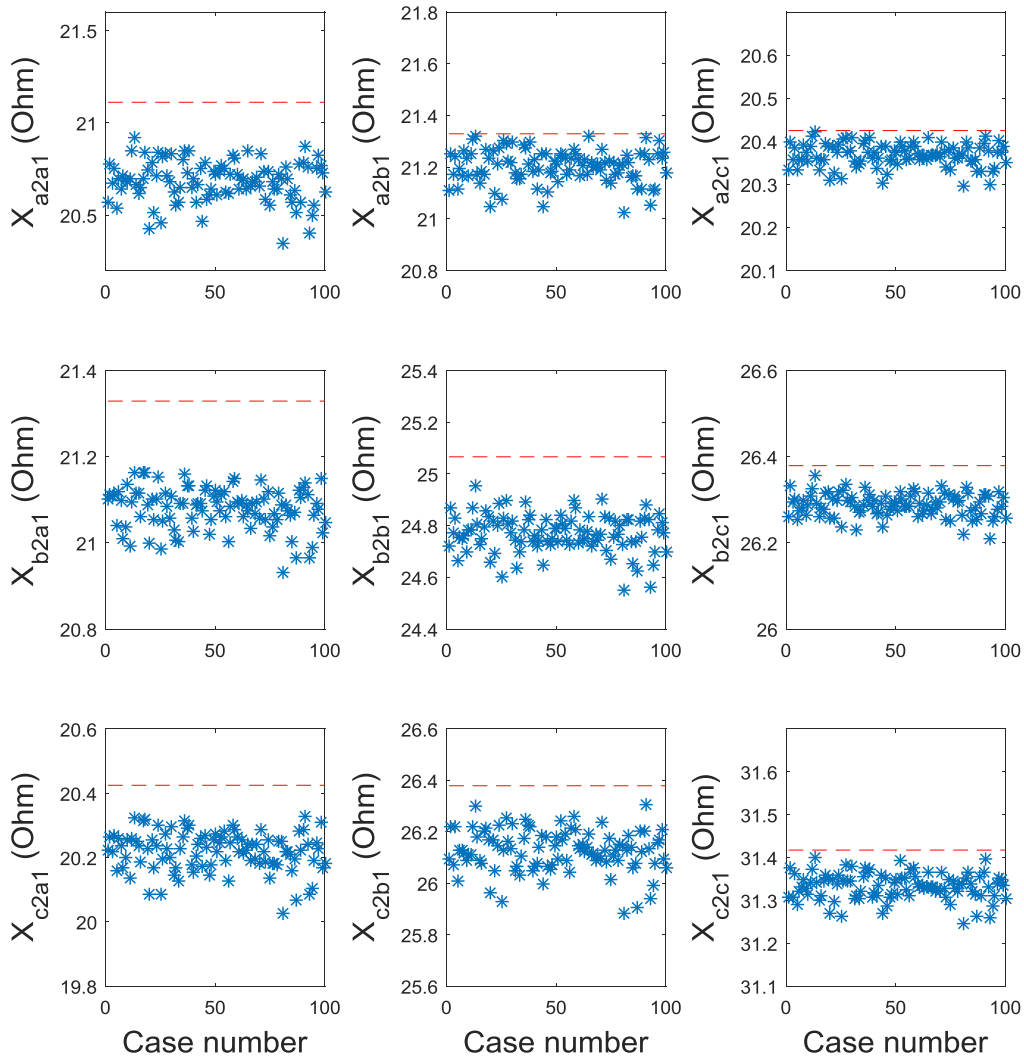


Figure 4.14 The mutual inductance values between the two lines obtained by the proposed method (blue stars) and the actual values (red dashed-line)

As it can be seen, the values obtained by the proposed method are close to the actual values. To summarize the results shown in Figure 4.9 to Figure 4.14, the accurate, mean, minimum, maximum, standard deviation, and average error of the line parameters are presented in TABLE 4.5 to TABLE 4.7

TABLE 4.5 The susceptances obtained by the proposed method compared with the accurate value

| Parameter | Accurate value (Mho) | Mean value (Mho) | Minimum value (Mho) | Maximum value (Mho) | Standard deviation (Mho) | Average error (%) |
|------------|----------------------|------------------|---------------------|---------------------|--------------------------|-------------------|
| B_{a2} | 6.1538e-4 | 6.1536e-4 | 6.1505e-4 | 6.1576e-4 | 1.2825e-7 | 0.0174 |
| B_{a2b2} | -1.0845e-4 | -1.0838e-4 | -1.0884e-4 | -1.0777e-4 | 2.2239e-7 | 0.1741 |
| B_{a2c2} | -3.3142e-5 | -3.3186e-5 | -3.3551e-5 | -3.2853e-5 | 1.3070e-7 | 0.3379 |
| B_{b2} | 6.1012e-4 | 6.0995e-4 | 6.0857e-4 | 6.1113e-4 | 5.3273e-7 | 0.0741 |
| B_{b2c2} | -1.0228e-4 | -1.0213e-4 | -1.0322e-4 | -1.0097e-4 | 4.9514e-7 | 0.4064 |
| B_{c2} | 6.2366e-4 | 6.2350e-4 | 6.2295e-4 | 6.2410e-4 | 2.3904e-7 | 0.0364 |
| B_{a2a1} | -6.7429e-5 | -6.7861e-5 | -7.2079e-5 | -6.2862e-5 | 1.7510e-6 | 2.2241 |
| B_{a2b1} | -3.8088e-5 | -3.8537e-5 | -4.2925e-5 | -3.3336e-5 | 1.8213e-6 | 4.0946 |
| B_{a2c1} | -1.9753e-5 | -2.0190e-5 | -2.4459e-5 | -1.5120e-5 | 1.7741e-6 | 7.6907 |
| B_{b2a1} | -3.8087e-5 | -3.6819e-5 | -4.7983e-5 | -2.5552e-5 | 4.9922e-6 | 10.9809 |
| B_{b2b1} | -3.9135e-5 | -3.7818e-5 | -4.9405e-5 | -2.6121e-5 | 5.1817e-6 | 11.0931 |
| B_{b2c1} | -3.2563e-5 | -3.1282e-5 | -4.2562e-5 | -1.9899e-5 | 5.0424e-6 | 12.9730 |
| B_{c2a1} | -1.9753e-5 | -2.1146e-5 | -2.5536e-5 | -1.5929e-5 | 1.8948e-6 | 9.6942 |
| B_{c2b1} | -3.2563e-5 | -3.4008e-5 | -3.8564e-5 | -2.8600e-5 | 1.9664e-6 | 6.1002 |
| B_{c2c1} | -5.3330e-5 | -5.4735e-5 | -5.9175e-5 | -4.9471e-5 | 1.9130e-6 | 3.6243 |

Chapter 4: Transmission Line Parameter Measurement

TABLE 4.6 The resistances obtained by the proposed method compared with the accurate value

| Parameter | Accurate value (Ohm) | Mean value (Ohm) | Minimum value (Ohm) | Maximum value (Ohm) | Standard deviation (Ohm) | Average error (%) |
|-------------------|----------------------|------------------|---------------------|---------------------|--------------------------|-------------------|
| R _{a2} | 13.9492 | 13.8457 | 13.7574 | 13.9366 | 0.0336 | 0.7420 |
| R _{a2b2} | 9.6049 | 9.5529 | 9.5163 | 9.5910 | 0.0145 | 0.5417 |
| R _{a2c2} | 9.0559 | 8.9944 | 8.9444 | 9.0432 | 0.0190 | 0.6784 |
| R _{b2} | 12.1766 | 12.2303 | 12.2056 | 12.2635 | 0.0111 | 0.4411 |
| R _{b2c2} | 8.5571 | 8.6084 | 8.5925 | 8.6310 | 0.0072 | 0.5990 |
| R _{c2} | 11.5820 | 11.6389 | 11.6250 | 11.6527 | 0.0059 | 0.4909 |
| R _{a2a1} | 9.9330 | 9.7047 | 9.5701 | 9.8474 | 0.0529 | 2.2981 |
| R _{a2b1} | 9.3014 | 8.8250 | 8.4739 | 9.1112 | 0.1179 | 5.1220 |
| R _{a2c1} | 8.9356 | 8.8462 | 8.7488 | 8.9533 | 0.0437 | 1.0065 |
| R _{b2a1} | 9.3014 | 9.5026 | 9.3970 | 9.6450 | 0.0462 | 2.1631 |
| R _{b2b1} | 8.7817 | 8.7867 | 8.7147 | 8.8483 | 0.0268 | 0.2335 |
| R _{b2c1} | 8.5049 | 8.5676 | 8.5220 | 8.6201 | 0.0206 | 0.7370 |
| R _{c2a1} | 8.9356 | 9.1613 | 9.0734 | 9.2789 | 0.0380 | 2.5255 |
| R _{c2b1} | 8.5049 | 8.5838 | 8.5425 | 8.6178 | 0.0149 | 0.9275 |
| R _{c2c1} | 8.2905 | 8.4013 | 8.3608 | 8.4622 | 0.0202 | 1.3355 |

TABLE 4.7 The reactances obtained by the proposed method compared with the accurate value

| Parameter | Accurate value (Ohm) | Mean value (Ohm) | Minimum value (Ohm) | Maximum value (Ohm) | Standard deviation (Ohm) | Average error (%) |
|------------|----------------------|------------------|---------------------|---------------------|--------------------------|-------------------|
| X_{a2} | 83.1056 | 83.0222 | 82.9289 | 83.0972 | 0.0339 | 0.1004 |
| X_{a2b2} | 28.6239 | 28.5436 | 28.4773 | 28.5998 | 0.0238 | 0.2805 |
| X_{a2c2} | 22.8355 | 22.7551 | 22.6743 | 22.8158 | 0.0280 | 0.3519 |
| X_{b2} | 91.0092 | 90.9597 | 90.9201 | 90.9897 | 0.0134 | 0.0544 |
| X_{b2c2} | 34.0982 | 34.0492 | 34.0079 | 34.0852 | 0.0143 | 0.1435 |
| X_{c2} | 94.6316 | 94.5920 | 94.5346 | 94.6351 | 0.0194 | 0.0420 |
| X_{a2a1} | 21.1113 | 20.6849 | 20.3443 | 20.9163 | 0.1094 | 2.0200 |
| X_{a2b1} | 21.3290 | 21.2026 | 21.0216 | 21.3211 | 0.0643 | 0.5926 |
| X_{a2c1} | 20.4249 | 20.3677 | 20.2955 | 20.4222 | 0.0266 | 0.2799 |
| X_{b2a1} | 21.3290 | 21.0798 | 20.9306 | 21.1647 | 0.0488 | 1.1683 |
| X_{b2b1} | 25.0662 | 24.7699 | 24.5523 | 24.9546 | 0.0733 | 1.1819 |
| X_{b2c1} | 26.3792 | 26.2881 | 26.2098 | 26.3561 | 0.0267 | 0.3453 |
| X_{c2a1} | 20.4249 | 20.2195 | 20.0245 | 20.3301 | 0.0606 | 1.0055 |
| X_{c2b1} | 26.3792 | 26.1270 | 25.8840 | 26.3067 | 0.0811 | 0.9558 |
| X_{c2c1} | 31.4174 | 31.3326 | 31.2470 | 31.3986 | 0.0310 | 0.2699 |

From the first six rows of TABLE 4.5 to TABLE 4.7, it can be seen that the method is very accurate in finding the parameters of the new line. The maximum errors for shunt susceptances, series resistances, and series inductance of the new line are 0.4064%, 0.7420%, and 0.3519%, respectively. The highest errors belong to the resistances because in transmission system the series impedances are highly inductive, i.e. the resistance values are much smaller than inductance values. Therefore, a small amount of noise or measurement error leads to larger errors in

the resistance parameters. The mutual parameters between the new line and the old line generally have larger errors, especially for shunt susceptances.

4.4 Conclusion

Transmission line electrical parameter measurement was addressed in this chapter. A method to find the parameters of a newly constructed transmission line in parallel with an existing transmission line was proposed. The main contributions of this chapter are: a) Proposing the idea of utilizing the induced voltages for measuring the line parameters, b) Proposing a proper data collection method based on different connections of the new line.

The proposed method did not require an external excitation source and could be applied without interrupting the normal operation of the old line. Synchronized voltage and current phasors at the two ends of the both lines were utilized to find the unknown parameters. Normal load variations in the network could be used to collect the required data points. After collecting the required measurement data, a two-step least-squares-based method was applied to find the unknown parameters.

To evaluate the performance of the proposed method, a test case including two medium length parallel transmission lines was considered. The π -circuit parameters of the new line were obtained by applying the method and compared with the actual parameters of the line. The results proved the efficacy of the method in finding the π -circuit parameters of the line with good accuracy even in presence of the measurement error and noise.

Chapter 5

Conclusions and Future Work

In this chapter, the main findings of the thesis are summarized and suggestions for future work are presented.

5.1 Thesis conclusions and contributions

This thesis proposed equivalent models for different power system studies. The conclusions and contributions are:

- A measurement-based approach to find multi-port Thevenin equivalent parameters of an external system was proposed in Chapter 2. The data obtained from PMUs located at the boundary nodes were utilized to obtain the unknown parameters using least-squares method. Two test cases were considered to evaluate the performance of the method. The results proved that the external equivalent model could represent the external system with good accuracy.
- Since the method proposed for parameters estimation in Chapter 2 was a measurement-based method, it was necessary to ensure that the external system has not changed during the identification process. Therefore, a disturbance side detection method was also proposed. The simulation results proved that the proposed method was able to correctly detect the source of the disturbance.
- Heuristic optimization based single-port FDNE methods were proposed in Chapter 3. To guarantee the passivity of the model, only passive elements, i.e.

positive resistance, inductance, capacitance, and conductance were used in the equivalent circuit. A new coding scheme based on the resonance frequencies was introduced to improve the convergence rate of the optimization methods. The performances of three optimization methods were compared and the best one was chosen. A strategy to determine the optimal number of branches was also proposed. Two case studies were considered and the results proved the efficacy of the method in finding equivalent models with high accuracy.

- For the multi-port case, since the non-diagonal elements of the admittance matrix could have negative real parts, a more general equivalent circuit consisting of branches with all positive elements and branches with all negative elements was proposed to fit the non-diagonal elements of the admittance matrix. Case studies were conducted to demonstrate the adequacy of the equivalent circuit. The results proved that the equivalent model could represent the original network with high accuracy.
- A method to measure the electrical parameters of a transmission line was proposed in Chapter 4. The method was specifically designed for newly constructed transmission line in parallel with an existing line. The advantage of the method was that it only relied on the induced voltages and currents from the old line and there was no need for interrupting the normal operation of the old line or connecting an additional voltage source to the new line.
- A data collection strategy based on different connections of the new line was also proposed to improve the parameter estimation accuracy. The collected data required for the estimation process were from normal load variations and there was no need to have scenarios like single line to ground faults in the old transmission line. A test case was considered to evaluate the performance of the method. The simulation results proved that the method was able to find the new line's parameters with high accuracy even in presence of the measurement error and noise.

5.2 Suggestions for future work

The suggestions for extending and modifying this research are as follows:

- In chapters 2 and 3, since the main focus was to evaluate the performance of the external system equivalent, the boundary zone was arbitrarily selected. But it was discussed that this area has an important effect on the overall accuracy of the equivalencing. A larger boundary area increases the accuracy but requires more computational capacity. Further studies on optimal size of the boundary zone are required to find a good balance between the accuracy and the size of the model.
- The line parameter measurement method proposed in chapter 4 is for newly constructed lines. The method proposed in this thesis is not applicable after the new line is connected to the grid. Therefore, an online method could be proposed to verify and track the parallel lines parameters using the measurement data when both lines are in service.

References

- [1] E. C. M. Costa and S. Kurokawa, "Estimation of transmission line parameters using multiple methods," *IET Generation, Transmission & Distribution*, vol. 9, no. 16, pp. 2617-2624, March 2015.
- [2] M. Asprou; E. Kyriakides, "Identification and Estimation of Erroneous Transmission Line Parameters Using PMU Measurements," *IEEE Transactions on Power Delivery*, doi: 10.1109/TPWRD.2017.2648881.
- [3] A. Abur and A. G. Exposito, *Power system state estimation: Theory and implementation*, New York: Basel, 2004.
- [4] K. J. Kusic and D. L. Garrison, "Measurement of transmission line parameters from SCADA data," *IEEE PES Power System Conference and Exposition*, New York, USA, Oct. 2004.
- [5] M. Gavrilas, O. Ivanov, and G. Gavrilas, "REI Equivalent Design for Electric Power Systems with Genetic Algorithms," *WSEAS Trans. Circuits & Systems*, vol. 7, no. 10, pp. 911-921, Oct. 2008.
- [6] X. Liu, J. Shen, A. Philip, E. Viray, M. Jiang, and D. Leon, "External WECC model reduction in on-line network applications for Alberta power grid," *IEEE Power and Energy Society General Meeting (PES)*, Vancouver, July 2013, pp. 1-5.
- [7] U. D. Annakkage et al., "Dynamic System Equivalents: A Survey of Available Techniques," *IEEE Transactions on Power Delivery*, vol.27, no.1, pp.411-420, Jan. 2012.
- [8] J. B. Ward, "Equivalent circuits for power-flow studies", *AIEE Transactions*, Vol. 68, pp. 373- 384, 1949.

Chapter 6: References

- [9] S. Deckmann, A. Pizzolante, A. Monticelli, B. Stott, and O. Alsac, "Numerical Testing of Power System Load Flow Equivalents," IEEE Transactions on Power Apparatus and Systems, vol. PAS-99, no. 6, pp. 2292-2300, Nov. 1980.
- [10] E. C. Housos, G. Irisarri, R. M. Porter, and A. M. Sasson, "Steady-state network equivalents for power system planning applications, " IEEE Trans. Power Appar. & Syst., vol. PAS-99, pp. 2113-2120, November 1980.
- [11] F.F. Wu and A. Monticelli, "A Critical Review on External Network Modeling for On-Line Security Analysis, " International Journal of Electrical Power and Energy Systems, vol. 5, no. 4, pp. 222-235, October, 1983.
- [12] E.K. Paulsson, "Network equivalents for on-line systems," presented at IEEE PAS Summer Meeting, Anaheim, July 1974.
- [13] D. Denzel, R. Graf and J. Verstege, "Practical use of equivalents for unobservable networks in on-line security monitoring", Power Systems Computation Conf., Cambridge, Sept. 1975.
- [14] A. Monticelli, S. Deckmann, A. Garcia, and B. Stott, "Real-Time External Equivalents for Static Security Analysis," IEEE Transactions on Power Apparatus and Systems, vol. PAS-98, no. 2, pp.498-508, March 1979.
- [15] P. Dimo, "Nodal Analysis of Power Systems," Abacus Press, Kent, England, 1975.
- [16] H. K. Singh and S. C. Srivastava, "A Sensitivity Based Network Reduction Technique for Power Transfer Assessment in Deregulated Electricity Environment," IEEE/PES Transmission and Distribution Conference and Exhibition Asia Pacific, 2002, pp.1976-1981.
- [17] O. Ivanov and M. Gavrilai, "Applying genetic algorithms to REI system equivalents," IEEE Power Tech Conf., 2009 Bucharest, Romania, June 28 - July 2.
- [18] T. E. DyLiacco, S. C. Savulescu, and K. A. Ramarao, "An On-Line Topological Equivalent of a Power System," IEEE Trans. Apparatus and Sys., vol. PAS-97, no. 5, pp. 1550-1563, Sept. 1978.
- [19] J. F. Dopazo, G. Irisarri, and A. M. Sasson, "Power Engineering Society 1981 Prize Paper Real-Time External System Equivalent for on-Line

Chapter 6: References

- Contingency Analysis," IEEE Power Engineering Review, vol. PER-1, no. 10, pp. 17-34, Oct. 1981.
- [20] E. Housos and G. Irisarri, "Real-time results with online network equivalents for control centre applications," IEEE Trans. Power Appar. & Syst., vol. PAS-100, pp. 4830-4837, December 1981.
- [21] H. Duran and N. Arvanitidis, "Simplification for Area Security Analysis: A New Look at Equivalencing," IEEE Trans. Power App. Syst., vol. PAS-91, pp. 670-679, March/April 1972.
- [22] E. H. Elkonyaly and F. L. Alvarado, "External System Static Equivalent for On-Line Implementation", IEEE PES Winter Meeting, New York, Jan. 1978.
- [23] A. J. Calvaer, "Power System Steady State Linearization around an Operating Point and Applications," CIGRE Committee 32, Minneapolis, May 1979.
- [24] J. F. Dopazo, M. H. Dwarakanath, J. J. Li, and A. M. Sasson, "An External System Equivalent Model Using Real-Time Measurements for System Security Evaluation," IEEE Trans. Power App. Syst., vol. 96, no. 2, pp. 431-446, March 1977.
- [25] A. S. Debs, "Estimation of External Network Equivalents from Internal System Data," IEEE Trans. Power App. Syst., vol. PAS-94, pp. 272-279, Mar./Apr.1975.
- [26] G. Contaxis and A. S. Debs, "Identification of External Equivalents for Steady State Security Assessment," IEEE Trans. Power App. Syst., vol. PAS - 97, pp. 409-414, March/April 1978.
- [27] H. Singh and A. Abur, "Multi-port equivalencing of external systems for simulation of switching transients," IEEE Trans. Power Syst., vol. 10, no. 1, pp. 374-382, Jan. 1995.
- [28] W. D. C. Boaventura, A. Semlyen, M. R. Iravani, and A. Lopes, "Sparse network equivalent based on time-domain fitting," IEEE Trans. Power Del., vol. 17, no. 1, pp. 182-189, Jan. 2002.

Chapter 6: References

- [29] Y. S. Mekonnen and J. E. Schutt-Ainé, "Fast macromodeling technique of sampled time/frequency data using s -domain vector-fitting method," in Proc. IEEE Electrical Performance of Electronic Packaging, 2007, pp. 47–50.
- [30] S. Grivet-Talocia, "Package macromodeling via time-domain vector fitting," IEEE Trans. Microw. Wireless Compon. Lett., vol. 13, no. 11, pp. 472–474, Nov. 2003.
- [31] A. Ubolli and B. Gustavsen, "Comparison of Methods for Rational Approximation of Simulated Time-Domain Responses: ARMA, ZD-VF, and TD-VF," IEEE Trans. on Power Del., vol. 26, no. 1, pp. 279-288, Jan. 2011.
- [32] B. Gustavsen and A. Semlyen, "Rational approximation of frequency domain responses by vector fitting," IEEE Trans. Power Del., vol. 14, no. 3, pp. 1052–1061, Jul. 1999.
- [33] B. Gustavsen "Improving the pole relocating properties of vector fitting," IEEE Trans. Power Del., vol. 21, no. 3, pp. 1587-1592, Jul. 2006.
- [34] B. Gustavsen and C. Heitz "Modal vector fitting: A tool for generating rational models of high accuracy with arbitrary terminal conditions," IEEE Trans. Adv. Packag., vol. 31, no. 4, pp.664 -672, Nov. 2008.
- [35] B. Gustavsen, "Computer code for rational approximation of frequency dependent admittance matrices," IEEE Trans. Power Del., vol. 17, no. 4, pp. 1093–1098, Oct. 2002.
- [36] B. Gustavsen and C. Heitz, "Fast Realization of the Modal Vector Fitting Method for Rational Modeling With Accurate Representation of Small Eigenvalues," IEEE Trans. Power Del., vol. 24, no. 3, pp. 1396-1405, July 2009.
- [37] S. Grivet-Talocia and A. Ubolli, "A comparative study of passivity enforcement schemes for linear lumped macromodels," IEEE Trans. Adv. Packag., vol. 31, pp.1-11, Nov. 2008.
- [38] B. Gustavsen and A. Semlyen, "Enforcing passivity for admittance matrices approximated by rational functions," IEEE Trans. Power Syst., vol. 16, pp.97-104, Feb. 2001.

Chapter 6: References

- [39] B. Gustavsen, "Computer code for passivity enforcement of rational macromodels by residue perturbation," *IEEE Trans. Adv. Packag.*, vol. 30, pp.209 -215, May 2007.
- [40] B. Gustavsen, "Fast passivity enforcement for pole-residue models by perturbation of residue matrix eigenvalues," *IEEE Trans. Power Del.*, vol. 23, no. 4, pp.2278 -2285, Oct. 2008.
- [41] I. R. Pordanjani, C. Y. Chung, H. E. Mazin, and W. Xu, "A Method to Construct Equivalent Circuit Model From Frequency Responses With Guaranteed Passivity," *IEEE Trans. on Power Del.*, vol. 26, no. 1, pp. 400-409, Jan. 2011.
- [42] I. R. Pordanjani, H. E. Mazin, and W. Xu, "A Novel Genetic Programming Approach for Frequency-Dependent Modeling," *IEEE Trans. on Evolutionary Computation*, vol. 17, no. 3, pp. 353-367, June 2013.
- [43] S. M. Chan, "Computing overhead line parameters," in *IEEE Computer Applications in Power*, vol. 6, no. 1, pp. 43-45, Jan. 1993.
- [44] H. W. Dommel, "Overhead Line Parameters From Handbook Formulas And Computer Programs," in *IEEE Transactions on Power Apparatus and Systems*, vol. PAS-104, no. 2, pp. 366-372, Feb. 1985.
- [45] X. Yang, G. Geng, Y. Wang, and T. Ding, "Method for accurately measuring the power-frequency parameters of EHV/UHV transmission lines," *IET Generation, Transmission & Distribution*, doi: 10.1049/iet-gtd.2016.1359.
- [46] S. Kurokawa, J. Pissolato, M. C. Tavares, C. M. Portela and A. J. Prado, "A new procedure to derive transmission-line parameters: applications and restrictions," in *IEEE Transactions on Power Delivery*, vol. 21, no. 1, pp. 492-498, Jan. 2006.
- [47] Y. Liao and M. Kezunovic, "Online Optimal Transmission Line Parameter Estimation for Relaying Applications," in *IEEE Transactions on Power Delivery*, vol. 24, no. 1, pp. 96-102, Jan. 2009.

Chapter 6: References

- [48] M. Bockarjova and G. Andersson, "Transmission line conductor temperature impact on state estimator accuracy," in IEEE PowerTech, Laussane, Jul. 2007.
- [49] Standardization Administration of the People's Republic of China: "Standard for hand-over test of electric equipment – electric equipment installation engineering (GB 50150-2006)", 2006.
- [50] North American Electric Reliability Corporation: 'Maintaining transmission line ratings consistent with as-built conditions: good utility practices', 2015, Available online at http://www.nerc.com/pa/rrm/bpsa/Facility_Ratings_Alert_DL/Maintaining_Transmission_Line_Ratings_Good_Utility_Practices_December_2015.pdf.
- [51] R. Schulze, P. Schegner and R. Zivanovic, "Parameter Identification of Unsymmetrical Transmission Lines Using Fault Records Obtained From Protective Relays," in IEEE Transactions on Power Delivery, vol. 26, no. 2, pp. 1265-1272, April 2011.
- [52] Y. Wang, W. Xu and J. Shen, "Online Tracking of Transmission-Line Parameters Using SCADA Data," in IEEE Transactions on Power Delivery, vol. 31, no. 2, pp. 674-682, April 2016.
- [53] I. D. Kim, J.R. Lee, Y.J., Ko, and Y. T. Jin: "A study on the condition monitoring of transmission line by on-line circuit parameter measurement", Int. J. Electr. Comput. Electron. Commun. Eng., vol. 7, no. 8, pp. 107–111, 2013.
- [54] Y. Du and Y. Liao, "On-line estimation of transmission line parameters, temperature and sag using PMU measurements," Electr. Power Syst. Res., vol. 93, pp. 39–45, July, 2012.
- [55] S. S. Mousavi-Seyedi, F. Aminifar, and S. Afsharnia, "Parameter estimation of multiterminal transmission lines using joint PMU and SCADA data," IEEE Trans. Power Del., vol. 30, no. 3, pp. 1077–1085, Jun. 2015.
- [56] C. Mishra, V. A. Centeno and A. Pal, "Kalman-filter based recursive regression for three-phase line parameter estimation using synchrophasor

Chapter 6: References

- measurements," 2015 IEEE Power & Energy Society General Meeting, Denver, CO, 2015, pp. 1-5.
- [57] Omicron Energy: "Impedance measurement on high-voltage lines", 2016. Available at <https://www.omicronenergy.com/en/products/transmission-lines/lineimpedance-measurement/cpc-100-cp-cu1/>.
- [58] B. Li, F. Guo, X. Li, et al.: "Circulating unbalanced currents of EHV/UHV untransposed double-circuit lines and their influence on pilot protection", IEEE Trans. Power Delivery, vol. 29, no. 2, pp. 825–833, 2014.
- [59] Z. Hu, M. Xiong, C. Li and P. Tang, "New Approach for Precisely Measuring the Zero-Sequence Parameters of Long-Distance Double-Circuit Transmission Lines," in IEEE Transactions on Power Delivery, vol. 31, no. 4, pp. 1627-1635, Aug. 2016.
- [60] A. S. Morched, J. H. Ottevangers, and L. Marti, "Multi-port frequency dependent network equivalents for the EMTP," IEEE Trans. Power Del., vol. 8, no. 3, pp. 1402–1412, Jul. 1993.
- [61] T. Noda, "Identification of a multiphase network equivalent for electromagnetic transient calculations using partitioned frequency response," IEEE Trans. Power Del., vol. 20, no. 2, pt. 1, pp. 1134–1142, Apr. 2005.
- [62] T. Noda, "A binary frequency-region partitioning algorithm for the identification of a multiphase network equivalent for EMT studies," IEEE Trans. Power Del., vol. 22, no. 2, pp. 1257–1258, Apr. 2007.
- [63] D. Chen and Z. Shen, "Bi-directional coupling between two coupled transmission lines," IEEE Microw. Wireless Compon. Lett., vol. 13, no. 12, pp. 514–516, Dec. 2003.
- [64] S. M. Abdelkader and D. J. Morrow, "Online Tracking of Thévenin Equivalent Parameters Using PMU Measurements," in IEEE Transactions on Power Systems, vol. 27, no. 2, pp. 975-983, May 2012.
- [65] I. D. Mayergoyz and W. Lawson, "Basic electric circuit theory: a one-semester text," Academic Press, Elsevier, 1997.

Chapter 6: References

- [66] L. M. Jin and S. P. Chan, "A unified and efficient approach for determining Thevenin (Norton) equivalent circuits," in *IEEE Transactions on Education*, vol. 32, no. 3, pp. 408-410, Aug. 1989.
- [67] S. M. Abdelkader and D. Flynn, "Graphical determination of network limits for wind power integration," in *IET Generation, Transmission & Distribution*, vol. 3, no. 9, pp. 841-849, September 2009.
- [68] G. Fusco and M. Russo, "Adaptive voltage regulator design for synchronous generator," *IEEE Trans. Energy Convers.*, vol. 23, no. 3, pp. 946–956, Sep. 2008.
- [69] M. Gol, and A. Abur, "LAV Based Robust State Estimation for Systems Measured by PMUs," *IEEE Trans. Smart Grid*, vol. 5, no. 4, pp. 1808-1814, July 2014.
- [70] I. R. Pordanjani, Y. Wang, and W. Xu, "Identification of Critical Components for Voltage Stability Assessment Using Channel Components Transform," *IEEE Trans. Smart Grid*, vol. 4, no. 2, pp. 1122-1132, June 2013.
- [71] A. A. Hajnoroozi, F. Aminifar, and H. Ayoubzadeh, "Generating Unit Model Validation and Calibration Through Synchrophasor Measurements," *IEEE Trans. Smart Grid*, vol. 6, no. 1, pp. 441-449, Jan. 2015.
- [72] J. Ma, P. Zhang, H. Fu, B. Bo, and Z. Dong, "Application of Phasor Measurement Unit on Locating Disturbance Source for Low-Frequency Oscillation," *IEEE Trans. Smart Grid*, vol. 1, no. 3, pp. 340-346, Dec. 2010.
- [73] A. Chakraborty, J. H. Chow, and A. Salazar, "A Measurement-Based Framework for Dynamic Equivalent of Large Power Systems Using Wide-Area Phasor Measurements," *IEEE Trans. Smart Grid*, vol. 2, no. 1, pp. 68-81, March 2011.
- [74] A. Chakraborty, "Wide-Area Damping Control of Power Systems Using Dynamic Clustering and TCSC-Based Redesigns," *IEEE Trans Smart Grid*, vol. 3, no. 3, pp. 1503-1514, Sept. 2012.
- [75] J. Wei, D. Kundur, and K. L. Butler-Purry, "A Novel Bio-Inspired Technique for Rapid Real-Time Generator Coherency Identification," *IEEE Trans. Smart Grid*, vol. 6, no. 1, pp. 178-188, Jan. 2015.

Chapter 6: References

- [76] S. M. Abdelkader and D. J. Morrow, "Online Thévenin Equivalent Determination Considering System Side Changes and Measurement Errors," *IEEE Trans. Power Sys*, vol. 30, no. 5, pp. 2716-2725, Sept. 2015.
- [77] W. Xu, I. R. Pordanjani, Y. Wang, and E. Vaahedi, "A Network Decoupling Transform for Phasor Data Based Voltage Stability Analysis and Monitoring," *IEEE Trans. on Smart Grid*, vol. 3, no. 1, pp. 261-270, March 2012.
- [78] S. A. Arefifar and W. Xu, "Online Tracking of Power System Impedance Parameters and Field Experiences," *IEEE Trans. Power Del.*, vol. 24, no. 4, pp. 1781-1788, Oct. 2009.
- [79] IEEE Standard for Synchrophasor Data Transfer for Power Systems, *IEEE Std. C37.118.1-2011*, Dec. 2011.
- [80] A. Asrari, S. Lotfifard and M. S. Payam, "Pareto Dominance-Based Multiobjective Optimization Method for Distribution Network Reconfiguration," *IEEE Trans. Smart Grid*, vol. 7, no. 3, pp. 1401-1410, May 2016.
- [81] A. R. Abbasi and A. R. Seifi, "Unified electrical and thermal energy expansion planning with considering network reconfiguration," *IET Generation, Transmission & Distribution*, vol. 9, no. 6, pp. 592-601, 4 20 2015.
- [82] H. Zeinoddini-Meymand, B. Vahidi, R. A. Naghizadeh and M. Moghimi Haji, "Optimal Surge Arrester Parameter Estimation Using a PSO-Based Multiobjective Approach," in *IEEE Transactions on Power Delivery*, vol. 28, no. 3, pp. 1758-1769, July 2013.
- [83] S. Jazebi, M. Moghimi Haji and R. A. Naghizadeh, "Distribution Network Reconfiguration in the Presence of Harmonic Loads: Optimization Techniques and Analysis," in *IEEE Transactions on Smart Grid*, vol. 5, no. 4, pp. 1929-1937, July 2014.
- [84] L. Meng, P. Gao, M. M. Haji and W. Xu, "Magnetic Sensor Array-Based AC Current Measurement for Multiconductor Cables Using Evolutionary

Chapter 6: References

- Computation Method," in IEEE Transactions on Instrumentation and Measurement, vol. 64, no. 10, pp. 2747-2758, Oct. 2015.
- [85] The vector fitting website, Vectfit3.m, Software package. (2009, Aug.). [Online]. Available: <http://www.energy.sintef.no/produkt/VECTFIT/-index.asp>.
- [86] J. J. Grainger and W. D. Stevenson, "Power System Analysis," McGraw-Hill, 1994.

Appendix A

Multi-port Thevenin Equivalent

A.1 Finding external network multi-port Thevenin equivalent parameters from known network data

The Thevenin equivalent of an external system can be calculated knowing the external system operating point and network data [1]. The following assumptions are made:

- Voltage sources are considered to be ideal
- Loads are converted to constant admittances and are included in the diagonal elements of the node admittance matrix
- Power flows from the internal system into the boundary nodes are assumed to be constant current injections

The following equation can be written for the external system:

$$\begin{bmatrix} I_b \\ I_g \\ 0 \end{bmatrix} = \begin{bmatrix} Y_{bb} & Y_{bg} & Y_{bl} \\ Y_{gb} & Y_{gg} & Y_{gl} \\ Y_{lb} & Y_{lg} & Y_{ll} \end{bmatrix} \begin{bmatrix} V_b \\ V_g \\ V_l \end{bmatrix} \quad (\text{A.1})$$

where I_b and V_b are current and voltage phasors of the boundary buses, respectively. I_g and V_g are current and voltage phasors of the PV buses, respectively. Finally, V_l is voltage phasor of the PQ buses.

The following equations are derived from (A.1):

$$I_b = Y_{bb}V_b + Y_{bg}V_g + Y_{bl}V_l \quad (\text{A.2})$$

Appendix A: Multi-port Thevenin Equivalent

$$V_l = -Y_{ll}^{-1}(Y_{lb}V_b + Y_{lg}V_g) \quad (\text{A.3})$$

Substituting V_l from (A.3) into (A.2) and rearranging the equation gives the following equations for calculating the external system Thevenin equivalent parameters:

$$Z_e = (Y_{bb} - Y_{bl}Y_{ll}^{-1}Y_{lb})^{-1} \quad (\text{A.4})$$

$$E = -Z_e(Y_{bg} - Y_{bl}Y_{ll}^{-1}Y_{lg})V_g \quad (\text{A.5})$$

A.2 Decoupling the multi-port Thevenin Equivalent

The multi-port Thevenin equivalent found above is in form of a coupled multi-port network. While some software might be compatible with such a matrix type equivalent, to be able to use this network in any simulation software, it is required to decouple the network and find the parameters of the decoupled network.

For instance, the decoupled network for a 4-port Thevenin equivalent is shown in Figure A.1.

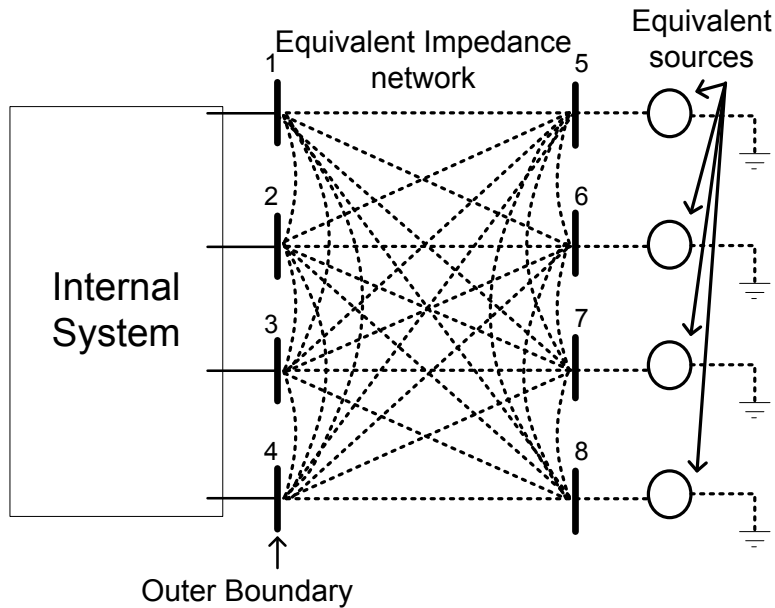


Figure A.1 Decoupled equivalent network configuration

Appendix A: Multi-port Thevenin Equivalent

The Thevenin equivalent is converted to the network shown in Figure A.1 using circuit theory principles [II]. The equivalent voltage sources shown in this figure are the same as the equivalent Thevenin voltage sources. To find the equivalent impedance network parameters, first the node incidence matrix is constructed as follows (assuming current flows from boundary nodes to the external system):

$$A_{inc} = \begin{bmatrix} 1 & 0 & 0 & 0 & -1 & 0 & 0 & 0 \\ 0 & 1 & 0 & 0 & 0 & -1 & 0 & 0 \\ 0 & 0 & 1 & 0 & 0 & 0 & -1 & 0 \\ 0 & 0 & 0 & 1 & 0 & 0 & 0 & -1 \end{bmatrix}^T \quad (\text{A.6})$$

Then, the equivalent node admittance matrix is:

$$Y_{bus_{eq}} = A_{inc} \times Z_e^{-1} \times A'_{inc} \quad (\text{A.7})$$

The values of the equivalent impedance network could be easily determined using the equivalent node admittance matrix.

A.3 IEEE 118 system

IEEE 118 bus system is used in Chapter 2. Bus 80 is considered to be the swing bus located in the internal system. For the first case, in addition to converting the PV buses of the external system to swing buses (i.e. ideal voltage sources), the values of some loads are modified as presented in TABLE A.1 to have more power transfer between the external system and boundary zone.

TABLE A.1 Modified loads in IEEE 118 bus system

| Bus number | P _{load} (MW) | Q _{load} (MVar) |
|------------|------------------------|--------------------------|
| 24 | 113 | 33 |
| 43 | 118 | 17 |
| 44 | 116 | 30 |
| 70 | 200 | 50 |

Appendix A: Multi-port Thevenin Equivalent

For the second case study, the PV buses with small capacity are converted to PQ buses instead of swing buses. Fixed shunts are added at these buses with values equal to the original reactive power injected at the respective buses. The modified buses along with the added fixed shunts are presented in TABLE A.2.

TABLE A.2 PV buses converted to PQ buses for case 2 of Chapter 2

| Bus number | Fixed shunt (MVar) | Bus number | Fixed shunt (MVar) | Bus number | Fixed shunt (MVar) |
|------------|--------------------|------------|--------------------|------------|--------------------|
| 1 | -3.1069 | 55 | 5.0 | 91 | -4.3 |
| 6 | 15.931 | 56 | 14.2 | 92 | 9.0 |
| 15 | 4.0197 | 62 | 2.5 | 99 | -17.1 |
| 18 | 26.0936 | 70 | 11.5 | 104 | 5.7 |
| 19 | -8.0 | 72 | -11.1 | 105 | -8.0 |
| 32 | -14.0 | 73 | 9.7 | 107 | 5.7 |
| 34 | 6.0 | 74 | -4.6 | 110 | 4.9 |
| 36 | 1.3286 | 76 | 7.7 | 112 | 41.5 |
| 40 | 33.0717 | 77 | 70.0 | 116 | 52.1 |
| 42 | 60.7179 | 85 | 3.5 | 49 | 122.9 |
| 24 | -15.8 | 90 | 81.7 | 65 | 88.1 |

Appendix B

Heuristic Optimization Methods

B.1 Shuffled frog-leaping algorithm

Shuffled frog-leaping algorithm (SFLA) is a population based meta-heuristic optimization algorithm inspired by natural memetics [III]. The algorithm can be summarized in the following steps:

1) The algorithm starts with creating N initial virtual frogs. The i^{th} frog is represented by $F_i = (F_i^1, F_i^2, \dots, F_i^D)$, where D is the number of optimization parameters.

2) The fitness function of each frog is calculated. The whole population is then sorted in an ascending order for a minimization problem which means that the frog with lowest (best) fitness function will be the first rank; the frog with the second lowest fitness function will be the second rank and so on.

3) The frogs are partitioned into m memeplexes with n frogs in each memeplex (i.e. $N=m \times n$). In the partitioning procedure, the first rank goes to the first memeplex, the second rank goes to the second memeplex and so on, until the m^{th} rank goes to the m^{th} memeplex. Then the $m+1^{\text{th}}$ rank goes back to the first memeplex, the $m+2^{\text{th}}$ rank goes to the second memeplex, and so on, until all of the frogs are placed in the corresponding memeplexes. The worst and best frogs in memeplex k are represented by WF^k and BF^k . Also, the best frog among the whole population is represented by GF .

4) Memetic evolution within each memeplex is done in which the worst frog in each memeplex tries to improve its performance (i.e. to lower its fitness function). The position of the worst frog is changed according to

$$WF_{new}^k = WF^k + c(BF^k - WF^k) \quad (B.1)$$

where c is an accelerating coefficient [IV]. If the performance of the frog improves in this way, the frog moves to the new location. Otherwise, BF^k is replaced with GF in (B.1) and the equation is applied a second time to try to improve the frog's performance. If the performance of the frog improves in this way, the frog moves to the new location. Otherwise, the frog's position is replaced with a new randomly generated position.

5) After a defined number of evolutionary steps are performed within each memeplex, the shuffling is done in which all of the frogs are put together in a single group. The population will be sorted again and new memeplexes will be formed.

6) The algorithm continues until a stopping criterion is satisfied. In this thesis, the algorithm stops after a defined maximum number of iteration is performed.

B.2 Particle Swarm Optimization

Particle swarm optimization (PSO) is a population-based algorithm introduced in 2005 by Kennedy and Eberhart [V]. The algorithm can be summarized in the following steps [VI]:

1) The algorithm starts with creating an initial population. An initial position and velocity is dedicated to each individual as $X_i = (X_i^1, X_i^2, \dots, X_i^D)$ and $V_i = (V_i^1, V_i^2, \dots, V_i^D)$, where D is the number of optimization parameters.

2) The fitness function of each particle is calculated. The position with the best fitness function is stored as G_{best} which represents the best position

Appendix B: Heuristic Optimization Methods

experienced by the whole swarm. Also, for each particle, the current position is stored as Pbest which represents the best position experienced by each particle.

3) At each evolutionary step, first the velocity of the particles is updated. Then, the positions are updated using the updated velocities using the following formulas:

$$V_i^{j,k+1} = \omega^k \cdot V_i^{j,k} + c_1 \cdot \text{rnd}_1 \cdot (Pbest_i^{j,k} - X_i^{j,k}) + c_2 \cdot \text{rnd}_2 \cdot (Gbest^{j,k} - X_i^{j,k}) \quad (\text{B.2})$$

$$X_i^{j,k+1} = X_i^{j,k} + V_i^{j,k+1} \quad (\text{B.3})$$

where $X_i^{j,k}$ and $V_i^{j,k}$ are the j^{th} element of position and velocity of the i^{th} particle at k^{th} iteration, respectively. c_1 and c_2 are accelerating coefficients. r_1 and r_2 are random numbers between zero and one. Finally, ω^k is the weighting factor obtained by

$$\omega^k = \omega_{\max} - \frac{\omega_{\max} - \omega_{\min}}{\max_iter} \times k \quad (\text{B.4})$$

where ω_{\max} and ω_{\min} are the maximum and minimum weight, respectively. \max_iter is the maximum number of iterations.

4) The fitness function of each particle is calculated and compared to its Pbest fitness function. If the particle has reached to a position with a better fitness function, the current position is stored as the new Pbest.

5) The best Pbest fitness value is found and compared to the Gbest fitness function. If the best Pbest has a better fitness function, its position replaces the Gbest which means that the whole swarm has found a new optimal position.

6) Equations (B.2) and (B.3) are applied again to update the velocity and position of each particle.

7) The algorithm continues until a stopping criterion is satisfied. In this thesis, the algorithm stops after a defined maximum number of iteration is performed.

B.3 Differential Evolution

Differential evolution (DE) is a parallel direct search method first introduced in 1995 [VII]. The algorithm can be summarized in the following steps [VII]:

1) The algorithm starts with randomly creating N_p parameter vectors as $X_i = (X_i^1, X_i^2, \dots, X_i^D)$, where D is the number of optimization parameters.

2) The fitness function of each vector is calculated. The best parameter vector X_{best} is stored for each generation/iteration.

3) A trial vector is generated for each vector X_i using

$$V_{i,\text{trial}} = X_{r_1} + F \cdot (X_{r_2} - X_{r_3}) \quad (\text{B.5})$$

where $r_1, r_2, r_3 \in [1, N_p]$ are mutually different random integers, different from i . F is positive real constant.

4) For each vector X_i , a new vector U_i is generated using

$$U_i^j = \begin{cases} V_i^j & \text{for } j \in S_{SD} \\ X_i^j & \text{otherwise} \end{cases} \quad (\text{B.6})$$

where SD is a subgroup of parameters.

5) The fitness function is calculated for the newly generated vectors. If U_i has a better fitness function compared to X_i , it will replace X_i for the next generation. Otherwise, U_i is discarded and X_i is retained.

6) The algorithm continues by generating new trial vectors. The process continues until a predefined fitness function value is reached or the maximum number of iteration is performed. The latter criterion is used in this thesis.

The MATLAB codes for implementing the algorithm are available online at University of California, Berkley website [VIII].

Appendix C

FDNE in EMTDC/PSCAD

C.1 Frequency Scan

The first step in finding the frequency dependent equivalent of an external network is to get the frequency scan results. The results could be expressed as impedance or admittance data. However, in FDNE application, it is more common to use the admittance data.

For the single-port problem, the built-in “Harmonic Impedance Component” shown in Figure C.1 can be used. This component gives the sequence impedances or phase impedances for a defined frequency range. However, this component can only be used for a single three-phase bus and cannot be used for multi-port problems.

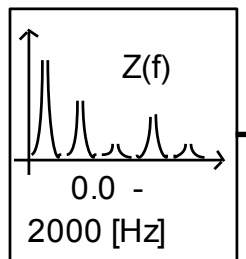


Figure C.1 The “Harmonic Impedance Component” in EMTDC/PSCAD

Appendix C: FDNE in EMTDC/PSCAD

An alternative approach is to replace all of the sources with their respective sub-synchronous impedance and then connect an external source with the desired frequency to the node. The admittance seen at this node can be obtained by

$$Y_k(f) = \frac{I_k(f)}{V_k(f)} \quad (\text{C.1})$$

where $Y_k(f)$, $I_k(f)$, and $V_k(f)$ are admittance seen at bus k at frequency f , injected current at bus k , and external source voltage magnitude connected to bus k , respectively. For simplicity, the magnitude of the voltage source can be set to 1. Therefore,

$$Y_k(f) = I_k(f) \quad (\text{C.2})$$

To automate the process, a staircase like waveform is generated to automatically change the frequency of the source. The duration of the steps is set to give enough time to the waveforms to reach the steady-state. An example of this waveform with 30Hz steps is shown in Figure C.2.

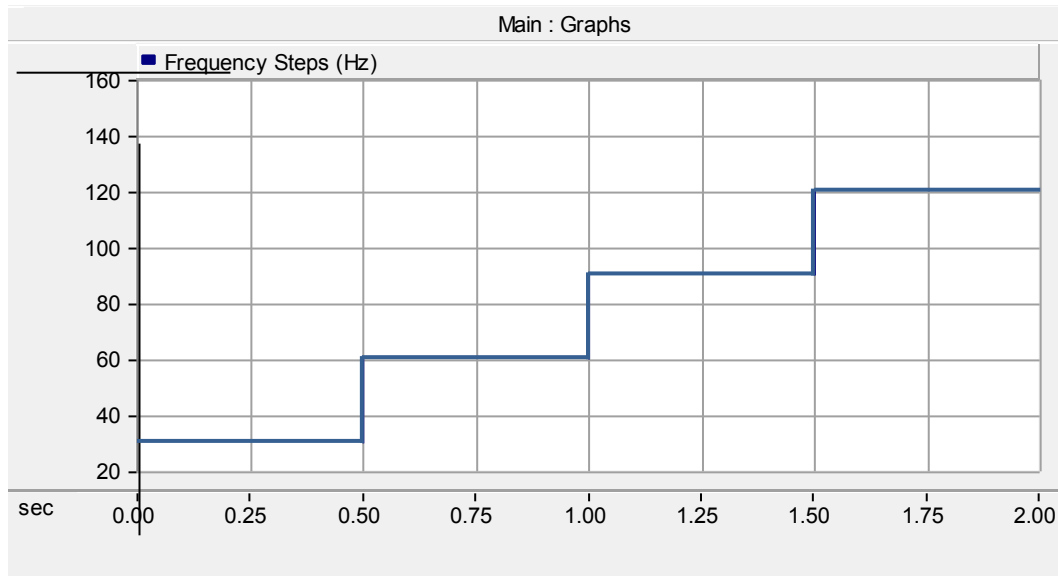


Figure C.2 The frequency steps given as the frequency input of the voltage source with external controls

Appendix C: FDNE in EMTDC/PSCAD

The frequency range can be increased by increasing the simulation time. In each frequency, the RMS value of the current, as well as the phase angle of the current with respect to the voltage source is recorded to calculate the admittance magnitude and angle at each frequency step using (C.2).

For the multi-port case, the following equation can be written at each frequency

$$\begin{bmatrix} I_1(f) \\ I_2(f) \\ \vdots \\ I_{N_b}(f) \end{bmatrix} = \begin{bmatrix} Y_{1,1}(f) & Y_{1,2}(f) & \dots & (f) \\ Y_{2,1}(f) & Y_{2,2}(f) & \dots & (f) \\ \vdots & \vdots & \vdots & \vdots \\ Y_{N_b,1}(f) & Y_{N_b,2}(f) & \dots & (f) \end{bmatrix} \begin{bmatrix} V_1(f) \\ V_2(f) \\ \vdots \\ V_{N_b}(f) \end{bmatrix} \quad (C.3)$$

Equation (C.4) can be written in impedance matrix form as

$$\begin{bmatrix} V_1(f) \\ V_2(f) \\ \vdots \\ V_{N_b}(f) \end{bmatrix} = \begin{bmatrix} Z_{1,1}(f) & Z_{1,2}(f) & \dots & (f) \\ Z_{2,1}(f) & Z_{2,2}(f) & \dots & (f) \\ \vdots & \vdots & \vdots & \vdots \\ Z_{N_b,1}(f) & Z_{N_b,2}(f) & \dots & (f) \end{bmatrix} \begin{bmatrix} I_1(f) \\ I_2(f) \\ \vdots \\ I_{N_b}(f) \end{bmatrix} \quad (C.4)$$

Similar to the single-port, to get the admittance matrix of the external network, first the sources are replaced with their sub-synchronous impedances. At each frequency, a voltage source is connected to each of the boundary nodes and the current and voltage magnitudes and phase angles at all of the boundary nodes are obtained. To better show the frequency scan method, an external system with N_b boundary nodes is considered as shown in Figure C.3.

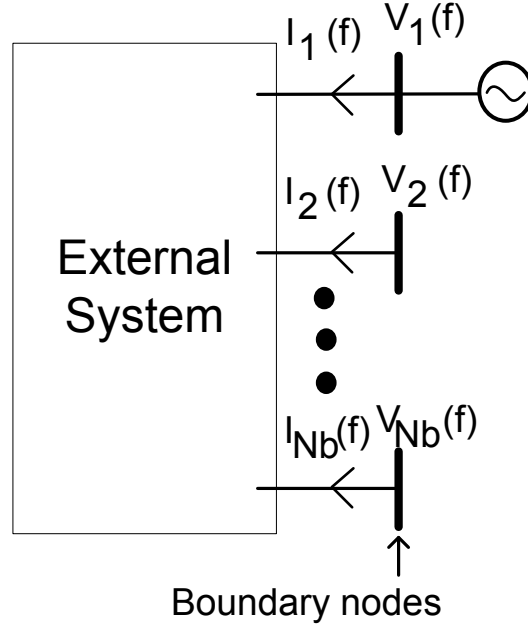


Figure C.3 An external source connected to node 1 in an external system with three boundary nodes

In Figure C.3, a voltage source is connected to node 1 and all of the voltage and current phasors are obtained. From (C.4) it can be deduced that

$$\begin{bmatrix} V_1(f) \\ V_2(f) \\ \vdots \\ V_{Nb}(f) \end{bmatrix} = \begin{bmatrix} Z_{1,1}(f) & Z_{1,2}(f) & \dots & (f) \\ Z_{2,1}(f) & Z_{2,2}(f) & \dots & (f) \\ \vdots & \vdots & \ddots & \vdots \\ Z_{Nb,1}(f) & Z_{Nb,2}(f) & \dots & (f) \end{bmatrix} \begin{bmatrix} I_1(f) \\ 0 \\ \vdots \\ 0 \end{bmatrix} \quad (C.5)$$

Therefore, the elements of the first of the harmonic impedance matrix can be calculated by

$$Z_{1,i}(f) = \frac{V_i(f)}{I_1(f)} \quad (C.6)$$

The rest of the elements of the impedance matrix can be calculated by connecting the voltage source at the other nodes and repeating the same process.

After calculating all of the elements of the harmonic impedance matrix, the harmonic admittance matrix can be calculated by inversion.

$$\begin{bmatrix} Y_{1,1}(f) & Y_{1,2}(f) & \dots & & & & & & \\ Y_{2,1}(f) & Y_{2,2}(f) & \dots & & & & & & \\ \vdots & \vdots & \ddots & \vdots & \vdots & \vdots & \ddots & \vdots & \\ Y_{Nb,1}(f) & Y_{Nb,2}(f) & \dots & & & & & & \end{bmatrix} \quad (C.7)$$

The same process is repeated to get the harmonic admittance matrix at all of the desired frequencies.

C.2 Creating the FDNE model in EMTDC/PSCAD

After finding the FDNE of the external network, the full external network should be replaced with the reduced order model. Considering case 4 of Chapter 3, the equivalent model is shown in Figure C.4.

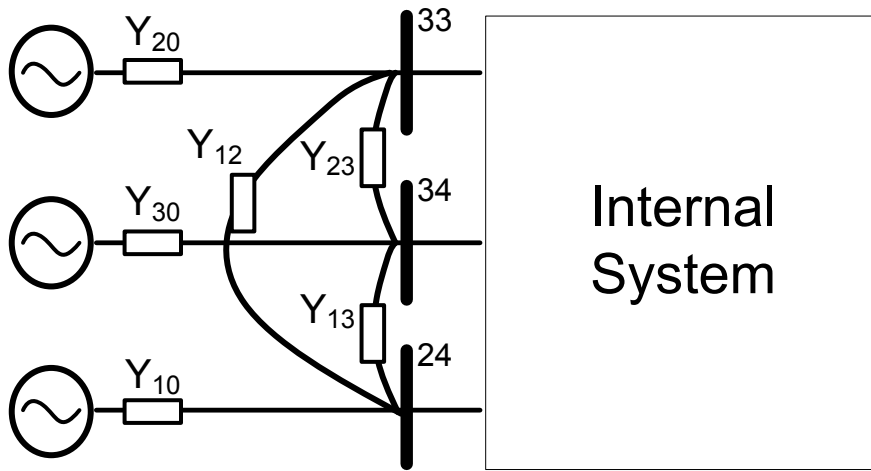


Figure C.4 Equivalent model for case 4 of Chapter 3

Each of the blocks shown in this figure should be replaced with a three-phase equivalent model consisting of parallel RLCG branches. For example, the branch between nodes 33 and 34 is shown in Figure C.5.

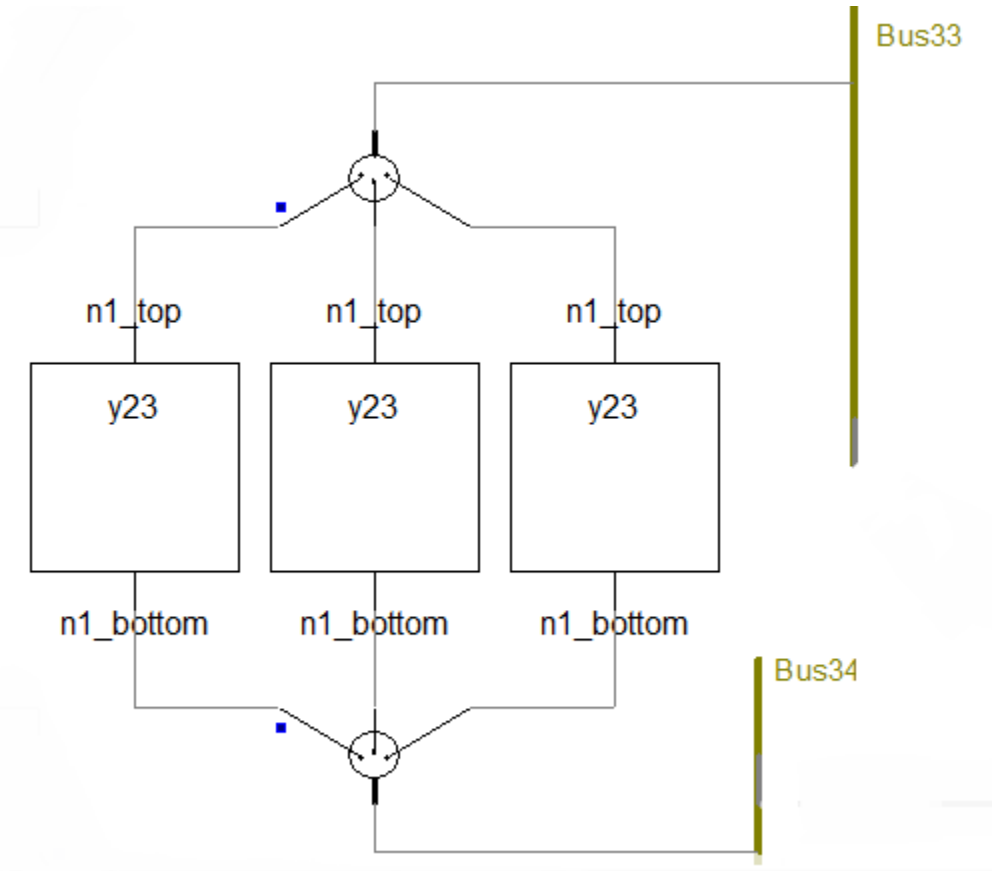


Figure C.5 The equivalent branch between nodes 33 and 34

The y23 modules in Figure C.5 are all the same and are in fact the parallel RLCG units/branches found by the FDNE method shown in Figure C.6.

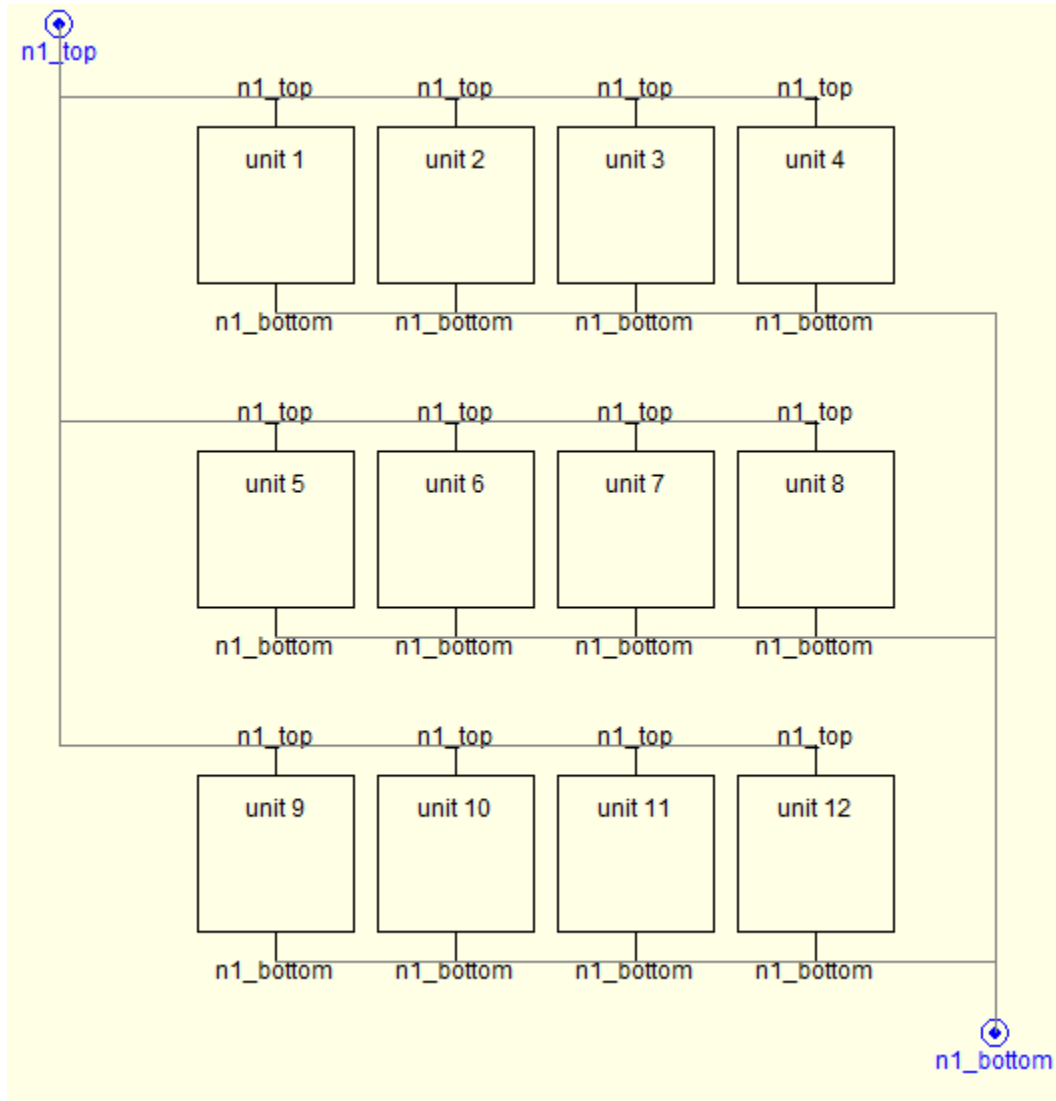


Figure C.6 The parallel RLCG units inside y23 modules of Figure C.5

Finally, each unit is a RLCG branch as shown in Figure C.7.

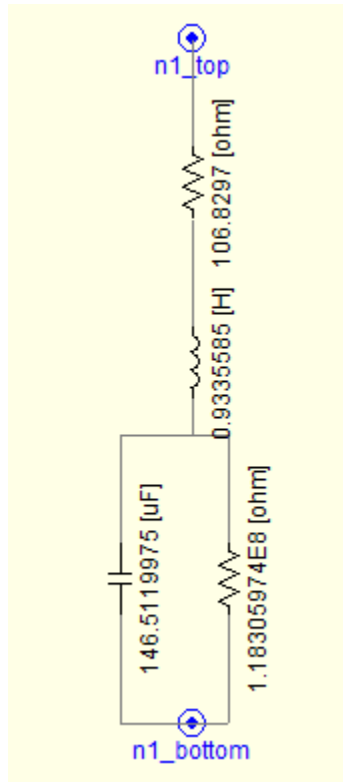


Figure C.7 The RLCG branch inside unit 1 of Figure C.6

Appendix D

Simulink Model

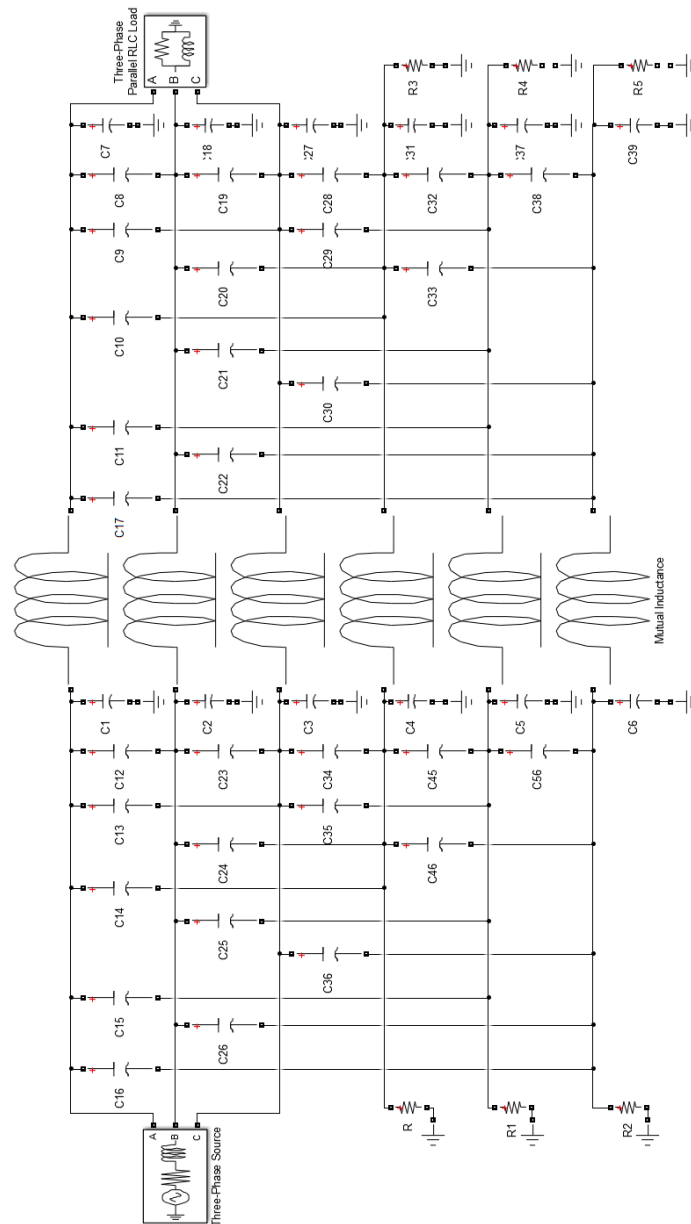


Figure D.1 Simulink model for chapter 4

References of Appendices

- [I] W. Xu, I. R. Pordanjani, Y. Wang, and E. Vaahedi, "A Network Decoupling Transform for Phasor Data Based Voltage Stability Analysis and Monitoring," IEEE Trans. on Smart Grid, vol. 3, no. 1, pp. 261-270, March 2012.
- [II] J. J. Grainger and W. D. Stevenson, "Power System Analysis," McGraw-Hill, 1994.
- [III] M. Eusuff, K. Lansey, and F. Pasha, "Shuffled frog-leaping algorithm: a memetic meta-heuristic for discrete optimization," Engineering Optimization, vol. 38, no. 2, pp. 129-154, March 2006.
- [IV] R. A. Naghizadeh, B. Vahidi and S. H. Hosseinian, "Modelling of inrush current in transformers using inverse Jiles–Atherton hysteresis model with a Neuro-shuffled frog-leaping algorithm approach," IET Electric Power Applications, vol. 6, no. 9, pp. 727-734, November 2012.
- [V] J. Kennedy and R. C. Eberhart, "Particle swarm optimization," in Proc. IEEE Int. Conf. Neural Networks (ICNN'95), Perth, Australia, 1995, vol. IV, pp. 1942–1948.
- [VI] J. B. Park, Y. W. Jeong, J. R. Shin and K. Y. Lee, "An Improved Particle Swarm Optimization for Nonconvex Economic Dispatch Problems," in IEEE Transactions on Power Systems, vol. 25, no. 1, pp. 156-166, Feb. 2010.
- [VII] Storn, R. and Price, K., "Differential Evolution - a Simple and Efficient Adaptive Scheme for Global Optimization over Continuous Spaces," Technical Report TR-95-012, ICSI, March 1995
- [VIII] Differential Evolution Homepage, Available online at <http://www1.icsi.berkeley.edu/~storn/code.html>